Development of modified graphite felt electrodes for the vanadium redox flow battery

Dissertation

zur Erlangung des Grades

des Doktors der Naturwissenschaften

der Naturwissenschaftlich-Technischen Fakultät

der Universität des Saarlandes

von

Sang Jun Yoon

Saarbrücken

2020

Tag des Kolloquiums:	09.06.2020
Dekan:	Prof. Dr. Guido Kickelbick
Berichterstatter:	Prof. Dr. Dr. h.c. Rolf Hempelmann
	Priv.-Doz. Dr.-Ing. Guido Falk
Vorsitz:	Prof. Dr. Michael Springborg
Akad. Mitarbeiter:	Dr. Francesco Arena

Eidesstattliche Versicherung

Hiermit versichere ich an Eides statt, dass ich die vorliegende Arbeit selbstständig und ohne Benutzung anderer als der angegebenen Hilfsmittel angefertigt habe. Die aus anderen Quellen oder indirekt übernommenen Daten und Konzepte sind unter Angabe der Quelle gekennzeichnet. Die Arbeit wurde bisher weder im In- noch im Ausland in gleicher oder ähnlicher Form in einem Verfahren zur Erlangung eines akademischen Grades vorgelegt.

Ort, Datum

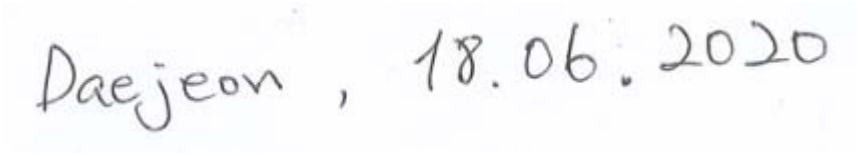

Unterschrift

Abstract

Redox flow batteries (RFBs) are one of the most promising candidates for stationary large-scale energy storage systems with regard to cost, cycle life, design flexibility, and safety. Among various RFBs, vanadium redox flow batteries (VRFBs) have the advantage of overcoming the cross-contamination of both electrolytes because VRFBs use the same V ion as the active species in both the anolyte and the catholyte. In spite of the various advantages of VRFBs, the performance of VRFBs needs to be further improved for the commercialization. The performance of VRFBs is significantly affected by the electrochemical activity of the electrode because the vanadium ion redox reactions take place at the graphite felt electrode surface during the charge-discharge process. To improve the electrochemical activity of graphite felt electrodes, facile methods for preparing nitrogen-doped carbon coated graphite felt electrodes using nitrogen-containing materials were developed. First, 1-ethyl-3-methylimidazolium dicyanamide (EMIM dca), an ionic liquid containing a high content of nitrogen, was used as an effective precursor for nitrogen doping on graphite felt surfaces. The effect of EMIM dca derived nitrogen doped graphite felt on the performance of VRFBs was investigated by various physical and electrochemical analyses. When employed in charge-discharge tests, the single cells with the nitrogen doped graphite felts showed outstanding performance. The improved performance is attributed to the high nitrogen content on the graphite felt, which increased the electrocatalytic activity of vanadium redox reactions. Second, polyacrylonitrile (PAN), which contains 26 wt% of nitrogen atoms, was employed to fabricate nitrogen-doped carbon materials on graphite felt surfaces. PAN was coated on graphite felt to improve the performance of VRFB single cell electrodes by utilizing the mechanism of the process of manufacturing carbon fiber from PAN. After optimizing the amount of PAN coated, a single cell with PAN derived nitrogen-doped graphite felt showed higher performance than a single cell with electrodes prepared by conventional treatment methods. In addition to improving the performance of the electrode by chemical methods, we examined the effect of local porosity of the electrodes on the electrolyte flow field in VRFBs at high current densities. The optimization of local porosity of the graphite felt electrode was carried out to improve the performance of VRFBs at high current density region.

Zusammenfassung

Redox-Fluss-Batterien (RFBs) gehören zu den vielversprechendsten Kandidaten für stationäre Energiespeichersysteme im großen Maßstab in Hinblick auf Kosten, Lebensdauer, Designflexibilität und Sicherheit. Vanadium-Redox-Fluss-Batterien (VRFBs) haben gegenüber anderen RFBs den Vorteil, dass sie keine Kreuzkontamination der Elektrolyte aufweisen, da VRFBs das gleiche V-Ion als aktive Spezies sowohl im Anolyten als auch im Katholyten verwenden. Trotz der verschiedenen Vorteile von VRFBs muss die Leistung von VRFBs für die Kommerzialisierung weiter verbessert werden. Die Leistung von VRFBs wird erheblich von der elektrochemischen Aktivität der Elektrode beeinflusst, da die Vanadiumionen-Redoxreaktionen an der Oberfläche der Graphitfilzelektrode während des Lade-Entlade-Prozesses stattfinden. Um die elektrochemische Aktivität von Graphitfilzelektroden zu verbessern, wurden einfache Verfahren zur Herstellung stickstoffdotierter kohlenstoffbeschichteter Graphitfilzelektroden unter Verwendung stickstoffhaltiger Materialien entwickelt. Zunächst wurde 1-Ethyl-3-methylimidazolium dicyanamid (EMIM dca), eine ionische Flüssigkeit mit hohem Stickstoffgehalt, als wirksame Vorstufe für die Stickstoffdotierung auf Graphitfilzoberflächen verwendet. Die Auswirkung von mit Stickstoff dotiertem Graphit, der von EMIM dca abgeleitet ist, auf die Leistung von VRFBs wurde durch verschiedene physikalische und elektrochemische Analysen untersucht. Bei Verwendung in Lade-Entlade-Tests zeigten die Einzelzellen mit den stickstoffdotierten Graphitfilzen eine hervorragende Leistung. Die verbesserte Leistung wird auf den hohen Stickstoffgehalt des Graphitfilzes zurückgeführt, der die elektrokatalytische Aktivität von Vanadium-Redox-Reaktionen erhöhte. Zweitens wurde Polyacrylnitril (PAN), das 26 Gew.-% Stickstoffatome enthält, verwendet, um mit Stickstoff dotierte Kohlenstoffmaterialien auf Graphitfilzoberflächen herzustellen. PAN wurde auf Graphitfilz aufgetragen, um die Leistung von VRFB-Einzelzellenelektroden zu verbessern, indem der Mechanismus des Prozesses zur Herstellung von Kohlenstofffasern aus PAN genutzt wurde. Nach Optimierung der Menge an beschichtetem PAN zeigte eine Einzelzelle mit PAN-abgeleitetem stickstoffdotiertem Graphitfilz eine höhere Leistung als eine Einzelzelle mit über herkömmliche Behandlungsmethoden hergestellten Elektroden. Zusätzlich zur Verbesserung der Leistung der Elektrode durch chemische Methoden untersuchten wir den Effekt der lokalen Porosität der Elektroden auf das Elektrolytflussfeld in VRFBs bei hohen Stromdichten. Die Optimierung der lokalen Porosität der Graphitfilzelektrode wurde durchgeführt, um die Leistung von VRFBs im Bereich hoher Stromdichte zu verbessern.

Table of contents

List of abbreviation

Abbreviation	Description
AEM	Anion exchange membrane
CE	Coulombic efficiency
CEM	Cation exchange membrane
CNT	Carbon nanotube
CV	Cyclic voltammetry
CVD	Chemical vapor deposition
EE	Energy efficiency
EMIM dca	1-ethyl-3-methylimidazolium dicyanamide
ICB	Iron/Chromium (Fe/Cr) Redox Flow Battery
IEM	Ion exchange membrane
MWCNT	Multi-walled carbon nanotube
NGS	N-doped graphene sheet
OCV	Open circuit voltage
ORMOSIL	Organically modified silicate
PAN	Polyacrylonitrile
PEMFC	Polymer electrolyte membrane fuel cell
PSB	Polysulphide/Bromine redox flow battery
RFB	Redox flow battery
SEM	Scanning electron microscopy
SOC	State of charge
SPEEK	Sulfonated polyether ether ketone)
TEOS	Tetraethylorthosilicate
TGA	Thermogravimetric analysis
VE	Voltage efficiency
VRFB	Vanadium redox flow battery
XPS	X-ray Photoelectron Spectroscopy
ZBB	Zinc/Bromine redox flow battery
ZrP	Zirconium phosphates

1. Introduction

There is a growing interest in renewable energy such as solar and wind power due to environmental issues such as global warming caused by the use of fossil fuels and rapid increase in energy consumption [1-3]. However, these energy sources have the disadvantage of being intermittent and often unpredictable. Therefore, there is a growing need for energy storage systems that can store such intermittently produced energy and use it at the required moment. Among various energy storage systems, the vanadium redox flow battery (VRFB), proposed by Kazacos and coworkers in the 1980s, has received much attention due to its many advantages such as long life time, low cost, high safety, fast response, and design flexibility [4-7]. Unlike other types of RFB, VRFB does not need to be concerned about the issue of cross contamination through the membrane because it uses the same material for both anode and cathode electrolytes.

In spite of the various advantages of VRFBs, the performance of VRFBs needs to be further improved for the commercialization. The performance of VRFBs is significantly affected by the electrochemical activity of the electrode because the vanadium ion redox reactions take place at the electrode surface during the charge-discharge process [8-10]. Graphite felt has been widely used as an electrode material for VRFBs because of its large surface area, high electrical conductivity, and stability in highly acidic electrolytes [11]. However, there is still a significant need to resolve the low electrochemical activity, poor wettability and kinetic reversibility of the graphite felt electrode for VRFBs system [12-16]

To improve the electrochemical activity of graphite felt electrodes, many researchers have performed various surface modifications for graphite felts such as thermal treatment [8], acid treatment [13], electrochemical oxidation [14], and the introducing of metal [12,15,17-19] and metal oxides [20-25]. In particular, non-metallic functionalization of the graphite felt via facile methods has been widely utilized due to cost efficiency. Most of these approaches have been used to employ oxygen-containing functional groups such as hydroxyl (-OH) and carboxyl (-COOH) groups on the graphite felt electrodes. These functional groups increase not only the electrochemical activity in the vanadium redox reactions, but also ensure good wettability of the graphite felt electrodes, thus decreasing the overpotential in VRFBs system.

In recent years, Nitrogen-doped carbon electrode materials have been explored and have been reported to exhibit improved electrocatalytic activity in vanadium redox reactions [26,27]. N-doped mesoporous carbon was prepared by a soft-template method and exhibited better electrochemical redox behavior than the widely used graphite felt electrode [28]. Also, PAN-based graphite felt, N-doped by a hydrothermal ammoniated treatment, was reported for VRFB

applications [29]. Wang et al. employed N-doped carbon nanotubes on graphite felt (N-CNT/GF) by a chemical vapor deposition (CVD) process and investigated the electrochemical performance in VRFB [30]. The cell with N-CNT/GF electrode showed higher energy efficiency than with pristine graphite felt electrode. The significantly improved performance was attributed to the unique porous structure and nitrogen doping of N-CNT/GF with increased surface area. Jin et al. developed N-doped graphene sheets (NGS) to increase the electrocatalytic performance [31]. NGS was synthesized by annealing graphite oxide with urea at 700-1050 °C and used as positive electrodes in VRFB. In particular, Kim et al. employed various nitrogen doping precursors such as polypyrrole, dopamine, and melamine to improve the electrochemical catalytic activity in vanadium redox reactions via various treatment techniques [32-34].

On the other hand, the proper distribution of electrolyte in a three-dimensional electrode is especially important at high current density because it is related to the reactant supply and the product removal near the electrode surface. Therefore, other studies examined the distribution of electrolyte in the electrode. Some studies have investigated the compressibility of carbon felt electrode to enhance the internal mass transport of electrolyte [35,36]. They increased the performance of the VRFBs system by finding an optimal relationship between the pressure drop and electrolyte flow rate. Other authors tried to distribute the electrolyte uniformly by introducing various flow-by channels (e.g. parallel, serpentine, and interdigitated ones) in the bipolar plate [37-39], thereby increasing the performance of VRFBs. Moreover, advanced designs of porous electrodes have been shown to improve the overall energy efficiency [40]. Yet, these designs could increase the system efficiency of VRFB system by reducing the pumping power but could not contribute to increase the power density of VRFB cell. In summary, the current power densities of VRFBs are still unsatisfactory despite many research efforts.

In this study, nitrogen-doped graphite felt was developed for VRFB electrode applications. First, we propose a facile preparation method for nitrogen-doped carbon coated graphite felts using a nitrogen-containing ionic liquid, 1-ethyl-3-methlimidazolium dicyanamide (EMIM dca), as a nitrogen doping precursor. EMIM dca not only has a high nitrogen content of 39.5 wt% but also becomes a nitrogen doped carbon material with 18 wt% of nitrogen when it is heated up to 900 °C in an inert gas [41,42]. EMIM dca has shown good electrocatalytic activity as a nitrogen containing carbon coating material in polymer electrolyte membrane fuel cell (PEMFC) applications [43,44]. For these reasons, various amounts of EMIM dca were coated on graphite felt electrodes and then thermally treated. The effect of EMIM dca derived nitrogen-doped graphite felt on the performance of VRFBs was investigated by various physical and

electrochemical analyses. Second, Polyacrylonitrile (PAN) was used to fabricate nitrogen-doped carbon coated graphite felts. PAN is commonly used as a precursor for producing carbon fibers and contains 26 wt% of nitrogen atoms in the molecule. Graphite felt, which is used as an electrode of VRFB, is also mostly manufactured using PAN as a precursor. In the process of manufacturing PAN-based carbon fibers from PAN, it could be confirmed that carbon material containing nitrogen can be produced through oxidation and carbonization [45]. PAN was coated on graphite felt to improve the performance of VRFB single cell electrodes by utilizing the mechanism of the process of manufacturing PAN from carbon fiber. This is expected not only to increase the surface area but also to improve the performance of the electrode by using the nitrogen-doping effect through nitrogen in the molecular structure of the prepared material. As a thermal treatment method for preparing PAN coated graphite felt, the oxidation and carbonization process of the conventional carbon fiber preparation process were used. To fabricate nitrogen doped graphite felt electrodes by coating PAN, two steps of thermal treatment were performed; (1) oxidation at 280°C for 3 hours under ambient atmosphere, (2) carbonization at 900°C for 1 hour under nitrogen atmosphere. Experiments were performed to optimize the amount of PAN coating to improve the performance of VRFBs. In addition, the effect of nitrogen doped graphite felt by coating PAN on the performance of VRFBs was investigated by various physical and electrochemical analyses. In addition, we tried to enhance the power density of VRFBs by optimizing the local porosity of the porous electrode. Three porous electrodes were considered: uniform porosity, low porosity at the electrolyte inlet, and low porosity at the outlet. Since the theoretical operating voltage of VRFBs is lower than that of other commercial rechargeable batteries, we tried to increase the power density of VRFBs by enhancing the energy efficiency at the high current density region through optimization of local porosity of the electrode. First, we analyzed numerical results of electrolyte flow fields for VRFBs with different electrode designs. Next, we examined the variation of charge-discharge curves and energy efficiencies of VRFBs depending on various current densities to understand the relationship between the variation of electrode porosity and current density. In addition, the effect of flow rate on the performance of VRFBs under various electrode designs were investigated in the high current density region. Lastly, we suggested an empirical equation of optimal distribution of local porosity according to the current density.

2. Theoratical background

2.1 Basic principle of redox flow battery

Redox flow batteries (RFBs) are electrochemical systems that can convert and store electrical energy to chemical energy by the oxidation and reduction of active electrolyte materials and releases it when required [46]. Generally, secondary batteries involve the transformation of chemical energy into electrical energy through simultaneous redox reactions taking place at solid electrodes including suitable electrolytes [47,48]. However, RFBs employ two redox couples dissolved in two circulating electrolytes (anolyte and catholyte) which are stored in separate external tanks and pumped into the redox flow cell where the electron transfer reactions take place at inert electrodes [49]. Figure 2.1 shows the basic concept of a redox flow battery.

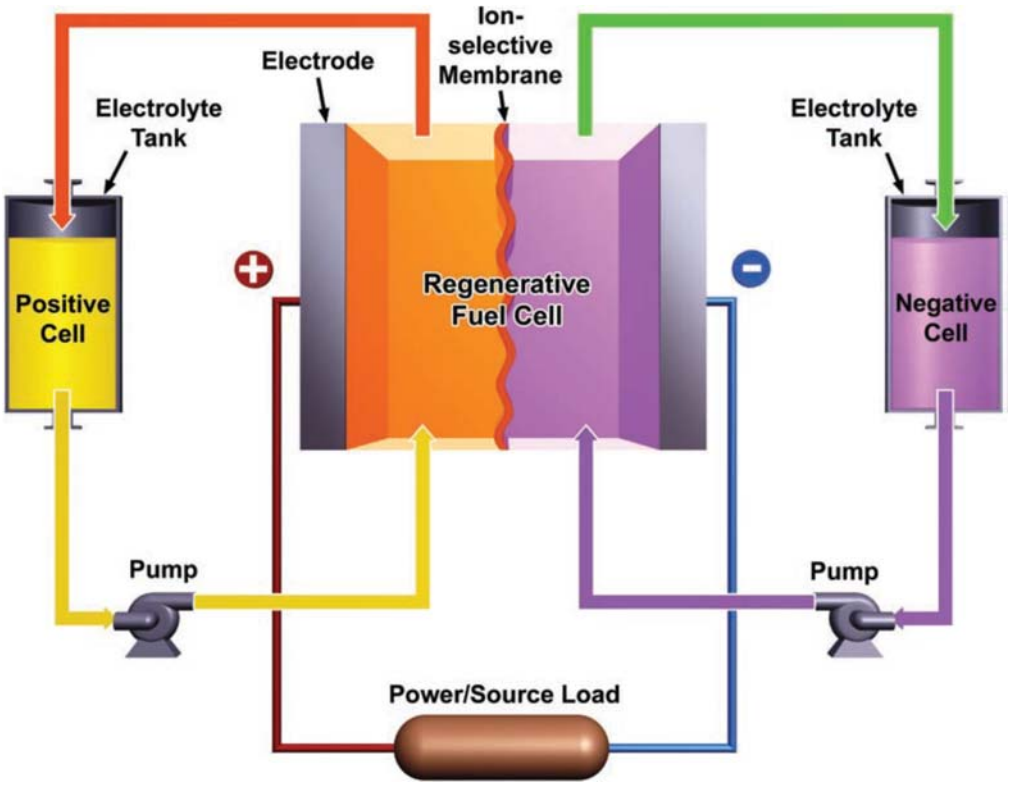

Figure 2.1 Schematic representation of the structure of a redox flow battery [46].

A RFB cell consists of two electrolytes (positive and negative electrolyte) and electrodes separated by the ion exchange membrane; each compartment is connected to an external electrolyte tank and a pump. The energy conversion between electrical energy and chemical energy takes place on the surface of the electrodes while the electrolyte from external electrolyte tanks circulates into the RFB cell. The reduction reaction at one side electrode extracts electrons and ions from one side electrolyte, while the oxidation reaction at the other side electrode recombines them into the other side electrolyte. The advantages of RFBs include durability for large numbers of charge/discharge cycles, high round-trip efficiency, an ability to respond rapidly to changes in load or input, and reasonable capital costs [50]. A key benefit of RFBs is the ability to separate power and storage capacity, which makes it possible to control the power and the electricity storage capacity independently.

The initial redox flow battery (RFB) was introduced by Lawrence Thaller of the National Aeronautics and Space Administration (NASA) in the 1970s [51]. The first RFB employed a Fe^{2+}/Fe^{3+} halide electrolyte solution in the positive half cell and a Cr^{2+}/Cr^{3+} halide electrolyte solution in the negative half cell. However, the cycling life was severely limited by the cross-contamination of the two half-cell electrolytes during charge/discharge processes. After this attempt, RFBs using various types of redox active materials have been developed as summarized in Table 2.1 [49].

Table 2.1 Various types of redox flow batteries [49].

Type	Positive half cell reaction	Negative half cell reaction	Electrolyte	Open cell Voltage / V
Fe/Cr [52]	$Fe^{2+} + e^- \rightleftharpoons Fe^{3+}$	$Cr^{2+} \rightleftharpoons Cr^{3+} + e^-$	1M $FeCl_2$/1M $CrCl_3$ in 2–3M HCl	1.18
All-Vanadium [53-55]	$VO_2^+ + e^- \rightleftharpoons VO^{2+}$	$V^{2+} \rightleftharpoons V^{3+} + e^-$	1.7–2 M V in 4–5 H_2SO_4	1.26
Zinc-Cerium [56]	$Zn \rightleftharpoons Zn^{2+} + 2e^-$	$2Ce^{4+} + 2e^- \rightleftharpoons 2Ce^{3+}$	1.5M $Zn(CH_3SO_3)_2$ / 0.2M $Ce(CH_3SO_3)_3$ in 0.5M CH_3SO_3H	2.43
Zinc-Bromine [57,58]	$Br_2 + 2e^- \rightleftharpoons 2Br^-$	$Zn \rightleftharpoons Zn^{2+} + 2e^-$	$ZnBr_2$ in excess of Br_2 ($ZnBr_2$ oil)	1.85
Fe/V [59]	$Fe^{2+} \rightleftharpoons Fe^{3+} + e^-$	$V^{2+} \rightleftharpoons V^{3+} + e^-$	1M $FeCl_2$ in 2M HCl / 2M V in 4M H_2SO_4	1.02
Br/V [60]	$Br_2 + 2e^- \rightleftharpoons 2Br^-$	$V^{2+} \rightleftharpoons V^{3+} + e^-$	3.5M V in 7M HBr + 2M HCl / 2M V in 4M H_2SO_4	1.30
Polysulfide/bromine (PSB) [7,61,62]	$Br_2 + 2e^- \rightleftharpoons 2Br^-$	$S_4^{2-} + 2e- \rightleftharpoons 2S_2^{2-}$	5M NaBr / 1.3M Na_2S_5 and 1M NaOH	1.36
Mn/V [63]	$Mn^{3+} + e^- \rightleftharpoons Mn^{2+}$	$V^{2+} \rightleftharpoons V^{3+} + e^-$	0.3M V^{3+} in 5M H_2SO_4 / 0.3M Mn^{2+} in 5M H_2SO_4	1.77
Zn/Ce [64]	CeIII - $e^- \rightleftharpoons$ CeIV	ZnII $+2e^- \rightleftharpoons$ Zn	1.0M MSA 0.152 CeIII, 4M MSA 0.152 CeIII	2.2
Pb/Ce [65]	$2CeIII \rightleftharpoons 2CeIV + 2e^-$	PbII $+ 2e^- \rightleftharpoons$ Pb	1.5M PbII methanesulfonate in 1.0M MSA(Negative); 1.0M CeIII methanesulfonate in 1.0M MSA (Positive)	1.7
Soluble-Pb [66,67]	$Pb^{2+} + 2H_2O + 2e^- \rightarrow PbO_2 + 4H^+$ (Charge)	$Pb^{2+} + 2e^- \rightarrow$ Pb0 (Charge)	Lead(II) in methanesulfonic acid	1.78
Fe/Fe [68]	$2Fe^{3+} + 2e^- \rightleftharpoons 2Fe^{2+}$	$Fe^{2+} + 2e^- \rightleftharpoons$ Fe0	$FeCl_2$ (Negative) $FeCl_2$ & $FeCl_3$ (Positive)	1.21
Zn/I [69]	$I_3^- + 2e^- \rightleftharpoons 3I^-$	$Zn \rightleftharpoons Zn^{2+} + 2e^-$	ZnI_2 in aqueous	1.29

2.2 Type of redox flow battery

2.2.1 All-vanadium redox flow battery (VRFB)

All vanadium redox flow battery (VRFB) is the most popular and promising technology of RFB. VRFB was first proposed by Skyllas-Kazacos and co-workers at the University of New South Wales (UNSW) in 1980s [53-55]. VRFB employs four different oxidation states of vanadium ions to form two redox couples with only one active component in both the anolyte and the catholyte. Because VRFB uses vanadium ions in the both side electrolyte, the inherent cross-contamination issue by diffusion of different redox ions through the membrane can be overcome, which allows the cycling life related to the capacity retention to be extended. The VRFB employs the V^{2+}/V^{3+} redox couple at the negative electrode and the VO^{2+}/VO_2^{+} redox couple ate the positive electrode with the following charge-discharge reactions.

At the positive electrode

$$VO^{2+} + H_2O \rightleftharpoons VO_2^{+} + 2H^{+} + e^{-} \qquad E° = 1.00\ V\ (vs\ SHE) \qquad (2-1)$$

At the negative electrode

$$V^{3+} + e^{-} \rightleftharpoons V^{2+} \qquad E° = -0.26\ V\ (vs\ SHE) \qquad (2-2)$$

Overall cell reaction

$$VO^{2+} + V^{3+} + H_2O \rightleftharpoons VO_2^{+} + V^{2+} + 2H^{+} \qquad E° = 1.26\ V \qquad (2-3)$$

The electrochemical overall cell reaction gives an open cell voltage of 1.26 V at 25 °C. As described in Figure 2.2, the electrolytes (anolyte and catholyte), which include the active vanadium redox couples, are circulated through the anode and cathode half cells that are separated by an ion exchange membrane. During the discharging process, VO_2^{+} is reduced to VO^{2+} at the positive electrode, while V^{2+} is oxidized to V^{3+} at the negative electrode. The hydrogen ions move through the membrane to maintain the electrical balance of the electrolytes. As the redox reactions proceed, color changes can be observed in both electrolytes, i.e., yellow/blue on the positive half cell and purple/green on the negative half cell.

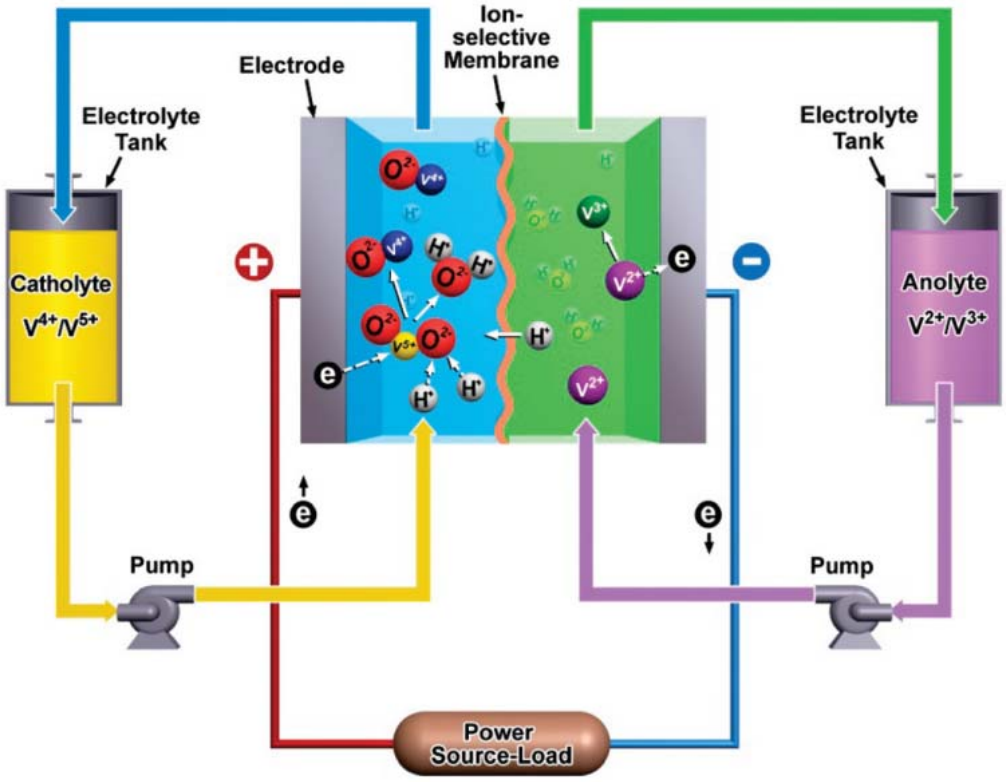

Figure 2.2 Schematic of an all vanadium redox flow battery [70]

Since the VRFB was first developed, continuous research has been conducted around the world. While meaningful progress was made in advancing RFB such as the demonstration of multiple MWh VRFB systems [71,72], the current technology is still not ready for the commercial market because of significant limitations caused by vanadium solubility and the stability of the electrolyte solutions. The thermal precipitation of V_2O_5 at temperature of 40°C and above [71,73,74] and the low solubility (< 1.7 M) of vanadium at the real operating temperature range restricts the energy capacity to < 25 Wh L^{-1} and the operating temperature range between 10 and 40°C [73-76]. Therefore, a heat management system is necessary for a practical VRFB system, which causes energy loss and overall operating costs [72]. Because overall improvement of the VRFB system with respect to energy capacity and stability[W1] has been still limited, more research is necessary to connect VRFB system with renewable energy sources.

2.2.2 Iron/chromium (Fe/Cr) redox flow battery

In the early 1970, Thaller at NASA invented the iron/chromium (Fe/Cr) redox flow battery (ICB) that employs a ferric/ferrous redox couple (Fe^{2+}/Fe^{3+}) as catholyte and a chromic/chromous redox couple (Cr^{2+}/Cr^{3+}) as anolyte in an acid medium [51]. After NASA's initial research, Mitsui Engineering and Shipbuilding, Kanasi Electric Power Inc. and Sumitomo Electric Industries Ltd produced a 10 − 60 kW test system in Japan in 1984 − 1989, which is based on the following redox reactions [7,71].

At the positive electrode

$$Fe^{2+} - e^{-} \rightleftharpoons Fe^{3+} \qquad E° = 0.77\ V\ (vs\ SHE) \qquad (2-4)$$

At the negative electrode

$$Cr^{3+} + e^{-} \rightleftharpoons Cr^{2+} \qquad E° = -0.41\ V\ (vs\ SHE) \qquad (2-5)$$

Overall cell reaction

$$Fe^{2+} + Cr^{3+} \rightleftharpoons Fe^{3+} + Cr^{2+} \qquad E° = 1.18\ V \qquad (2-6)$$

The cell reaction offers a standard voltage of 1.18 V. The ICB employs a cation or anion exchange membrane and carbon fiber, carbon felt or graphite as electrode materials. While the redox reaction of Fe^{2+}/Fe^{3+} shows a very high reversibility and fast kinetics on the electrodes, the redox reaction of Cr^{2+}/Cr^{3+} exhibits relatively slow kinetics on the electrodes. To improve its electrode kinetics, expensive noble metal catalysts are used for Cr^{2+}/Cr^{3+} redox reaction, which leads to an increase in ICB cost [77,78]. Additionally, the low redox potential of Cr^{2+}/Cr^{3+} (-0.41 V) causes hydrogen evolution, which restricts the fuel use (~60%) and reduces the coulombic efficiency. In early ICB system, the problem of cross mixing of iron and chromium active species across the membrane was solved by using mixed electrolytes at both cathode and anode side [79]. However, ICB system was not commercially developed due to problems of low energy density for the mixed electrolyte cell, membrane fouling and the slow chromium redox reaction.

2.2.3 Zinc/bromine (Zn/Br) redox flow battery

The zinc/bromine redox flow battery (ZBB) system employs bromide ion/bromine conversion at the positive electrode and the zinc metal dissolution/plating redox reaction at the negative electrode. The charge and discharge of ZBB cells proceed via the following electrode reactions.

At the positive electrode

$$2Br^- - 2e^- \rightleftharpoons Br_2 \qquad E° = 1.087 \text{ V (vs SHE)} \qquad (2-7)$$

At the negative electrode

$$Zn^{2+} + 2e^- \rightleftharpoons Zn \qquad E° = 0.763 \text{ V (vs SHE)} \qquad (2-8)$$

Overall cell reaction

$$2Br^- + Zn^{2+} \rightleftharpoons Br_2 + Zn \qquad E° = 1.85 \text{ V} \qquad (2-9)$$

The ZBB cell reaction offers a standard voltage of 1.85 V. At the positive electrode, bromide ions are converted to bromine during charging or vice versa during discharging. Complexing agents are employed to reduce the bromine evolution which is a serious health hazard. At the negative electrode, zinc is reversibly deposited from ions. Unlike the traditional redox flow systems, the ZBB system has less design flexibility with regard to power and storage capacity because its total available energy capacity is restricted by the electrode area for plating zinc. The ZBB system has a high energy density due to a high cell voltage, good reversibility, and expectation of low material costs. However, the demonstration of ZBB has been limited due to material corrosion, dendrite formation, electrical shorting, its low energy efficiencies, high self-discharge rate, and short cycling life [50,80-82].

2.2.4 Polysulphide/bromine redox flow battery

In the polysulphide/bromine redox flow battery (PSB) system, the positive electrolyte is sodium bromide, and the negative electrolyte is sodium polysulfide. A standard cell voltage of 1.36 V is given by the following electrochemical reactions.

At the positive electrode

$3Br^- - 2e^- \rightleftharpoons Br_3^-$ $E° = 1.09$ V (vs SHE) (2−10)

At the negative electrode

$S_4^{2-} + 2e^- \rightleftharpoons 2S_2^{2-}$ $E° = -0.265$ V (vs SHE) (2−11)

Overall cell reaction

$3Br^- + S_4^{2-} \rightleftharpoons Br_3^- + 2S_2^{2-}$ $E° = 1.36$ V (2−12)

During the charge process, the bromide ions are oxidized to bromine and complexed as tribromide ions in the positive side, and the soluble polysulfide anion is reduced to sulfide ion in the negative side. During the discharge process, the sulfide ion is oxidized, and the tribromide ion is reduced. In this system, because all of the electroactive species are anions, a cation-exchange membrane is used to prevent mixing of the anolyte and catholyte. The PSB system was found to be attractive for RFB applications due to abundance of the electrolyte, reasonable cost of materials and high solubility in aqueous media. However, this system is suffered from the cross-contamination problems of both electrolyte solutions, the possibility of deposition of Sulphur species on the membrane, and the formation of $H_2S(g)$ and $Br_2(g)$ [7,71,83].

2.3 Component of redox flow battery

2.3.1 Electrode

The electrodes in a RFB are required to have a high surface area, suitable porosity, low electronic resistance, and high electrochemical activity toward the redox reactions to optimize the performance of the RFB. Due to the commonly corrosive environment in a RFB, there are limited choices of materials to fabricate electrodes. The early RFB, the Fe/Cr redox flow battery (ICB) which was invented and developed at NASA, employed carbon fiber, carbon felt, or graphite as electrode materials. Because of inadequate electrochemical activity, however, the electrodes in an ICB require a catalyst coating for facile redox reactions [7,71]. Although the carbon based electrodes often show inadequate electrochemical activity and kinetic reversibility toward the electrochemical reactions between the redox species, graphite- or carbon-based materials have been used as electrodes due to their inert and high-surface-area properties in other RFBs such as all vanadium redox flow battery (VRFB), polysulfide/bromine flow battery (PSB), zinc/bromine flow battery (ZBB) and vanadium/cerium flow battery [4,7,8,11,12,13,16,28,71,84-95]. Among the RFBs, research on electrodes for the VRFB has been the most performed by many research groups. The electrode materials used in a VRFB must satisfy the following properties: (1) the electrode must have high electrical conductivity and active surface area; (2) the electrode must be chemically stable in acidic and corrosive environments; (3) the electrode must be electrochemically stable in the VRFB operating potential window; (4) the electrode must have optimum porosity and good wettability for electrolytes. This section provides a short introduction and overview of the technical trends in VRFB electrodes.

Since the VRFB was first proposed by Skyllas-Kazacos [4,6], several research groups have reported various outcomes about the VRFB electrodes to increase the electrochemical properties. In early research, various approaches including heat treatment, chemical treatment, electrochemical oxidation, and metal doping on carbon materials were employed to improve the electrochemical properties.

Sun and Skyllas-Kazacos adopted heat treatment of graphite felt in 1992 to improve its electrochemical activity [8]. As a result of heating at 400°C for 30 h, the energy efficiency of the VRFB could reach about 86% at a current density of 40 mA cm^{-2}. The improved activity was attributed to the enhanced surface hydrophilicity and the formation of the oxygen functional groups of C−O−H and C=O groups on the graphite felt surface, because the C−O groups on the electrode surface played a role as active sites and catalyzed the electrochemical

reactions of the vanadium species. Figure 2.3 illustrates the reaction mechanisms which were proposed by the authors [16]. Another method to modify the surface of graphite felt electrode is chemical treatment. Sun and Skyllas-Kazacos employed chemical treatments with nitric acid or sulfuric acid solution to increase electrochemical properties of the graphite felt electrode [13]. A significant enhancement in VRFB performance was achieved after the graphite felt electrode was treated with concentrated sulfuric acid solution. The improved activity was also attributed to the increased oxygen functional groups of COOH and C=O groups which were formed during chemical treatment. After chemical treatment with concentrated sulfuric acid solution for 5h, the energy efficiency of the VRFB could reach about 88% at a current density of 25 mA cm^{-2}.

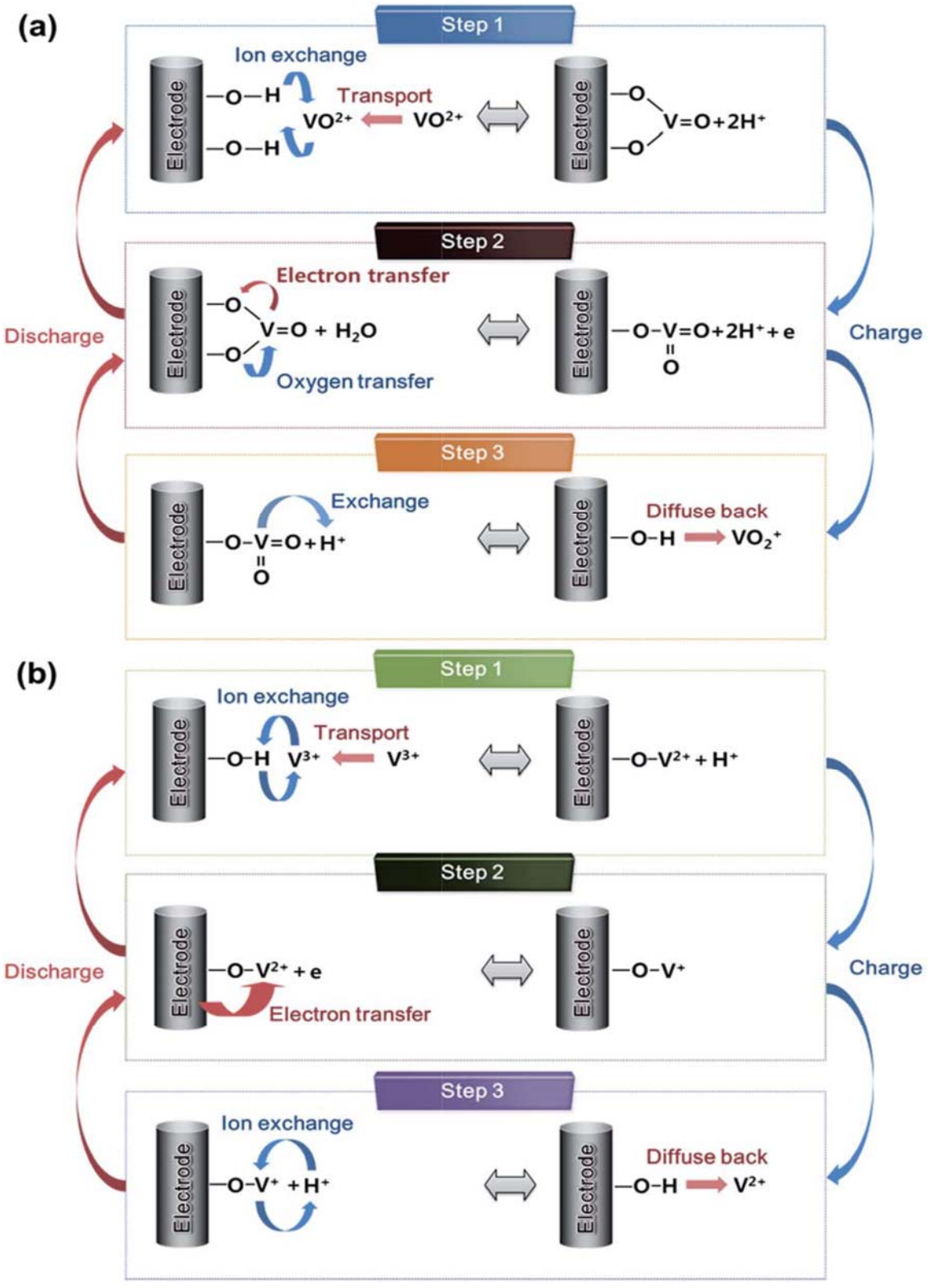

Figure 2.3 Schematic illustration of the redox reaction mechanism proposed by Skyllas-Kazacos et al. [16] and reproduced by Kim et al. [16] for (a) VO^{2+}/VO_2^{+} redox couples in the catholyte, (b) V^{2+}/V^{3+} redox couples in the anolyte on the surface of the carbon felt electrode in VRFB.

Another method to increase the electrochemical activity of graphite felt electrode for the VRFB is a combination of heating and chemical treatment [70]. The graphite felt was firstly treated in 98 wt% in sulfuric acid solution for 5h and then kept at 450 ℃ for 2 h. The synergetic effect of heat treatment and chemical treatment increased the concentration of the COOH oxygen functional groups on the graphite electrode surface and enlarged the specific surface area of the graphite felt electrode from 0.31m^2/g to 0.45 m^2/g. As a result, improved reactivity of the graphite felt electrode was attributed to the increased number of COOH oxygen functional groups that behave as active sites, catalyzing the reactions of redox species and facilitating the transfer of electron and oxygen effectively. Li et al. employed the chemical treatment on the graphite felt electrode using mixed acids (nitric acid / phosphoric acid = 3:1) [96]. The improved electrochemical properties of the treated graphite felt electrode was ascribed to the increase of the interaction between vanadium ions with OH groups that were formed on the surface of graphite felt electrode by mixed acid treatment. After the mixed acid treatment for 8h at 80℃, the energy efficiency of the VRFB could reach about 78% at a current density of 20 mA cm^{-2}.

Electrochemical oxidation is another method to modify the graphite felts to improve their electrochemical activity toward reactions between redox species. Li et al. studied characteristics of graphite felt electrodes that were treated by electrochemical oxidation for the VRFB [97]. After electrochemical oxidation treatment, the specific surface area of the graphite felt electrode increased from 0.33 m^2/g to 0.49 m^2/g. The improvement of electrochemical activity for the electrode is ascribed to the increase of the number of COOH group and the special surface of graphite felt electrode. Tan et al. investigated the activation mechanism of electrochemical treated graphite felt by electrochemical impedance spectrum [98]. The changes in the value of electrochemical impedance can be explained by the increase of COOH group on the graphite felt surfaces after electrochemical oxidation treatment. Zhang et al. studied the electrochemical activation of graphite felt at a range of oxidation degrees [14]. The graphite felt electrode was modified through electrochemical oxidation at a current density of 100 mA cm^{-2} in 1 M sulfuric acid solution. The increase of oxidized graphite felt activity could be ascribed to the formation of the C−OH and COOH oxygen functional groups on the oxidized graphite felt surface, which provided active sites for VO^{2+}/VO_2^+ redox reactions. As a result, the voltage efficiency and energy efficiency of VRFBs with oxidized graphite felt electrodes were 4-5% higher than of VRFBs with pristine graphite felt electrodes.

The deposition of metals on the surface of graphite felt was used to improve the electrochemical activity of redox species in VRFB. Sun et al. proposed metal incorporation on

graphite fiber electrodes by impregnation or ion-exchange with solutions containing Pt^{4+}, Pd^{2+}, Au^{4+}, In^{3+}, Mn^{2+}, Te^{4+}, or Ir^{3+}[12]. Among these, the electrode modified by Ir^{3+} showed the best electrochemical behavior for the vanadium redox species. Wang et al. reported Ir-modified carbon felt as the positive electrode of VRFB [17]. The carbon felt was modified by pyrolysis of Ir reduced from H_2IrCl_6 to improve the electrochemical reactivity. Ir-modification of carbon felt improved the electro-conductivity of electrode materials and the Ir-material coated on the carbon felt electrode surface decreased the cell internal resistance. Jeong et al. proposed platinum-based electrocatalyst synthesized by polyol process to increase the VRFB performance [99]. To increase the slow reaction rate of the VO^{2+}/VO_2^+ redox couple, Pt/C catalyst was synthesized and coated on the surface of graphite felt using air spray for VRFB cell test. A significant improvement in catalytic activity and reaction reversibility was ascribed to positively charged Pts that behave as active sites for VO^{2+}/VO_2^+ redox reaction.

Apart from results by using noble metals, Gonzalez et al. proposed graphite felt modified with nanodispersed bismuth as electrode in the positive half-cell of VRFB [100]. The graphite felt was modified by immersion in a Bi_2O_3 solution in 0.01M HCl under vacuum for 3h and then treated in air at 450°C for 3h. After the treatment, Bi-modified graphite felt contains 1.09 at% bismuth on the surface of the fibers and presents a high concentration of defects or holes. As a result, Bi-modified graphite felt showed excellent electrochemical performance and the improved results were attributed to the dispersion of bismuth nanoparticles on the carbon surface that served as stable active sites to facilitate the reactions. Furthermore, they reported an additional achievement by incorporating Bi nanoparticles into the graphite felt electrode in the negative half-cell of VRFB [101]. Unlike previous study, Bismuth was electrodeposited onto thermal oxidized graphite, which was treated in air at 450℃ for 3h in advance, by immersing the graphite felt in 0.005M $Bi(NO_3)_3$/ 1.0M HNO_3 solution and applying -0.2V for 1min. And then the graphite felt was treated in air at 450°C for 30min to stabilize the electrodeposited bismuth. The reversibility of the V^{3+}/V^{2+} redox reactions and the long-term cycling performance of the electrode were improved by preventing H_2 evolution through incorporating Bi nanoparticles into the graphite felt. In this process, Bi nanoparticles on the graphite felt inhibit H_2 evolution by forming BiH_x which is formed as an intermediate in the H_2 evolution, but reduces V^{3+} to V^{2+}.

For the practical use of VRFB, many researchers have investigated metal oxide catalysts that have relatively low price and comparable catalytic properties against compared with noble metals [16]. Kim et al. investigated catalytic effects of Mn_3O_4 nanoparticles on the carbon felt electrode for VRFBs [21]. Mn_3O_4 nanoparticles were incorporated onto the surface of carbon

felts using a hydrothermal treatment. A carbon felt was soaked in 1M manganese acetate solution and heated to 200°C for 12h for hydrothermal reaction. And then Mn_3O_4-modified carbon felt was treated at 500°C for 5h under an Ar atmosphere for Mn_3O_4 attachment on the carbon felt. After the modification, the electrochemical properties of Mn_3O_4-modified carbon felt were increased because of well-dispersed Mn_3O_4 nanoparticles, which serve as an electrocatalyst for the VO^{2+}/VO_2^+ redox reaction. As a result, the VRFB using Mn_3O_4-modified carbon felts exhibited improved coulomb, voltage, and energy efficiencies compared to the cell using pristine carbon felts. Li et al. proposed Nb_2O_5 nanorod as powerful catalysts toward both VO^{2+}/VO_2^+ and V^{2+}/V^{3+} redox couples to increase the electrochemical performance of the graphite felt electrode in VRFB [22]. They investigated and optimized the amount, size, and distribution of Nb_2O_5 nanorod catalysts on graphite felt surfaces and added salt containing W in the precursor solutions during synthesis for more uniform distribution and minimum agglomeration. VRFB using Nb_2O_5 nanorod catalyst on graphite felt electrode exhibited about 10.7% higher energy efficiency at 150 mA cm^{-2} as compared with the cell without catalysts on graphite felt electrode. Tseng et al. investigated the effects of adding titanium dioxide (TiO_2) particles to the negative electrode in VRFB [102]. Hydrophilic TiO_2/C composite electrodes were prepared by a sol–gel method. The electrode specific capacitance and charge–discharge efficiency of VRFB were improved by adding an adequate amount of TiO_2 particles to the carbon electrode. Wu et al. employed lead dioxide (PbO_2) catalyst on graphite felt to improve electrochemical properties [24]. Lead dioxide (PbO_2) was prepared through pulse electrodeposition method and PbO_2 showed excellent electro-catalytic activity and reactive velocity to vanadium redox couples. As a result, the efficiencies of VRFB using PbO_2-modified graphite felt electrodes were higher than the cell using bare graphite felt electrodes. Zhou et al. proposed CeO_2 decorated graphite felt as a high-performance electrode for VRFB [23]. CeO_2 nanoparticle decorated graphite felts were prepared by a facile precipitation method and showed higher activity and reversibility towards the VO^{2+}/VO_2^+ redox reaction than the pristine graphite felts. The cell using CeO_2 decorated graphite felt which was optimized at the CeO_2 content of 0.2wt% exhibited the highest energy efficiency.

Carbon nanotubes (CNTs) have been used as fuel cell catalyst support because of their high specific surface area, chemical stability, and excellent electrical conductivity [103-106]. Zhu et al. firstly proposed graphite-carbon nanotube composite electrodes for VRFB [107]. Yan et al. also employed CNTs as an electrode reaction catalyst for VRFB [108]. Multi-walled carbon nanotubes (MWCNTs) and hydroxyl and carboxyl functional MWCNTs were coated on the surface of the carbon electrode. Modified carbon electrode showed increased electrochemical activities, and the electrocatalytic kinetics of the redox reactions are in the order of carboxyl

MWCNTs > hydroxyl MWCNTs > pristine MWCNTs. The VRFB using the carboxyl MWCNTs modified carbon electrode exhibited excellent storage efficiency, suggesting the oxygen functional groups could significantly facilitate the VO^{2+}/VO_2^+ redox reaction. In addition to this research, this group has reported various results about the electocatalytic effect of CNTs for VRFB [109-111].

Nitrogen-doped carbon electrode materials have been explored and have been reported to exhibit improved electrocatalytic activity compared with pristine carbon electrode materials [112-118]. For use in VRFB, N-doped mesoporous carbon was prepared by soft-template method and exhibited increased electrochemical redox behavior for the couple than the widely used graphite felt electrode [28]. Also, N-doped PAN-based graphite felt by a hydrothermal ammoniated treatment was reported for VRFB applications [29]. Wang et al. employed N-doped carbon nanotubes on graphite felt (N-CNT/GF) by a chemical vapor deposition (CVD) process and investigated the electrochemical performance in VRFB [30]. The cell using N-CNT/GF electrode showed increased energy efficiency compared with pristine graphite felt electrode. The significantly improved performance was attributed to the unique porous structure and nitrogen doping of N-CNT/GF with increased surface area. Jin et al. developed N-doped graphene sheet (NGS) to increase electrocatalytic performance [31]. NGS was synthesized by annealing graphite oxide with urea at 700-1050°C and used as positive electrodes in VRFB. Figure 2.4 shows the VO^{2+}/VO_2^+ redox reaction mechanism on nitrogen-doped carbon materials. In this study, the authors confirmed that the increased catalytic activity was ascribed not to the nitrogen doping level but to the nitrogen type in the graphene sheets. There are four types of nitrogen species doped into the graphene lattice including pyridinic-N, pyrrolic-N, quaternary nitrogen, and oxidic-N. Among them, the quaternary nitrogen was verified as catalytic active center for the VO^{2+}/VO_2^+ redox couple reaction.

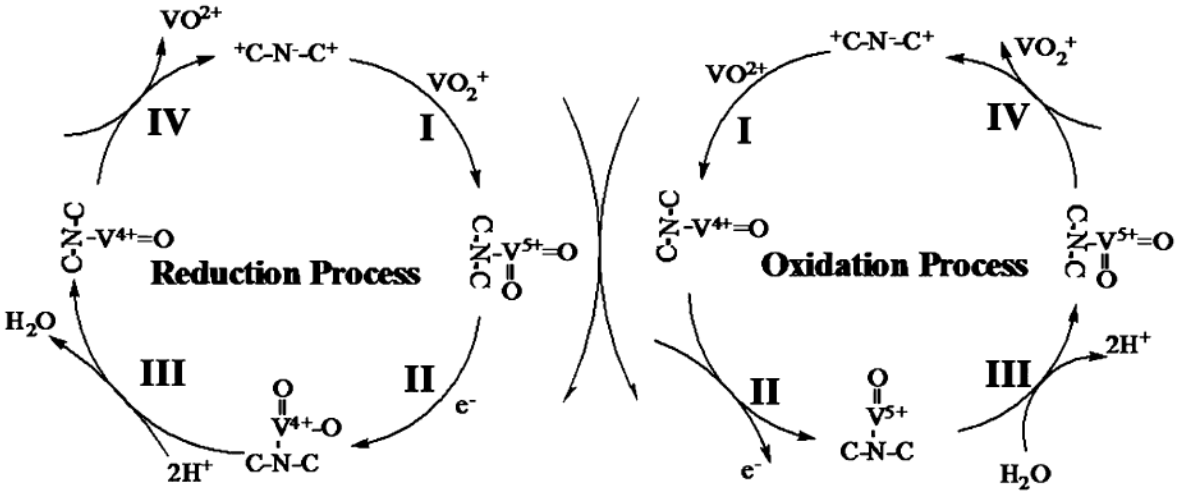

Figure 2.4 VO^{2+}/VO_2^+ redox reaction mechanism on nitrogen-doped carbon materials [31].

Bio-derived carbon materials were also investigated as electrodes for the VRFB. Park et al. employed carbon-based catalysts by corn protein self-assembly [119]. Corresponding carbon black nanoparticles were coated with nitrogen-doped graphite layers with oxygen-rich functionalities. This treatment increased the catalytic activity towards both V^{2+}/V^{3+} and VO^{2+}/VO_2^+ redox couples. As a result, a significant improvement in the energy efficiency of VRFB was observed. The improved performances are attributed to the abundant oxygen active sites and nitrogen defects in the corn protein-derived nitrogen-doped carbon black by enhancing the electron transfer rate and vanadium ion transfer kinetics. Ulaganathan et al. investigated the multi-couple reaction in VRFB by using bio-mass (coconut shell) derived mesoporous carbon as electrode [120]. The modified electrode showed enhanced electrochemical performance. It is believed that the increased cell performance was ascribed to the improved electro-catalytic activity of coconut shell-derived high surface area mesoporous carbon.

Recently, many researchers are continuing to report their results about electrode for VRFB with various approaches. Park et al. proposed new fabrication method for highly porous graphite felt electrode with high-performance [121]. They conducted the etching treatment on graphite felt by repetition of a NiO/Ni redox reaction cycle to produce a high surface area. The etched graphite felt has stepped edges incorporating oxygen defects which show increased catalytic effect and wettability, and it led to enhanced electrochemical performance. Gonzalez et al. employed graphene-modified graphite felt as electrode for VRFB by electrophoretic deposition technology form graphene oxide suspension [122]. The graphene modified graphite felt enhanced the electrochemical activity and kinetic reversibility towards the VO^{2+}/VO_2^+ redox reaction. It is believed that 3D-architecture consisting of fibers interconnected by graphene

sheets is beneficial to the vanadium redox reaction. Blasi et al. employed an electrospinning method to fabricate carbon nanofibers with oxide materials [123,124]. Electrospun oxide-carbon nanofiber samples showed improved electrochemical properties for VRFB. Apart from these studies that were focused on electrode materials, Bhattarai et al. investigated different designs of flow channels in porous electrodes of VRFB [40]. Electrodes with flow channels improved the overall energy efficiency by reducing pumping power and enhancing flow distribution of electrolyte.

2.3.2 Membrane

In redox flow batteries, membranes separate the cathode and anode compartments, preventing mixing of anolyte and catholyte. They are permeable for charge carriers, such as protons or sulfates, to make the electrochemical system maintain its electrical neutrality. On the other hand, membranes should be impermeable for the active species and chemically stable against oxidation and acid-catalyzed reactions. While the membrane must have excellent chemical stability in VRFB systems due to the severe acidic environment and strong oxidative VO_2^+ ions, hydrocarbon-based membranes which have relatively week chemical stability can be used in ICB systems because of less corrosive active materials. To decrease the resistance and thus power losses, the membrane needs to have a high ionic conductivity. In general, the membrane is required to be hydrophilic at the interface between the electrolyte and membrane surface to facilitate the ion transfer. Additionally, the fast ion transfer needs to be highly selective; the transfer of active species should be minimized to decrease the energy and capacity loss. Water transport across the membrane should also be restricted to balance catholyte and anolyte. A membrane with low cost, high stability, and excellent conductivity is significantly important for the commercialization of RFBs [70,125].

Generally, membranes can be classified as ion exchange membranes (IEMs) and microporous membranes (separators). Ion exchange membranes can be further separated into two types: cation exchange membranes (CEMs) and anion exchange membranes (AEMs). Both cation and anion exchange membranes have been investigated for VRFB applications. Nafion, a perfluorinated polymer membrane, has been studied the most in VRFB systems because it can withstand the severe acidic environment and strong oxidative VO_2^+ ions in the positive half-cell electrolyte. The Nafion membrane also is highly conductive to protons [126]. Although the Nafion membrane has excellent chemical stability and proton conductivity, high vanadium ion permeability which leads to loss of cell capacity and reduction of coulombic efficiency remains a concern for VRFB systems.

Therefore many chemical and physical modifications of Nafion membranes were performed to enhance ion selectivity. Qiu's group prepared Nafion/SiO_2 hybrid membranes by using the sol-gel method to decrease vanadium ion permeability [92]. The incorporation of SiO_2 into Nafion can clearly decrease the crossover of vanadium because the polar clusters of the pristine Nafion were filled with SiO_2 nanoparticles during the in-situ sol-gel reaction of tetraethylorthosilicate (TEOS). The VRFB single cell with Nafion/SiO_2 hybrid membrane shows a higher coulombic and energy efficiencies and a lower self-discharge rate than that with a pristine Nafion system. On the other hand, other types of inorganic hybrid Nafion membranes were developed and employed in VRFB systems. These kinds of inorganic hybrid membranes also focused on enhancing coulombic efficiency of the VRFB by increasing the ion selectivity of Nafion. These membranes usually include organically modified silicate (ORMOSIL), organic silica modified TiO_2, and zirconium phosphates (ZrP) [127-129].

Hydrocarbon-based membranes have received broad attention in VRFBs due to their low cost, high mechanical stability and high ion selectivity. In recent years, studies related to hydrocarbon-based membranes have been focusing on sulfonated aromatic polymers because their rigid main chain and less connected ionic cluster can prevent vanadium ion crossover [130]. Chen et al. prepared sulfonated poly(arylene thioether), sulfonated poly(fluorenyl ether ketone), sulfonated poly(fluorenyl ether ketone) with embedded SiO_2, sulfonated poly(arylene ether sulfone), and sulfonated poly(fluorenyl ether thioether ketone) membranes for VRFBs [131-135]. Sulfonated poly(tetramethydiphenylether ether ketone) (SPEEK) membranes were also prepared and employed in VRFBs by Zhang's group [136]. These membrane showed much lower vanadium ion permeability and higher coulombic efficiency than the Nafion membrane. In addition, (hydrocarbon-based) anion exchange membranes raised attention because of their repellent effect to positive vanadium ions, which leads to minimize vanadium ion transfer cross membranes. Various anion exchange membranes were also prepared and employed in VRFBs by several research groups [137-142].

Another type of membrane for RFB applications is the microporous membrane (separator). These membranes have received continuous interest due to their obviously lower cost compared to the Nafion membrane. Microporous membranes have been widely used in other type of batteries such as Li-ion batteris and lead-acid batteries and water treatment systems. Unlike the Nafion membrane and hydrocarbon-based membranes, microporous separator foils generally have much larger pore sizes and thicknesses. Compared with the Nafion membrane, microporous separators show higher ionic transport, but the ion selectivity is relatively lower. Although the difference in transport rate of the different chemical species in the electrolyte

allows the electrochemical system of VRFBs to activate, the degradation of VRFB performance due to high vanadium ion permeability is inevitable. To minimize the vanadium ion crossover, the Daramic[W2] membranes were optimized with various modifications and used for VRFBs [143-148]. Despite the low ion selectivity problem, which has not yet been solved, the significantly lower cost makes the separator foils attractive for the RFBs.

2.3.3 Electrolyte

In RFB systems, the electrolyte is the most important component, which can directly affect the capacity and power of RFBs. Because the RFB utilizes two soluble chemicals as active materials, the concentration of the electrolyte can determine the power density of the RFB. Thus, the higher the solubility of the electrolyte, the more energy density it can have. The temperature stability of the electrolyte is also significant, because the operation temperature window of the RFB was determined by the temperature stability of the electrolyte. It is worth noting that the electrolyte must have the electrochemical stability over the entire charge/discharge range. When the state of charge (SOC) is 0% or 100%, the electrolyte could be in the most detrimental condition during cell operation. The operating voltage windows is generally limited by the water electrolysis potential of aqueous RFBs. Additionally, the redox reaction potential of the RFB should be within the stable electrolyte potential window to prevent electrolyte decomposition. The ionic conductivity of the electrolyte is also important to provide proper rate capability of the RFB. Viscosity needs to be controlled to avoid high pressure drop due to high viscosity. The characteristics of the electrolyte, such as the acidity, flammability, stability against oxygen/water, etc., also are important factors in RFB system design and durability. The electrolytes used in the various types of RFB systems are summarized in Table 2.1 above.

3. Characterization techniques

3.1 Electron microscopy techniques

3.1.1 Scanning electron microscopy (SEM)

Scanning electron microscopy has traditionally been used to directly obtain the morphology information of the used materials. SEM images were taken with Hitachi S-4700 microscope (Japan) operated at an acceleration voltage of 10kV.

3.2 Thermal characterization

3.2.1 Thermogravimetric analysis (TGA)

Thermogravimetric analysis (TGA) is a method of thermal analysis in which the mass of a sample is measured over time as the temperature changes. TGA can provide information about physical phenomena, such as phase transitions, absorption, adsorption and desorption as well as chemical phenomena including chemisorption, thermal decomposition, and solid-gas reactions. In this study, TGA (Pyris 1, PerkinElmer) was used to determine the thermal stability of the sample. TGA consists of a precision balance with a platinum sample pan located inside a furnace with a programmable control temperature. TGA was carried out from 25 to 1000 °C under a nitrogen atmosphere using a heating rate of 10 °C/min.

3.3 Spectroscopic characterization

3.3.1 X-ray photoelectron spectroscopy (XPS)

X-ray photoelectron spectroscopy (XPS) measurements can provide valuable information about the chemical composition and bond structure of carbon supports and the surface interaction between atoms. The XPS spectra were taken by a KRATOS AXIS NOVA XPS system with a monochromated Al-Kα (150 W) source. The XPS energy scale was calibrated by setting the binding energy of the carbon support to exactly 284.6 eV referenced to the Fermi level. The deconvolutions of the XPS spectra were carried out using OriginPro 8.5 software.

The relative concentrations of the surface species are equal to the corresponding deconvoluted peak areas divided by the total XPS signal area extracted from the experimental XPS core level regions of N 1s and C 1s.

3.4 Electrochemical characterization

3.4.1 Cyclic voltammetry (CV)

Cyclic voltammetry (CV) is an electrochemical technique which measures the current that arises in an electrochemical cell under conditions where voltage is in excess of that of predicted by the Nernst equation. In this study, CV was performed in 0.05 M $VOSO_4$ + 3.0 M H_2SO_4 electrolyte using a three-electrode cell. The graphite felt sample as a working electrode was prepared with 1 cm diameter and 0.46 cm height by using a punch. It was loaded to a sample holder with a glassy carbon disc as a current collector. The electrolyte was placed in the sample holder and air bubbles were removed using a vacuum oven. Platinum wire and Ag/AgCl electrode were used as counter and reference electrodes, respectively. The CV test was performed over the voltage range from 0 to 1.6 V vs. Ag/AgCl at a scan rate of 10 mV s^{-1} using a Bio-Logic VMP3 multichannel potentiostat (France).

3.4.2 Charge/discharge test

Charge/discharge test is generally used to measure electrochemical performance of rechargeable batteries. Figure 3.1 shows a lab-scale vanadium redox flow battery (VRFB) set-up for charge/discharge tests. The vanadium redox flow battery single cell used for charge-discharge tests consisted of electrolytes, electrodes, bipolar plates, ion exchange membranes, tanks, and pumps. The electrolyte from the inlet enters the flow path of the graphite bipolar plate, undergoes an electrochemical reaction at the electrode, and exits through the outlet. Protons produced through electrochemical reactions at the electrodes pass through the membrane to the opposite compartment and electrons pass through the graphite bipolar plate and the current collector. Commercial vanadium electrolyte with a total vanadium concentration of 1.6 M (50% VO^{2+} and 50% V^{3+}) in 2 M H_2SO_4 (GfE Metalle und Materialien GmbH, Germany) was used. The electrolyte volumes on both the positive and negative sides were 15 mL or 30mL and the area of the prepared graphite felt electrodes on both side was 4 cm^2 or 25 cm^2 depending on the experimental purpose. A Nafion membrane (N115, Dupont)

was used as a separator. Charge-discharge cycle tests were measured with a potentiostat/galvanostat (WonATech WBCS3000M2, Korea). The unit cells were charged and discharged in the 1.6-1.0 V range (voltage under current, not OCV) at current densities between 25 and 150 mA cm^{-2} at room temperature. The electrolyte flow rate was varied from 13 to 25 mL min^{-1} depending on the experimental purpose, which was controlled by a peristaltic pump (Ismatec, Germany).

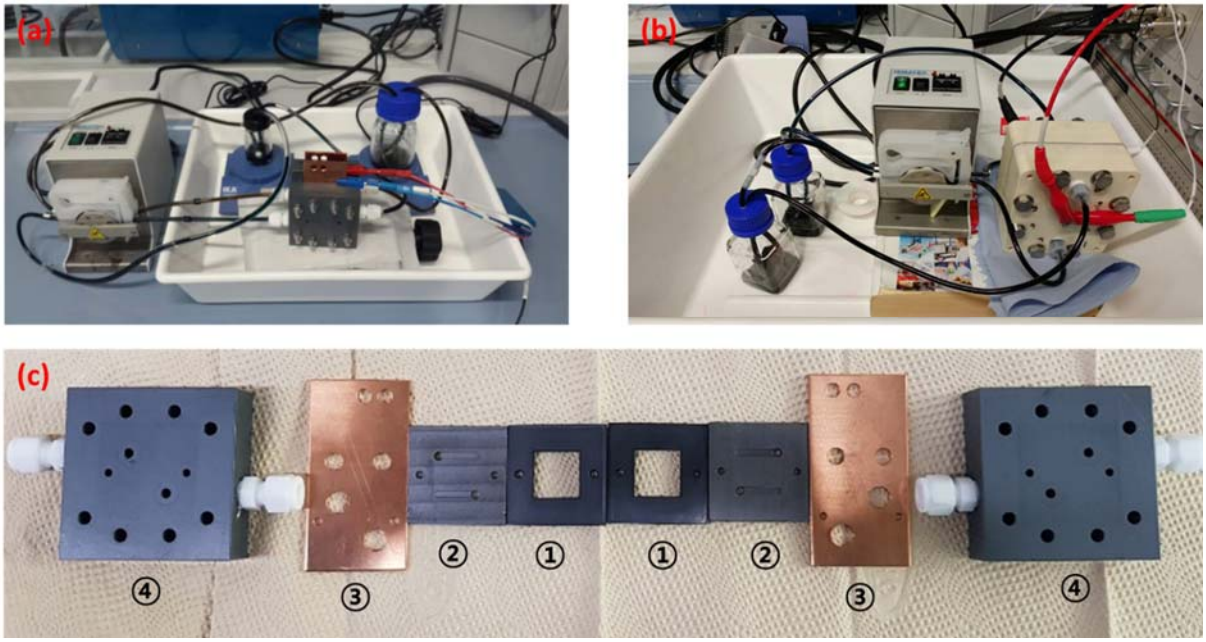

Figure 3.1 Vanadium redox flow battery (VRFB) set-up, (a) 2 x 2 cm^2 VRFB setting, (b) 5 x 5 cm^2 VRFB setting, (c) VRFB cell components (2 x 2 cm^2), ① gasket, ② graphite bipolar plate, ③ copper current collector, ④ end plate

4. Ionic liquid derived nitrogen doped graphite felt electrodes for vanadium redox flow batteries

In this chapter, we report a facile preparation method for nitrogen-doped carbon coated graphite felts using a nitrogen-containing ionic liquid, 1-ethyl-3-methlimidazolium dicyanamide (EMIM dca), as a nitrogen doping precursor. EMIM dca not only has a high nitrogen content of 39.5 wt% but also becomes a nitrogen doped carbon material with 18 wt% of nitrogen when it is heated up to 900 °C in an inert gas. EMIM dca has shown good electrocatalytic activity as a nitrogen containing carbon coating material in polymer electrolyte membrane fuel cell (PEMFC) applications. For these reasons, various amounts of EMIM dca were coated on graphite felt electrodes and then thermally treated. The effect of EMIM dca derived nitrogen-doped graphite felt on the performance of VRFBs was investigated by various physical and electrochemical analyses.

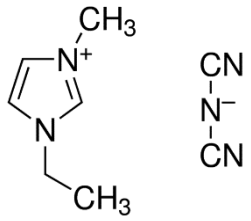

Figure 4.1 Molecular structure of 1-Ethyl-3-methylimidazolium dicyanamide (EMIM dca)

4.1 Experimental

4.1.1 Preparation of the nitrogen-doped graphite felt electrodes

EMIM dca coated graphite felt was prepared by thermal treatment of EMIM dca on graphite felt (SGL group, GFD 4.6EA, 2cm × 2cm). To coat graphite felt, EMIM dca was diluted in acetone with various concentrations (1 wt%-50 wt%). The graphite felt samples were named GF-Ed1 (EMIM dca 1 wt%), GF-Ed5 (EMIM dca 5 wt%), GF-Ed10 (EMIM dca 10 wt%) and so on according to the concentration of EMIM dca. After the EMIM solution was coated on the

graphite felt, the sample was placed in the hood for 3 hours to evaporate the solvent. The prepared product was heated in a quartz tube under N_2 atmosphere at 900 °C for 1h. For comparison purpose, pristine graphite felt was also heated under air atmosphere at 400 °C for 30 h, named GF-Ref [8].

4.1.2 Physical and electrochemical characterization

The surface morphology of graphite felt was investigated by scanning electron microscopy (SEM) using a Hitachi S-4700 microscope (Japan) operated at an acceleration voltage of 10kV. The graphite felt surface composition was analyzed using X-ray photoelectron spectroscopy (XPS) with a KRATOS AXIS NOVA XPS system with a monochromated Al-Kα (150 W) source. To investigate the electrochemical properties of the graphite felt electrodes, cyclic voltammetry (CV) was performed in 0.05 M $VOSO_4$ + 3.0 M H_2SO_4 electrolyte using a three-electrode cell. The graphite felt sample as a working electrode was prepared with 1 cm diameter and 0.46 cm height by using a punch. It was loaded to a sample holder with a glassy carbon disc as a current collector. The electrolyte was placed in the sample holder and air bubbles were removed using a vacuum oven. Platinum wire and Ag/AgCl electrode were used as counter and reference electrodes, respectively. The CV test was performed over the voltage range from 0 to 1.6 V vs. Ag/AgCl at a scan rate of 10 mV s^{-1} using a Bio-Logic VMP3 multichannel potentiostat (France).

4.1.3 Single cell test

The vanadium redox flow battery single cell used for charge-discharge tests consisted of electrolytes, electrodes, bipolar plates, ion exchange membranes, tanks, and pumps. Commercial vanadium electrolyte with a total vanadium concentration of 1.6 M (50% VO^{2+} and 50% V^{3+}) in 2 M H_2SO_4 (GfE Metalle und Materialien GmbH, Germany) was used. The electrolyte volumes on both the positive and negative sides were 15 mL and the area of the prepared graphite felt electrodes on both side was 4 cm^2. A Nafion membrane (N115, Dupont) was used as a separator. Charge-discharge cycle tests were measured with a potentiostat/galvanostat (WonATech WBCS3000M2, Korea). The single cells were charged and discharged in the 1.6-1.0 V range (voltage under current, not OCV) at current densities between 50 and 150 mA cm^{-2} at room temperature. The flow rate was fixed at 20 mL min^{-1}, which was controlled by a peristaltic pump (Ismatec, Germany).

4.2 Results and discussion

4.2.1 Thermal stability of nitrogen-doping precursor

Thermogravimetric analysis (TGA) was carried out to analyze carbonization and mass yield of the nitrogen-doping precursor, EMM dca, as shown in Figure 4.2.

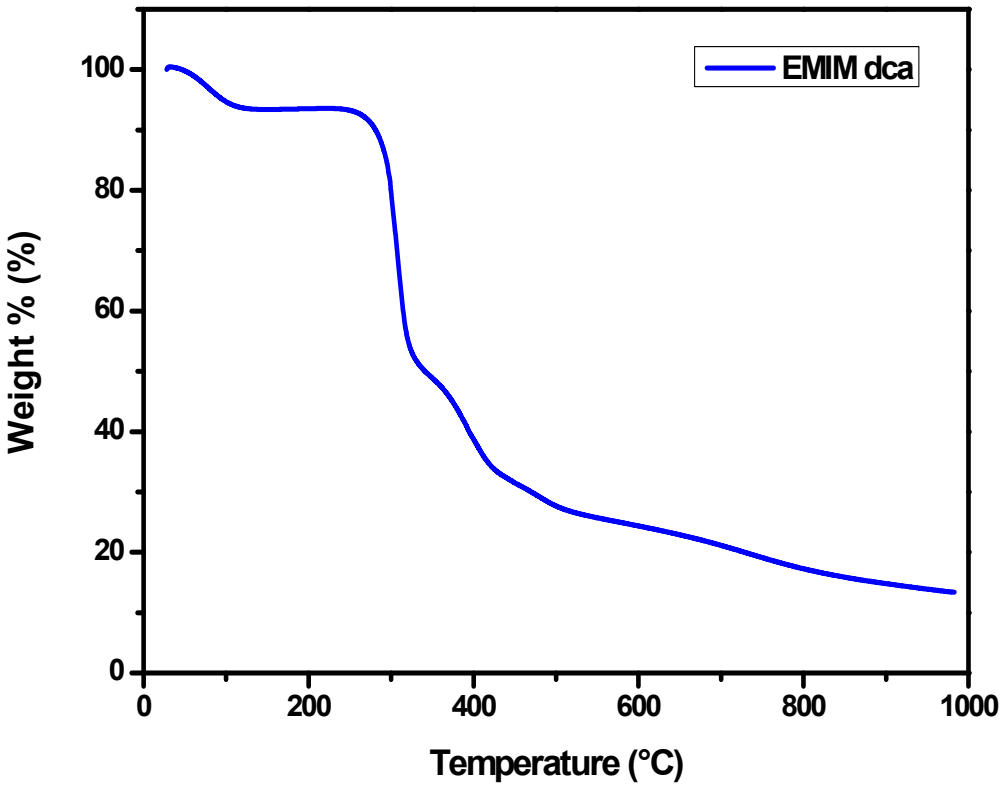

Figure 4.2 TGA of nitrogen-doping precursor (EMMI dca)

EMIM dca shows no significant weight loss up to a temperature of 300 °C and residual mass of EMIM dca of 13% are detected at 1000 °C. Paraknowitsch et al. performed a more detailed thermal analysis. As shown Figure 4.3, elemental analysis indicates that the carbon content is increased over the whole temperature range, but the hydrogen and nitrogen contents are decreased [41]. While the hydrogen content is less than 0.5%, the nitrogen content is about 10% at 1000 °C. These results show that EMIM dca is suitable as a nitrogen doping material.

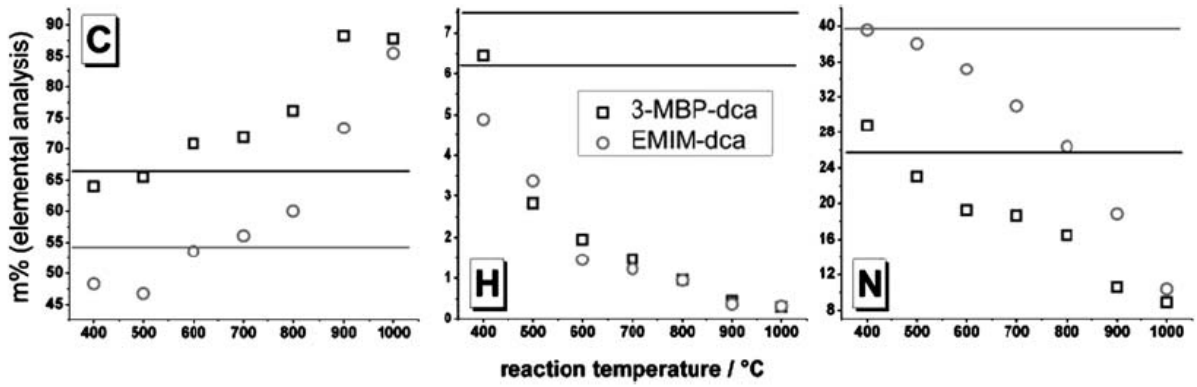

Figure 4.3 Course of the elemental composition of the material at different reaction temperatures. [42]

4.2.2 Morphology of nitrogen doped graphite felts

Nitrogen doped graphite felts were prepared by performing thermal treatment on EMIM dca coated graphite felt under a N_2 atmosphere at 900 °C for 1h. EMIM dca has been previously used as a precursor for nitrogen doped carbon materials which were obtained by a thermal decomposition [43,44]. It was reported that the products possessed high nitrogen content, local graphitic order, and good conductivities at high carbonization temperatures [3,41]. The nitrogen content and the electrical resistance of EMIM dca depend strongly on the carbonization temperature. For this reason, the thermal treatment on EMIM dca coated graphite felt was performed at 900 °C, resulting in the formation of nitrogen-doped graphite felt. Figure 4.4 shows the SEM images to demonstrate the surface morphologies of GF-Ed5 (Figure 4.4 a), GF-Ed10 (Figure 4.4 b), GF-Ed20 (Figure 4.4 c), and GF-Ed50 (Figure 4.4 d). Only few and small particles were observed on the surface of GF-Ed5, and more and larger particles were observed on the surface of GF-Ed10. When the concentration of the coated EMIM dca solution was increased to 20 wt% (GF-Ed20), it could be confirmed that most of the surface of the graphite felt was covered with coating materials. On the other hand, when the concentration of the coated EMIM dca solution was increased to 50 wt% (GF-Ed50), it was observed that excessive coating materials were generated on the surface of the graphite felt.

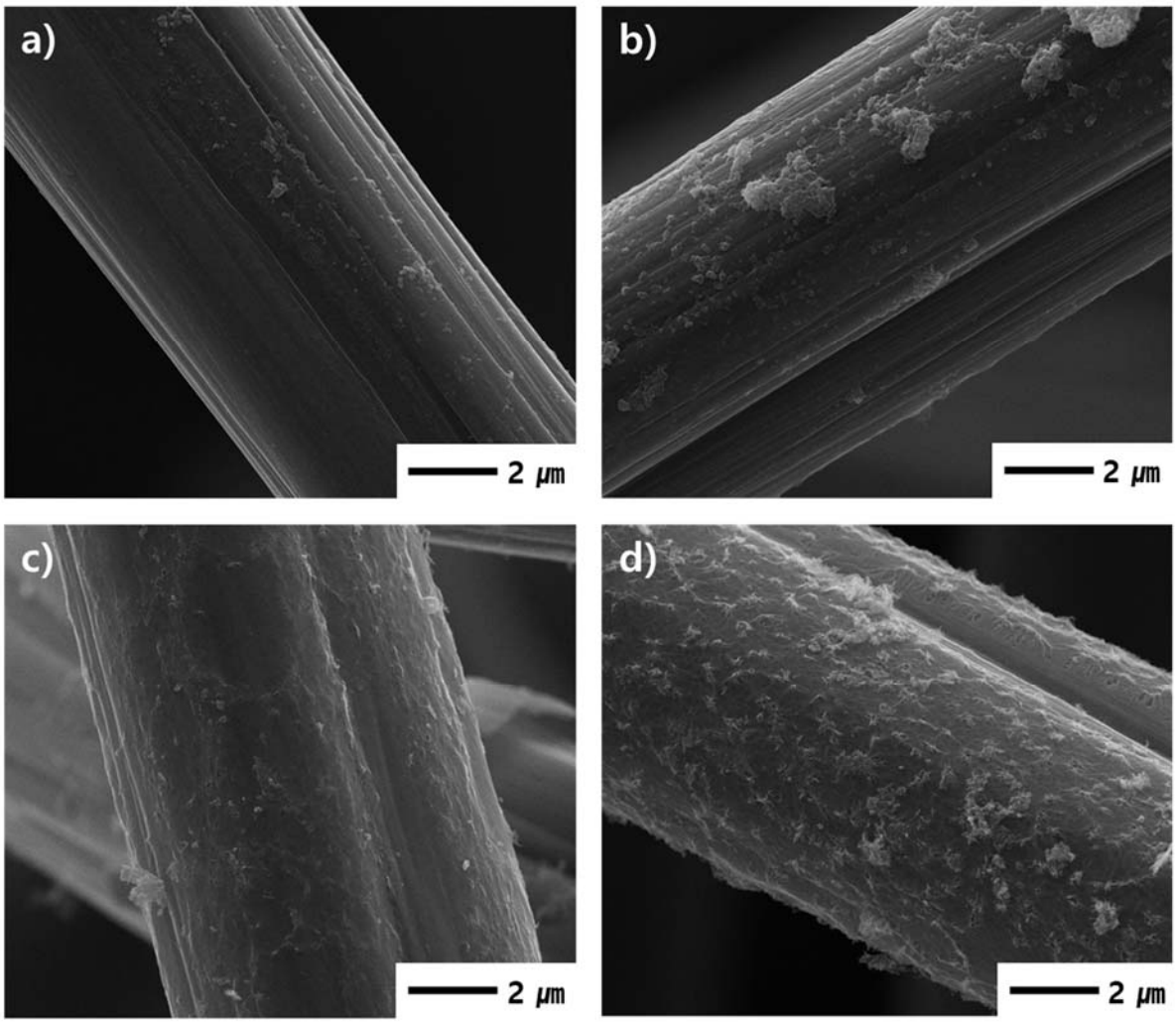

Figure 4.4 SEM image of (a) GF-Ed5, (b) GF-Ed10, (c) GF-Ed20, and (d) GF-Ed50.

4.2.3 Cyclic voltammetry analysis

Cyclic voltammetry tests were carried out using the three-electrode system in 0.05 M $VOSO_4$ + 3.0 M H_2SO_4 electrolyte to evaluate the electrochemical activity of the prepared electrodes. In cyclic voltammetry analysis, the peak potential difference ($\Delta E_p = E_{pa} - E_{pc}$), redox onset potential, the peak oxidation and reduction current and their ratio (I_{pa} / I_{pc}) are investigated to evaluate electrocatalytic activities for the V^{4+}/V^{5+} redox reaction. As shown in Figure 4.5, the peak potential difference of GF-Ref (ΔE_p = 427 mV) is smaller than of GF-Ed1 (ΔE_p = 530 mV), and the ratio of the oxidation and reduction peak currents was closer to 1 for GF-Ref (I_{pa} / I_{pc} = 1.36) than for GF-Ed1 (I_{pa} / I_{pc} = 1.65). These results mean that GF-Ed1 has lower electrochemical activity and reversibility for the vanadium V^{4+}/V^{5+} redox reaction than GF-Ref. GF-Ref with the oxygen functional groups prepared by the conventional heat treatment method

in air at 400 °C for 30h showed better performance than GF-Ed1 coated with less EMIM dca. However, as the amount of EMIM dca coated on the graphite felt increased, the electrochemical performance increased, showing better electrochemical activity and reversibility for GF-Ed20 (ΔE_p = 414 mV, I_{pa} / I_{pc} = 1.32) and GF-Ed50 (ΔE_p = 351 mV, I_{pa} / I_{pc} = 1.23) than for GF-Ref.

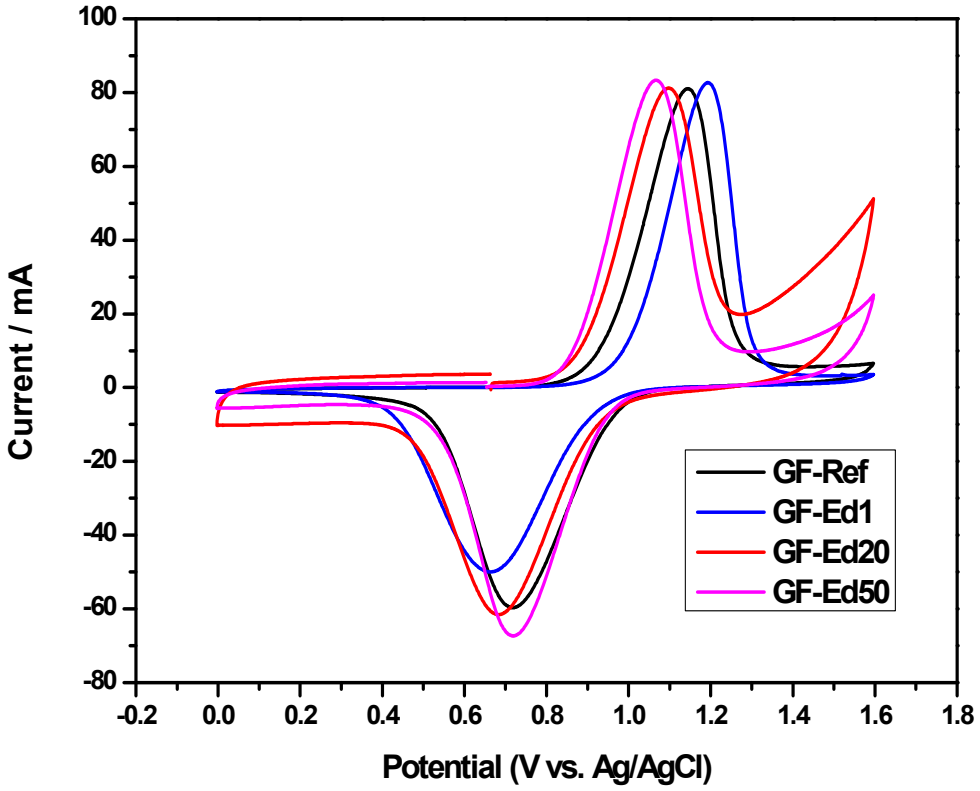

Figure 4.5 Cyclic voltammograms of GF-Ref and EMIM dca coating graphite felts with different loadings in 0.05M $VOSO_4$ + 3.0M H_2SO_4 electrolyte at a scan rate of 10 mVs^{-1} with a potential window of 0.0 V to 1.6 V vs. Ag/AgCl, i.e. for the V^{4+}/V^{5+} redox reactions.

4.2.3 XPS characterization

To describe the effect of EMIM dca coating to improve the electrochemical activity, XPS analysis was carried out for the prepared electrodes. According to the survey XPS spectra as shown in Figure 4.6 a, it was difficult to identify nitrogen peaks in the GF-Ref. For the case of GF-Ed20, a nitrogen peak could be observed and the elemental compositions are summarized in Table 4.1. GF-Ref and GF-Ed20 showed nitrogen contents of 0.5 at% and 6.1 at%, respectively. These results confirm that the graphite felt was doped with nitrogen through the EMIM dca coating. To investigate the effect of the nitrogen doping on the EMIM dca coated graphite felt, the N 1s spectra were deconvoluted into two peaks, which corresponded to graphitic-N (401.0 eV) and pyridinic-N (398.3 eV) [41,42,149]. According to the intensity of the deconvoluted contribution, the amount of graphitic N is higher than pyridinic N. In addition, the C 1s spectra were obtained to confirm the nitrogen bonding structure. As shown in Figure 4.6c, the C 1s spectra exhibited pyridinic C (285.6 eV) and purely aromatic carbon (284.7 eV) [41,42]. These results indicate that nitrogen atoms were successfully incorporated into the carbon structure. Nitrogen doped carbon materials have been reported to improve their electrical conductivity and oxidation stability [150-154]. It is known that the strong electronic affinity of the nitrogen atoms causes modification of the electronic properties of carbon atoms, which enhance the electron transfer between the graphite felt electrode and vanadium ions and improve the wettability of the electrolyte [29,34]. Therefore, a high surface concentration of nitrogenous groups improves the electrocatalytic activity of the felt for vanadium redox reaction.

Table 4.1 Elemental composition of EMIM dca coating graphite felt electrodes

Sample	Carbon (at. %)	Nitrogen (at. %)	Oxygen (at. %)
GF-Ref	92.7	0.5	6.8
GF-Ed20	91	6.1	2.9

(a)

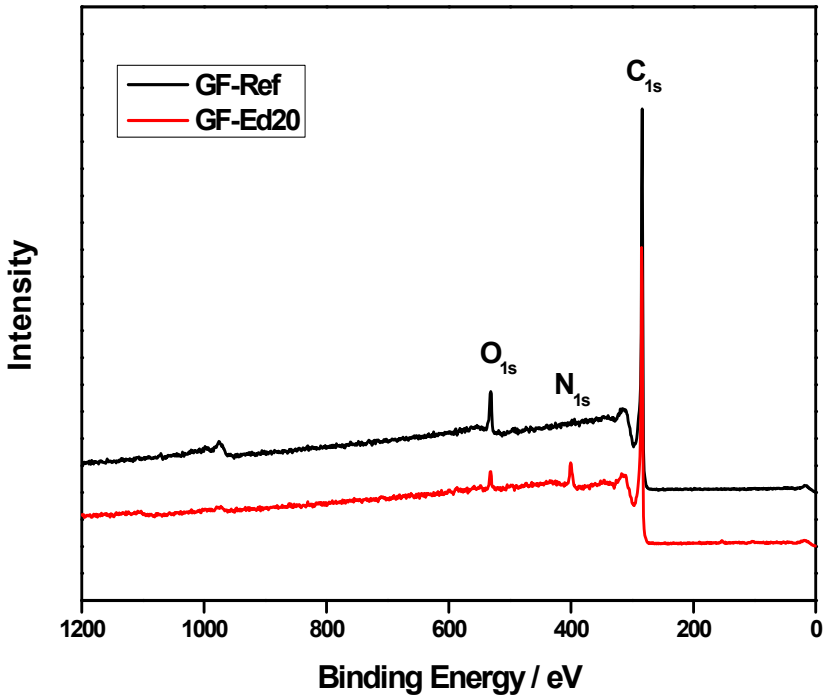
GF-Ref
GF-Ed20
C1s
O1s
N1s
Intensity
1200
1000
800
600
400
200
0
Binding Energy / eV

(b)

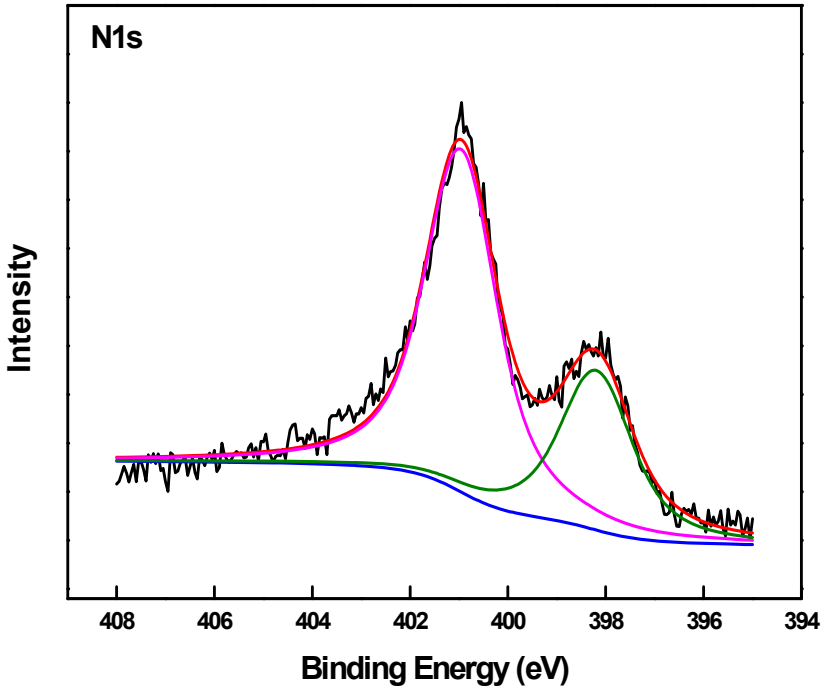
N1s
Intensity
408
406
404
402
400
398
396
394
Binding Energy (eV)

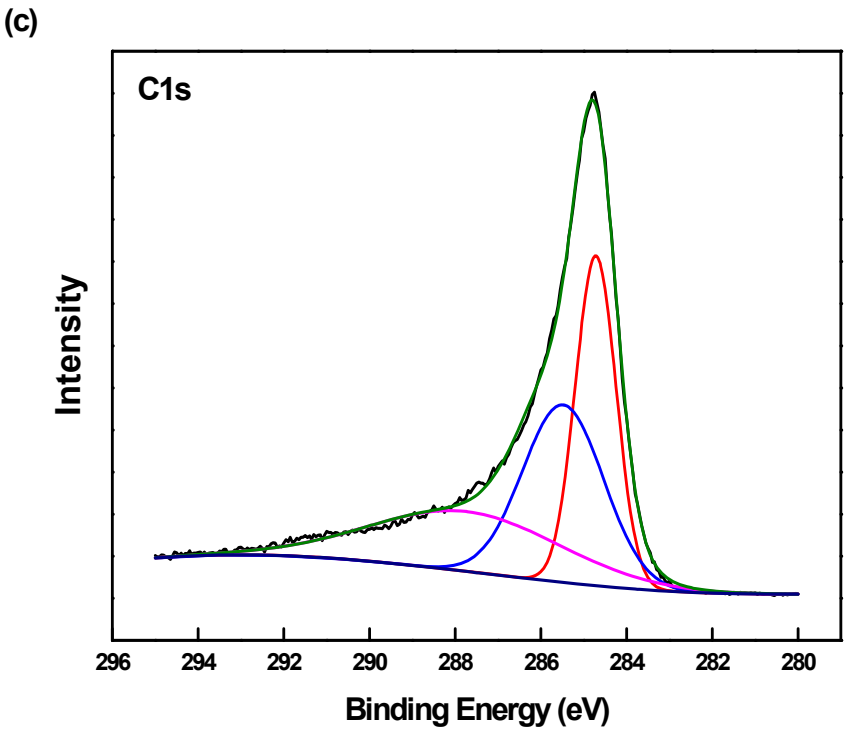

Figure 4.6 (a) Survey XPS spectra of GF-Ref and GF-Ed20 (b) N1s XPS spectra of GF-Ed20 (c) C1s XPS spectra of GF-Ed20

4.2.4 Charge/discharge test

The charge/discharge experiments were carried out using a VRFB single cell to verify the improved electrochemical activity for the nitrogen doping graphite felt electrodes. EMIM dca coating graphite felt samples were prepared by coating 0.5, 1, and 5 wt% EMIM dca solutions on graphite felts. Prior to EMIM dca coating, the pristine graphite felts were heated at 400°C for 30 hours under air atmosphere in a box furnace and EMIM dca coated graphite felt samples were heated at 600 °C for 1hour under nitrogen atmosphere in a tube furnace. The prepared samples were named 2H-GF-Ed0.5 (EMIM dca 0.5 wt%), 2H-GF-Ed1 (EMIM dca 1 wt%), and 2H-GF-Ed5 (EMIM dca 5 wt%). The rate performances were measured by varying the current density from 25 to 150 mA cm^{-2}. Figure 4.7 shows the charge-discharge curves at a constant current density of 75 mA cm^{-2}. When the charge-discharge process was performed with an upper limiting voltage of 1.6 V, the VRFB cells employing the EMIM dca coating electrodes exhibited lower charge-discharge capacities than the GF-Ref prepared by the conventional heat treatment method. Among the cells with the EMIM dca coating electrodes, as the amount of EMIM dca coating increases, the charge-discharge capacities decrease and the

overpotential during the charge and discharge processes increases. In the case of 2H-GF-Ed5 which had the worst performance, the discharge capacity decreased from 445 mAh to 153 mAh, and the voltage loss at the beginning of discharge process increased by 229 mV compared to GF-Ref at the current density of 75 mA/cm^{-2}

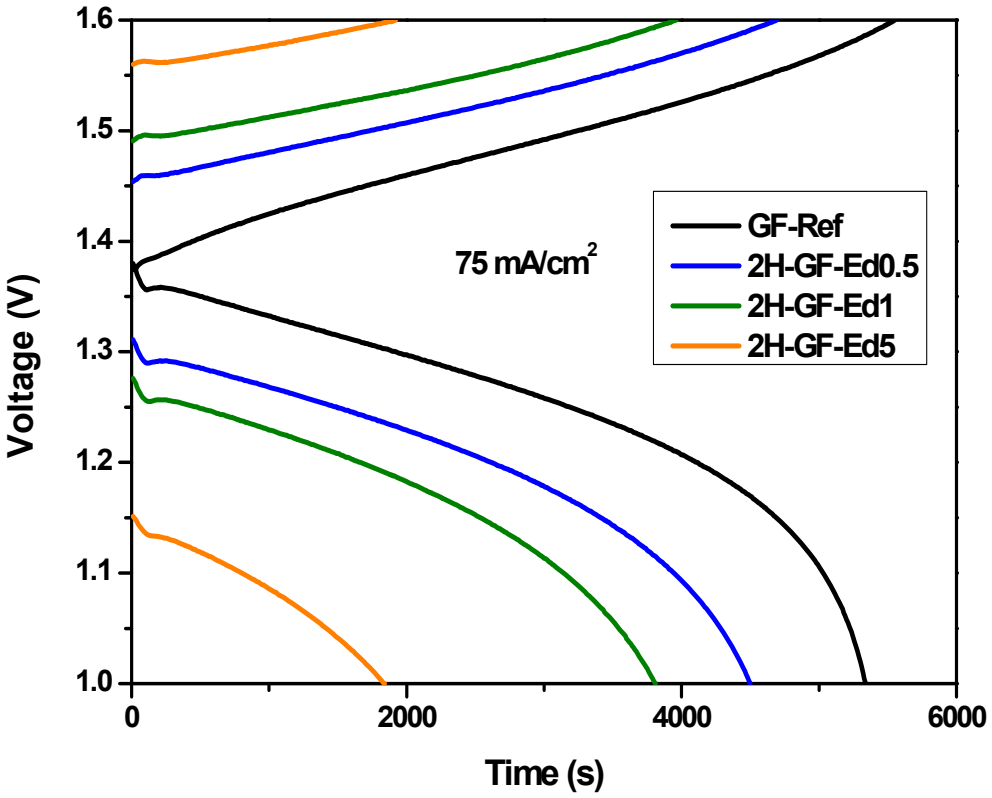

Figure 4.7 Charge/discharge curves for VRFBs employing the graphite felts coated with various amounts of EMIM dca at the current density of 75 mA/cm^2.

Figure 4.8 shows the coulombic efficiency (CE), voltage efficiency (VE), and energy efficiency (EE) of the VRFBs at various current densities during the charge/discharge cycles. However, the charge/discharge results could not be obtained at the overall current densities because of high overpotential caused by two steps heated EMIM dca coating graphite felt electrodes. When graphite felt coated with 5 wt% EMIM dca solution (2H-GF-Ed5) was used, the charge/discharge test did not proceed at current densities higher than 75 mAcm^{-2}. Even with

graphite felt coated with 0.5 wt% and 1 wt% EMIM dca solutions (2H-GF-Ed0.5 and 2H-GF-Ed1), charge/discharge tests were not successful at a current density higher than 125 mA cm^{-2}. There was no notable difference between the CE values (~96%) of all prepared electrodes. However, the VE of cells with EMIM dca coated electrodes decreased from 79% to 69% at 75 mA cm^{-2} as the amount of EMIM dca coating increases. This values are lower than the VE of cell using GF-Ref which was heated without EMIM dca, indicating that EMIM dca coating electrodes heated at 600 °C has reduced the electrochemical activity of the graphite felt for the vanadium redox reaction. Finally, the cells with EMIM dca coated electrodes showed lower energy efficiencies than the cell using GF-Ref at the overall current densities, suggesting that the thermal treatment of EMIM dca at 600 °C is not suitable for increasing VRFB performance.

(a)

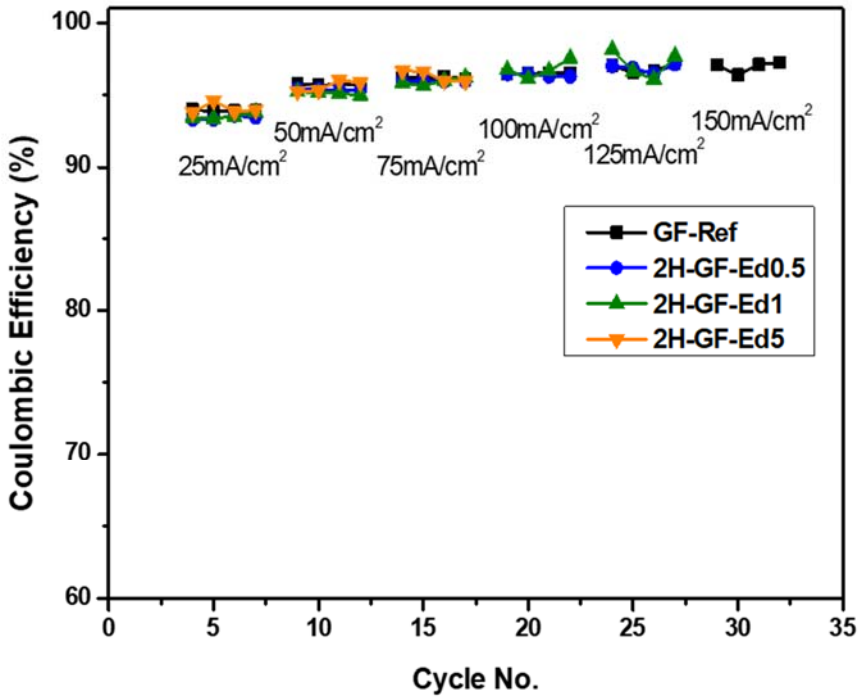

(b)

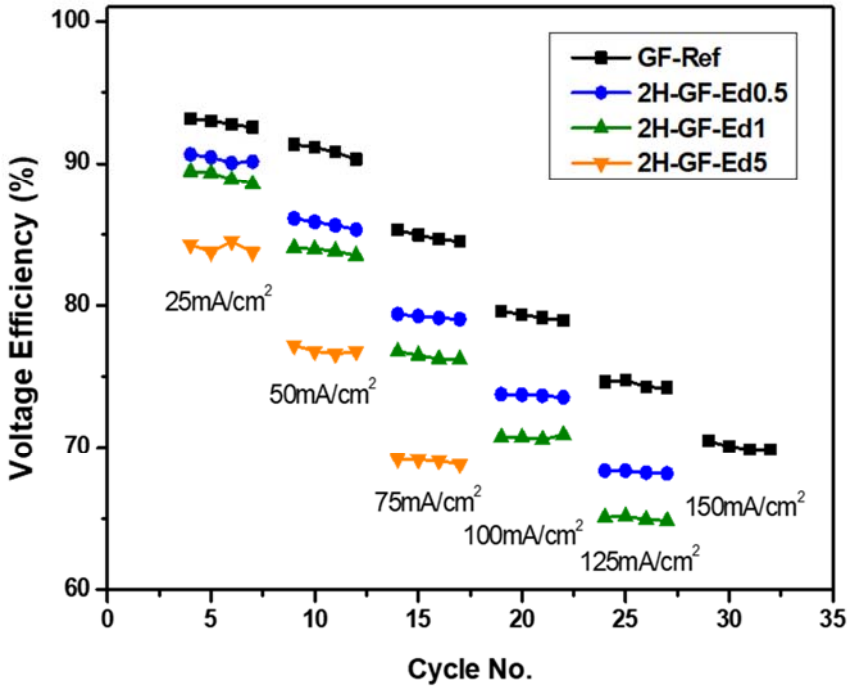

(c)

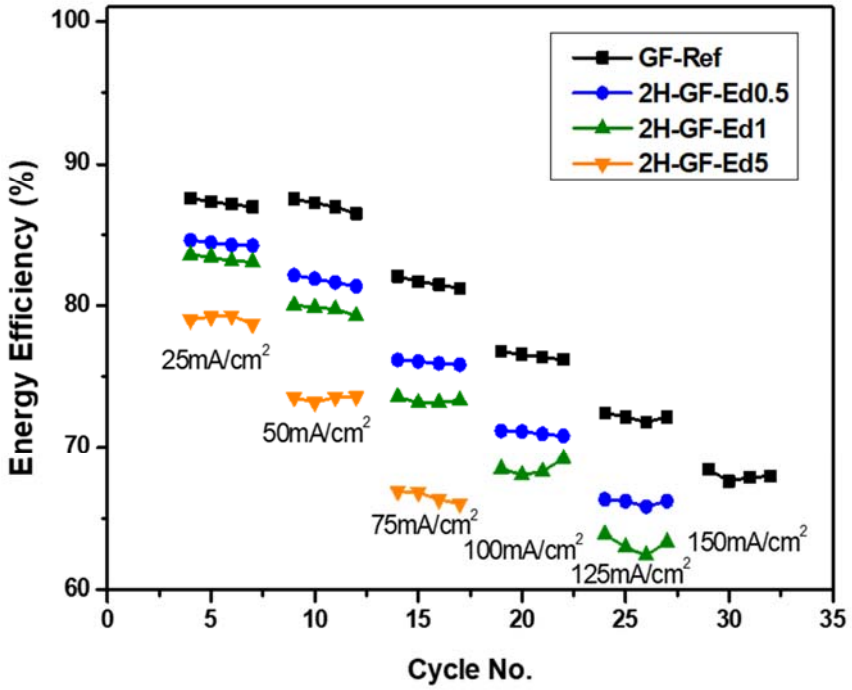

Figure 4.8 Cycling performance of VRFBs employing the prepared graphite felts with various amounts of EMIM dca at different current densities; (a) coulombic efficiency, (b) voltage efficiency, and (c) energy efficiency.

Second, charge/discharge tests were carried out with EMIM dca coating graphite felts, which had been heated at 900°C for 1 hour under nitrogen atmosphere, to verify the improved electrochemical activity for the nitrogen doping graphite felt electrodes. The prepared graphite felt samples were named GF-Ed1 (EMIM dca 1 wt%), GF-Ed5 (EMIM dca 5 wt%), GF-Ed10 (EMIM dca 10 wt%) and so on according to the concentration of EMIM dca. The rate performances were measured by varying the current density from 50 to 150 mA cm^{-2}. Figure 4.9 shows the charge-discharge curve at a constant current density of 150 mA cm^{-2}. When the charge/discharge process was performed with an upper limiting voltage of 1.6 V, the VRFB cells employing the EMIM dca coating electrodes exhibited higher charge-discharge capacities than the GF-Reference prepared by the conventional heat treatment method. Among the cells with the EMIM dca coating electrodes, as the amount of EMIM dca coating increases, the charge/discharge capacities increase and the overpotential during the charge and discharge processes decreases. In the case of GF-Ed20 which had the best performance, the discharge capacity increased by 195%, from 8.2 Ah L^{-1} to 24.2 Ah L^{-1}, and the voltage loss at the beginning of discharge process decreased by 154 mV compared to GF-Ref at the current density of 150 mA/cm^{-2}. On the other hand, for the more EMIM dca coated GF-Ed50, the voltage loss at the beginning of discharge process was similar to that of GF-Ed20, whereas the discharge capacity was reduced by 9% due to the diffusion layer transport loss derived by the excess coating material which caused EMIM dca coated graphite felt to be hard and brittle.

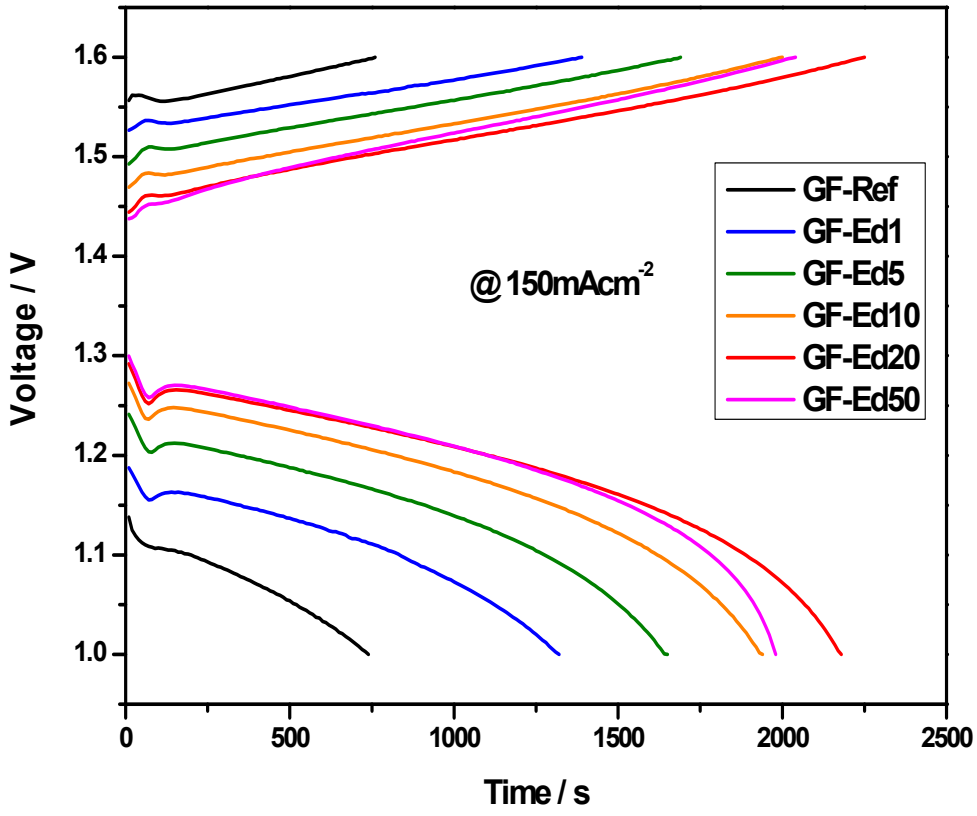

Figure 4.9 Charge/discharge curves for VRFBs employing the prepared graphite felts with different EMIM dca coating at the current density of 150 mA/cm^2.

Figure 4.10 shows the coulombic efficiency (CE), voltage efficiency (VE), and energy efficiency (EE) of the VRFBs at various current densities during the charge-discharge cycles. There are hardly any differences between the CE values (~97%) of all prepared electrodes. However, the VE of cells with EMIM dca coated electrodes increased from 71% to 78% (GF-Ref, 68%) at 150 mA cm^{-2} as the amount of EMIM dca coating increases, suggesting that EMIM dca coated electrodes has enhanced the electrochemical activity of the felt for the vanadium redox reaction. Finally, the cells with sufficient amount of EMIM dca-coated electrodes (GF-Ed20, GF-Ed50) showed about 10% higher energy efficiencies than the cell using GF-Ref at 150 mA cm^{-2}.

(a)

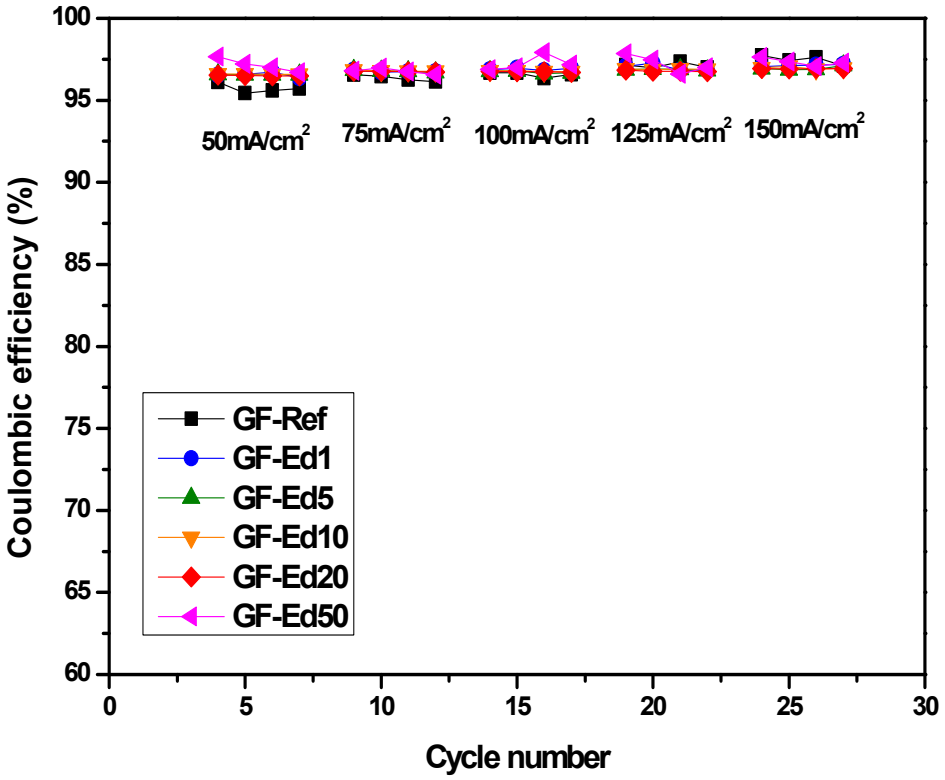
Coulombic efficiency (%)
Cycle number
50mA/cm2
75mA/cm2
100mA/cm2
125mA/cm2
150mA/cm2
GF-Ref
GF-Ed1
GF-Ed5
GF-Ed10
GF-Ed20
GF-Ed50

(b)

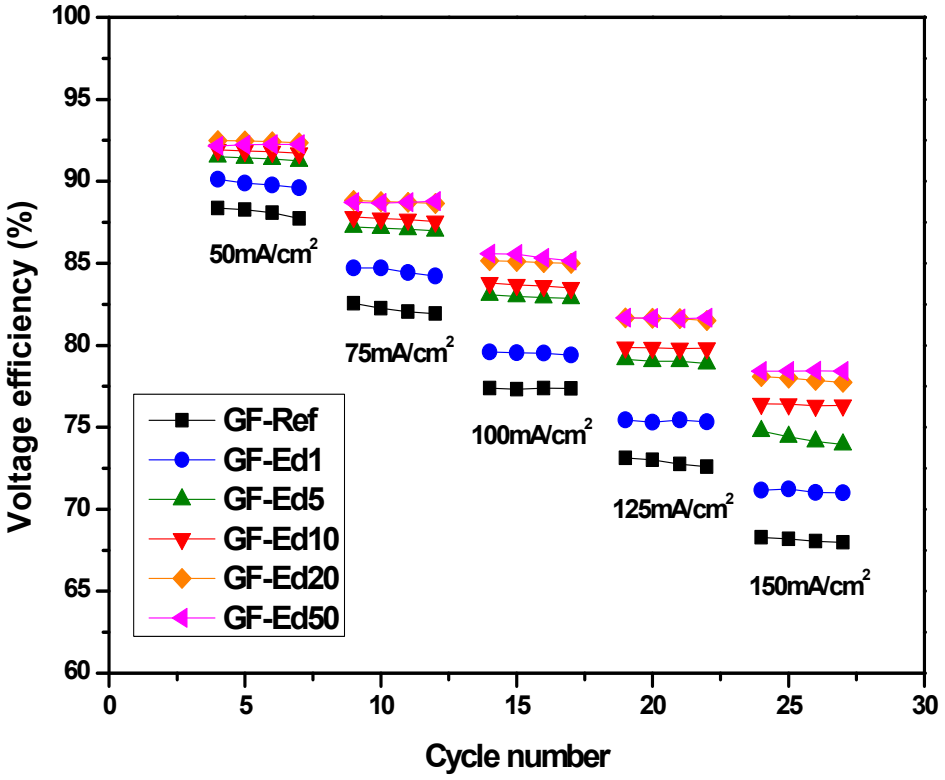
Voltage efficiency (%)
Cycle number
50mA/cm2
75mA/cm2
100mA/cm2
125mA/cm2
150mA/cm2
GF-Ref
GF-Ed1
GF-Ed5
GF-Ed10
GF-Ed20
GF-Ed50

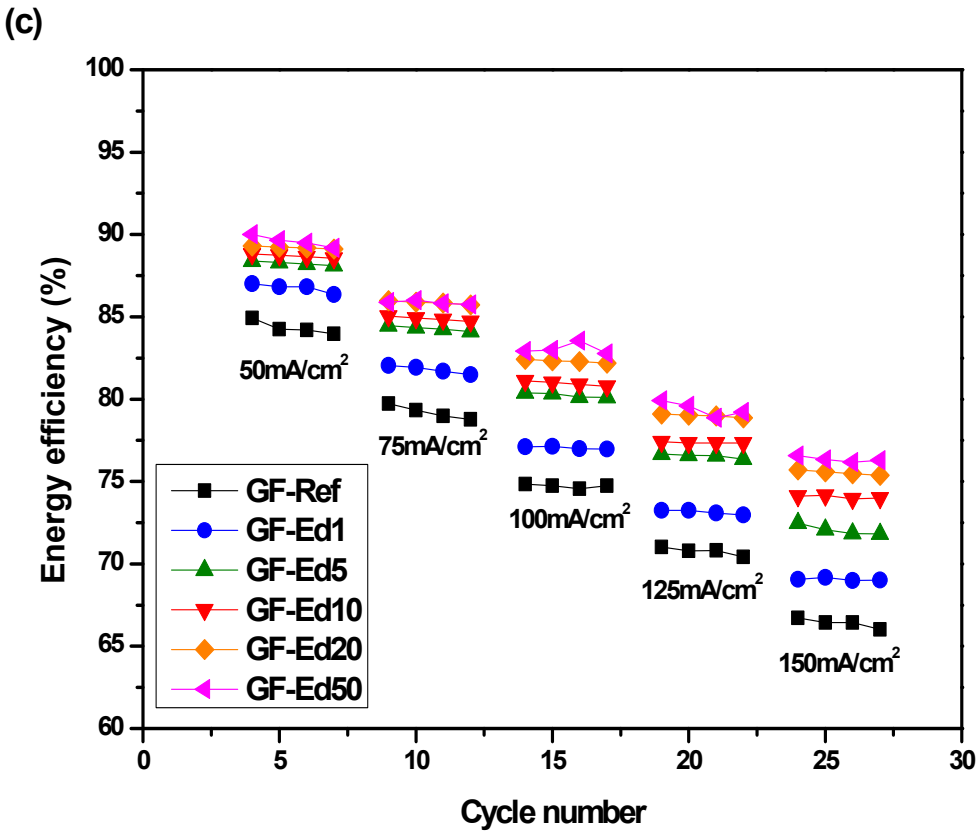

Figure 4.10 Cycling performance of VRFBs employing the prepared graphite felts with different EMIM dca coating at different current densities; (a) coulombic efficiency, (b) voltage efficiency, and (c) energy efficiency.

Figure 4.11 shows the efficiencies and discharge capacities for the cells with GF-Ed20 and GF-Ref during 100 charge/discharge cycles at 100 mA cm^{-2}. In CE results, no obvious difference was observed for 100 cycles. As shown in VE results, GF-Ed20 presents higher stability (deterioration from 85% to 81%) than GF-Ref (from 84% to 72%) during 100 cycles, leading to higher EE in the VRFB cell. After 100 charge-discharge cycles, the discharge capacity of the cell with GF-Ed20 was maintained at 81%, while the discharge capacity of GF-Ref was reduced to 52% from the initial capacity. These results indicate that the EMIM dca coating not only improves the electrochemical activity but also enhances the stability of the graphite felt electrode.

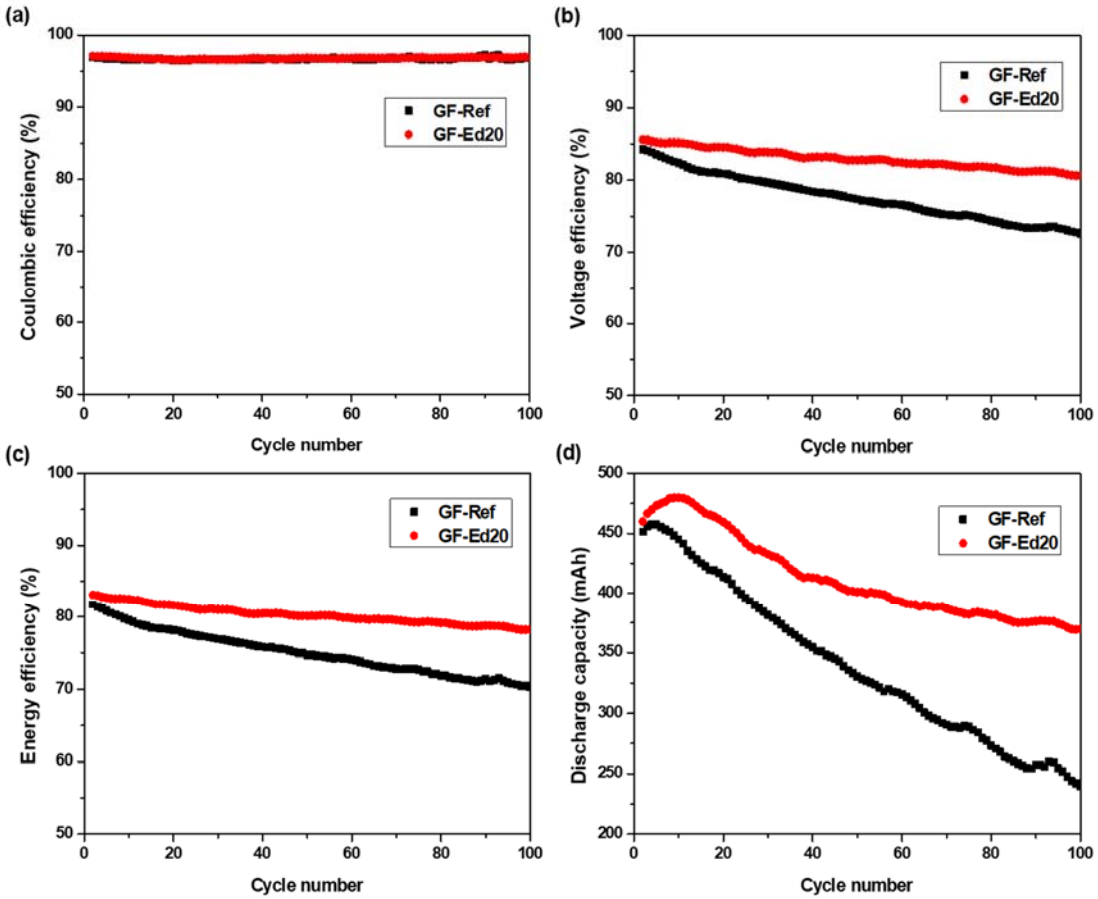

Figure 4.11 Cycling stability of VRFBs with GF-Ref and GF-Ed20 at the current density of 100 $mAcm^{-2}$; (a) coulombic efficiency, (b) voltage efficiency, (c) energy efficiency, and (d) discharge capacity.

4.2.5 Conclusion

Nitrogen doped graphite felts were prepared by a thermal coating process of a nitrogen containing ionic liquid on the pristine graphite felt for VRFB electrode applications. Ethylmethylimidazolium dicyanamide (EMIM dca) was used as a precursor for the high performance nitrogen-doped graphite felt electrode due to its high nitrogen content. According to the experimental results, via EMIM dca a nitrogen-containing carbon material has been successfully deposited on the surface of the graphite felt. From the results of CV, EMIM dca coated graphite felts showed higher electrocatalytic activity than the graphite felt with the oxygen functional groups which was prepared by the conventional heat treatment (GF-Ref). The charge-discharge test results showed that EMIM dca coated graphite felts had much

higher performance than GF-Ref. Working with a upper limiting voltage of 1.6 V the discharge capacity of the 20 wt% EMIM dca solution coated graphite felt (GF-Ed20) was 24 Ah L^{-1} at the current density of 150 mA cm^{-2}, which is three times higher than that of GF-Ref. The cells with GF-Ed20 also showed about 10% higher energy efficiency than the cell using GF-Ref at 150 mA/cm^{-2}. More specifically, the capacity retention and energy efficiency of the cell with GF-Ed20 were higher than those of GF-Ref after 100 charge-discharge cycle test, which indicates that the EMIM dca coating improved both the electrochemical activity and the stability of the graphite felt electrode.

5. Nitrogen doped graphite felt electrodes by coating polyacrylonitrile (PAN) for vanadium redox flow batteries

In this chapter, we report a facile preparation method for nitrogen-doped carbon coated graphite felts using polyacrylonitrile (PAN). PAN is commonly used as a precursor for producing carbon fibers and at the same time contains 26 wt% of nitrogen atoms in the molecule [45,155]. Graphite felt, which is used as an electrode of VRFB, is also mostly manufactured using PAN as a precursor. In the process of manufacturing carbon fiber from PAN as shown in Figure 5.1, it can be confirmed that carbon material containing nitrogen can be produced through oxidation and carbonization.

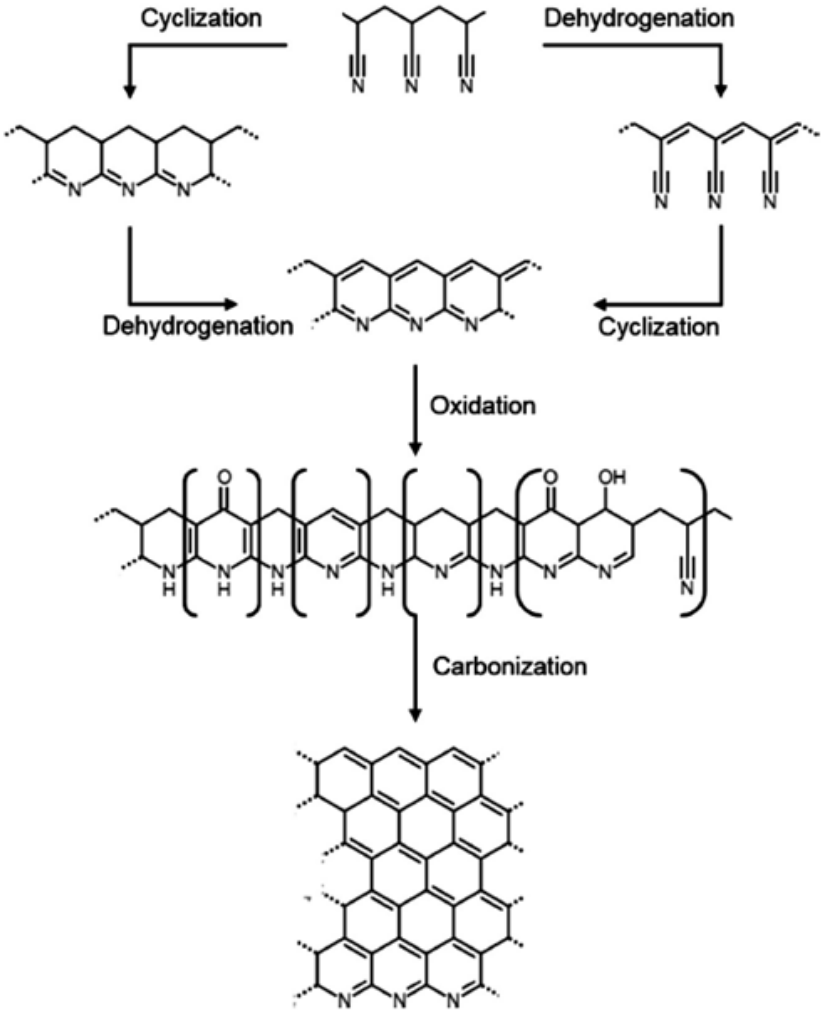

Figure 5.1 Chemical reactions during the stabilization and carbonization of PAN based carbon fiber [45]

In this study, the PAN is coated on graphite felt to improve the performance of VRFB single cell electrodes by utilizing the mechanism of the process of manufacturing PAN from carbon fiber. This is expected not only to increase the surface area but also to improve the performance of the electrode by using the nitrogen doping effect through nitrogen in the molecular structure of the prepared material. As a thermal treatment method for preparing PAN coated graphite felt, the oxidation and carbonization process of the conventional carbon fiber preparation process are used. In the oxidation process, it is known that the ring structure is formed as a result of thermal treatment of the PAN, however it is not clear about its exact mechanism. A lot of studies have been conducted to uncover the mechanism, and the various structures of oxidized PAN are shown in Figure 5.2 [156].

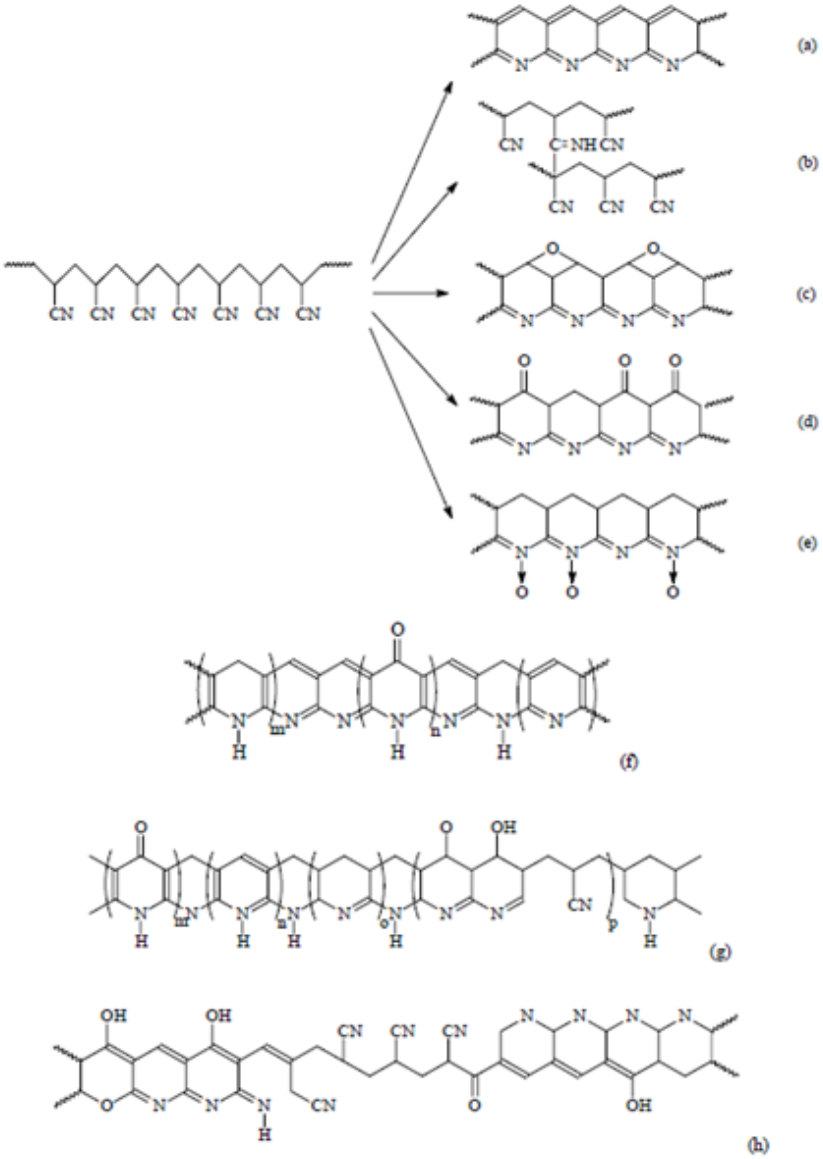

Figure 5.2 Oxidation of PAN [156]

To fabricate nitrogen-doped graphite felt electrodes by coating PAN, three kinds of thermal treatment were performed; (1) oxidation at 280°C for 3 hours under ambient atmosphere, (2) carbonization at 900°C for 1 hour under nitrogen atmosphere, (3) both oxidation and carbonization. Experiments have been carried out on optimizing the heat treatment process and the amount of PAN coating to improve the performance of VRFBs. In addition, the effect of nitrogen-doped graphite felt by coating PAN on the performance of VRFBs was investigated by various physical and electrochemical analyses.

5.1 Experimental

5.1.1 Preparation of PAN coated graphite felt electrodes

Nitrogen doped graphite felt by coating PAN was prepared by thermal treatment of PAN on graphite felt (SGL group, GFD 4.6EA, 2cm × 2cm). To coat PAN on graphite felt, PAN was dissolved in dimethyl sulfoxide with various concentrations (0.5 wt% - 8 wt%). The graphite felt samples were named GF-P0.5 (PAN 0.5 wt%), GF-P1 (PAN 1 wt%), GF-P2 (PAN 2 wt%) and so on according to the concentration of PAN. After the PAN solution was coated on the graphite felt, the sample was placed in the convection oven at 60 °C for 24 hours to evaporate the solvent. The prepared product was heated for each purpose in different method; (1) oxidation at 280°C for 3 hours under atmosphere in a box furnace, (2) carbonization at 900 °C for 1hour under nitrogen atmosphere in a tube furnace, (3) both oxidation and carbonization. For comparison purpose, pristine graphite felt was also heated at 400 °C for 30 hours under ambient atmosphere, named GF-Ref [8].

5.1.2 Physical and electrochemical characterization

The surface morphology of graphite felt was investigated by scanning electron microscopy (SEM) using a Hitachi S-4700 microscope (Japan) operated at an acceleration voltage of 10kV.

The graphite felt surface composition was analyzed using X-ray photoelectron spectroscopy (XPS) with a KRATOS AXIS NOVA XPS system with a monochromated Al-Kα (150 W) source. To investigate the electrochemical properties of the graphite felt electrodes, cyclic voltammetry (CV) was performed in 0.05 M $VOSO_4$ + 3.0 M H_2SO_4 electrolyte using a three-electrode cell. The graphite felt sample as a working electrode was prepared with 1 cm diameter and 0.46 cm height by using a punch. It was loaded to a sample holder with a glassy carbon disc as a current collector. The electrolyte was placed in the sample holder and air bubbles were removed using a vacuum oven. Platinum wire and Ag/AgCl electrode were used as counter and reference electrodes, respectively. The CV test was performed over the voltage range from 0 to 1.6 V vs. Ag/AgCl at a scan rate of 30 mV s^{-1} using a Bio-Logic VMP3 multichannel potentiostat (France).

5.1.3 Single cell test

The vanadium redox flow battery single cell used for charge/discharge tests consisted of electrolytes, electrodes, bipolar plates, ion exchange membranes, tanks, and pumps. Commercial vanadium electrolyte with a total vanadium concentration of 1.6 M (50% VO^{2+} and 50% V^{3+}) in 2 M H_2SO_4 (GfE Metalle und Materialien GmbH, Germany) was used. The electrolyte volumes on both the positive and negative sides were 15 mL and the area of the prepared graphite felt electrodes on both side was 4 cm^2. A Nafion membrane (N115, Dupont) was used as a separator. Charge-discharge cycle tests were measured with a potentiostat/galvanostat (WonATech WBCS3000M2, Korea). The single cells were charged and discharged in the 1.6-1.0 V range at current densities between 25 and 150 mA cm^{-2} at room temperature. The flow rate was fixed at 20 mL min^{-1}, which was controlled by a peristaltic pump (Ismatec, Germany).

5.2 Results and discussion

5.2.1 Thermal stability of nitrogen doping precursor

Thermogravimetric analysis (TGA) was carried out to analyze carbonization and mass yield of the nitrogen doping precursors, pristine PAN and Oxi-PAN which was heated at 280°C for 3 hours under ambient atmosphere, as shown in Figure 5.3.

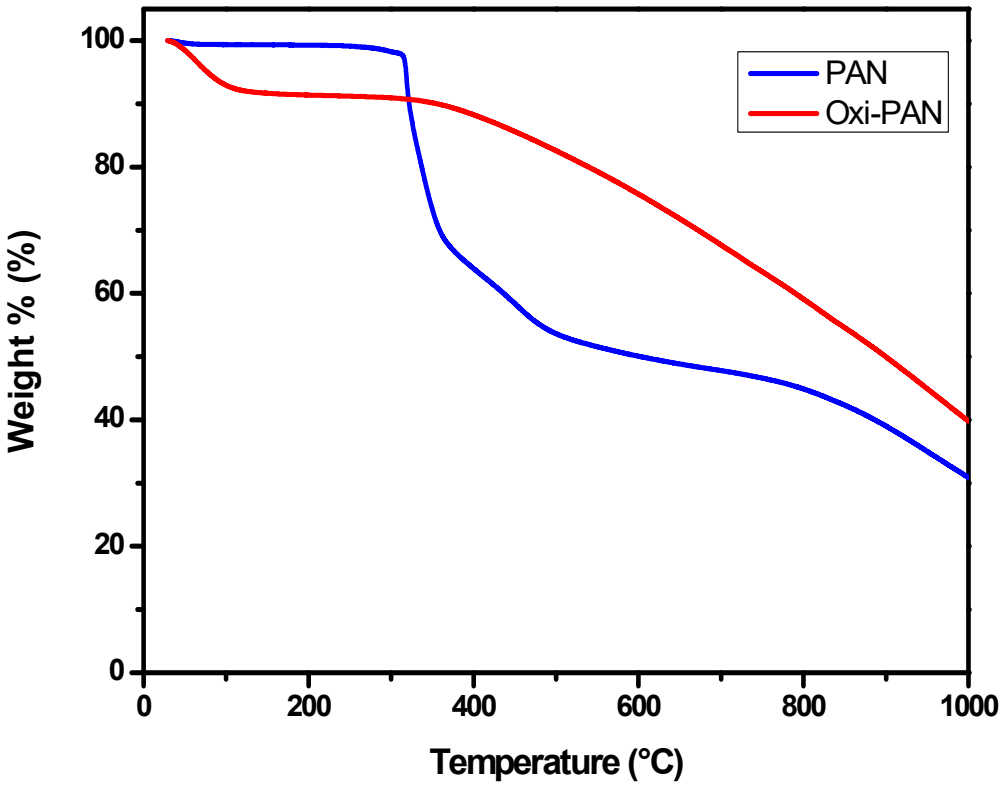

Figure 5.3 TGA of PAN and Oxi-PAN

PAN shows no significant weight loss up to a temperature of 315 °C, however rapid pyrolysis occurs as the temperature increases further. Eventually, the weight loss increases with increasing temperature, showing a residual mass of 39% at 900 °C and 31% at 1000 °C, respectively. In the case of Oxi-PAN, a weight loss of about 8% occurs up to 100 °C, which

appears to be due to the moisture inside the sample. It shows little weight loss from 100 °C to 350 °C, after which the weight of the sample gradually decreases. After all, the weight loss increases with increasing temperature, showing a residual mass of 50% at 900 °C and 40% at 1000 °C, respectively. However, considering the influence of moisture in the range below 100 °C, it shows a residual mass of about 58% at 900 °C. These results indicate that Oxi-PAN has a higher thermal stability than pristine PAN. At the same time, as shown in Figure 5.4, in the case of PAN, since nitrogen-containing material can be generated through heat treatment of less than 1000 °C, it can be used as nitrogen doping precursor [157].

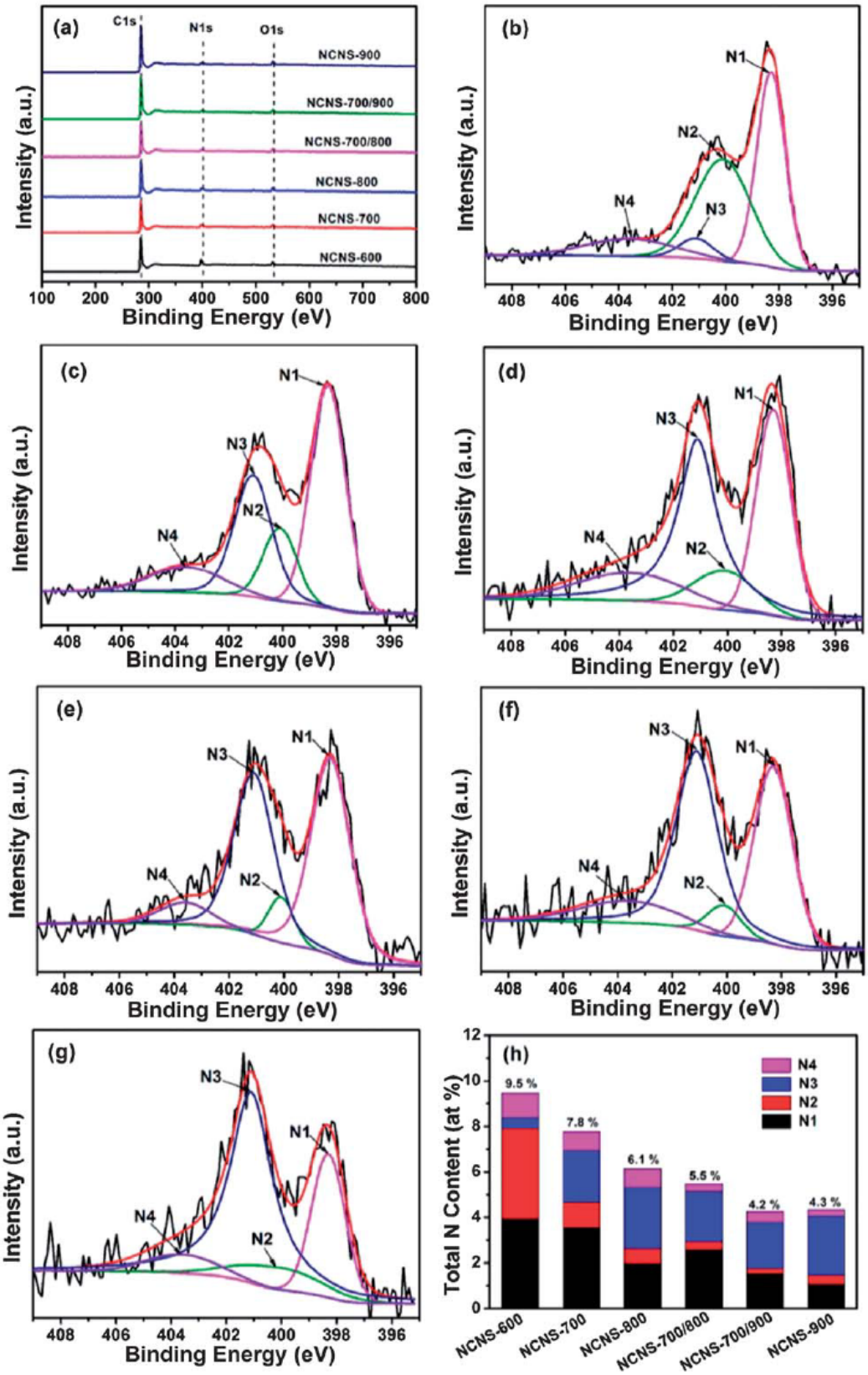

Figure 5.4 XPS survey spectra (a), N1s XPS spectra (b-g) and atomic percentages of different nitrogen species (h) for PAN derived nitrogen-doped carbon nanosheet prepared from various temperatures (from 600 °C to 900 °C) [157].

5.2.2 Morphology of nitrogen-doped graphite felts

Nitrogen doped graphite felts were prepared by performing two steps of thermal treatment on PAN coated graphite felt at 280 °C for 3 hours under ambient atmosphere and at 900 °C for 1 hour under nitrogen atmosphere. PAN is generally used as a precursor for producing carbon fibers [45,155], and Graphite felt which is used as an electrode of VRFB is also mostly fabricated using PAN as a precursor. The conventional carbonization process of carbon fiber is performed at 1000 ~ 1700 °C [45], and there is little nitrogen in the structure of the carbonized PAN at temperatures above 1000 °C. In addition, because the electrical conductivity of PAN rapidly decreased when the carbonization occurred below 1000 °C [158,159], the carbonization in this study was carried out at 900 °C to maintain the electrical conductivity and use nitrogen doping effect on PAN coating. Figure 5.5 shows the SEM images to demonstrate the surface morphologies of GF-Ref (Figure 5.5 a, b), GF-P4 (Figure 5.5 c, d) and GF-P8 (Figure 5.5 e, f). While the surface of GF-Ref without PAN coating was smooth, the coating material was easily found on the surfaces of PAN coated GF-P4 and GF-P8. Furthermore, when excess PAN was coated on the graphite felt, such as GF-P8, it was confirmed that pores of the graphite felt were blocked by the coating material derived from PAN.

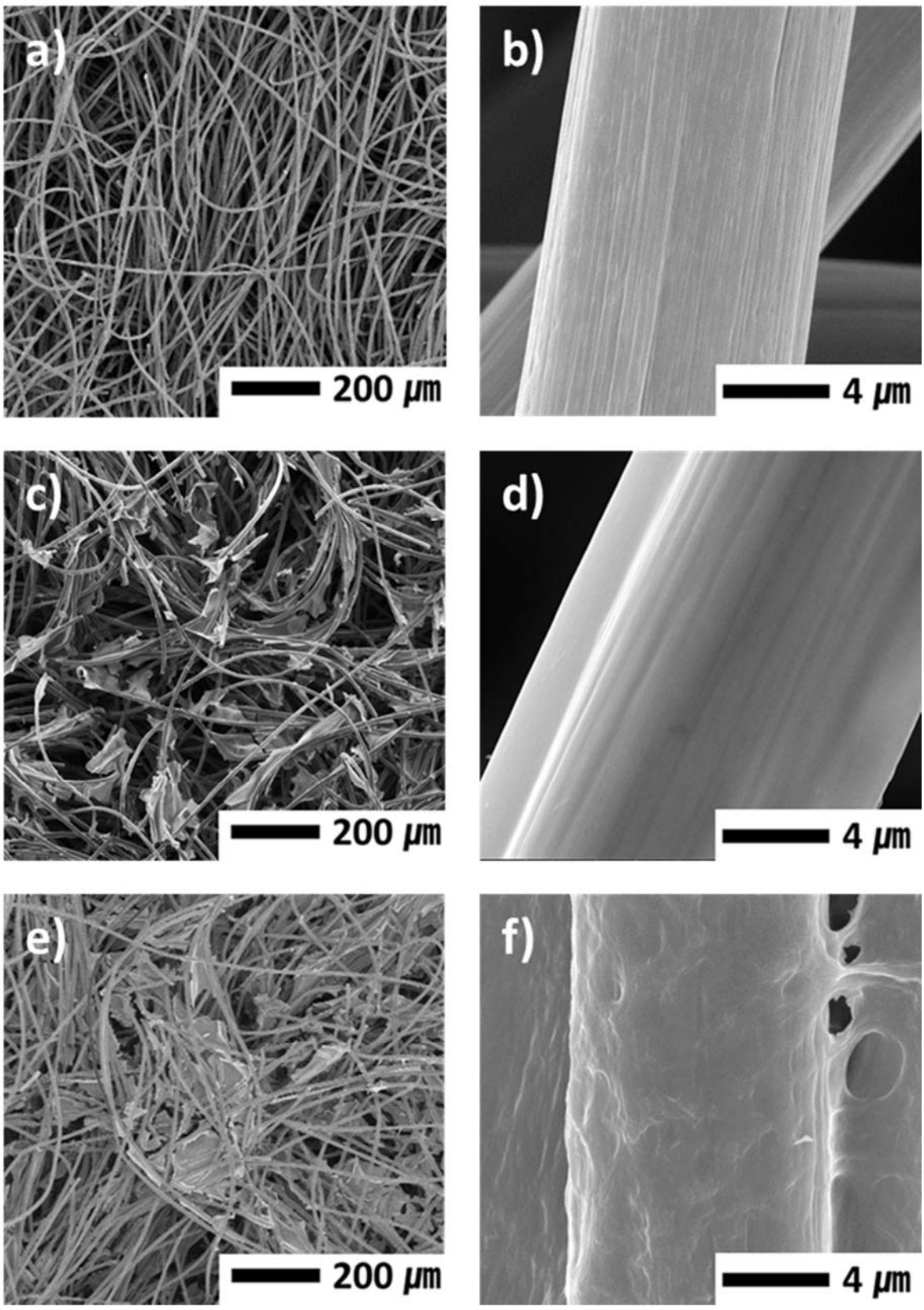

Figure 5.5 (a) SEM image of GF-Ref, (b) A magnified image of GF-Ref, (c) SEM image of GF-P4, (d) A magnified image of GF-P4, (e) SEM image of GF-P8, and (f) A magnified image of GF-P8.

5.2.3 Cyclic voltammetry analysis

Cyclic voltammetry (CV) tests were carried out using the three-electrode system in 0.05 M $VOSO_4$ + 3.0 M H_2SO_4 electrolyte to evaluate the electrochemical activity of the prepared electrodes. In cyclic voltammetry analysis, the peak potential difference ($\Delta E_p = E_{pa} - E_{pc}$), redox onset potential, the peak oxidation and reduction current and their ratio (I_{pa} / I_{pc}) are investigated to evaluate the electrocatalytic activity for the V^{4+}/V^{5+} redox reaction. For comparison purposes, CV results of GF-Ref were shown with other PAN coating samples. The peak potential difference of GF-Ref was 783 mV, and the ratio of the oxidation and reduction peak currents was 1.50. As shown in Figure 5.6, the peak potential difference of GF-P0.5 (ΔE_p = 836 mV) was higher than of GF-Ref. This result indicates that GF-P0.5 has lower electrochemical activity for the vanadium V^{4+}/V^{5+} redox reaction than GF-Ref. GF-Ref with the oxygen functional groups prepared by the conventional heat treatment method in the air at 400 °C for 30h showed better performance than GF-P0.5 coated with the little amount of PAN. However, as the amount of PAN coated on the graphite felt increased, the electrochemical performance increased, showing better electrochemical activity and reversibility for GF-P4 (ΔE_p = 711 mV, I_{pa} / I_{pc} = 1.31) than those for GF-Ref.

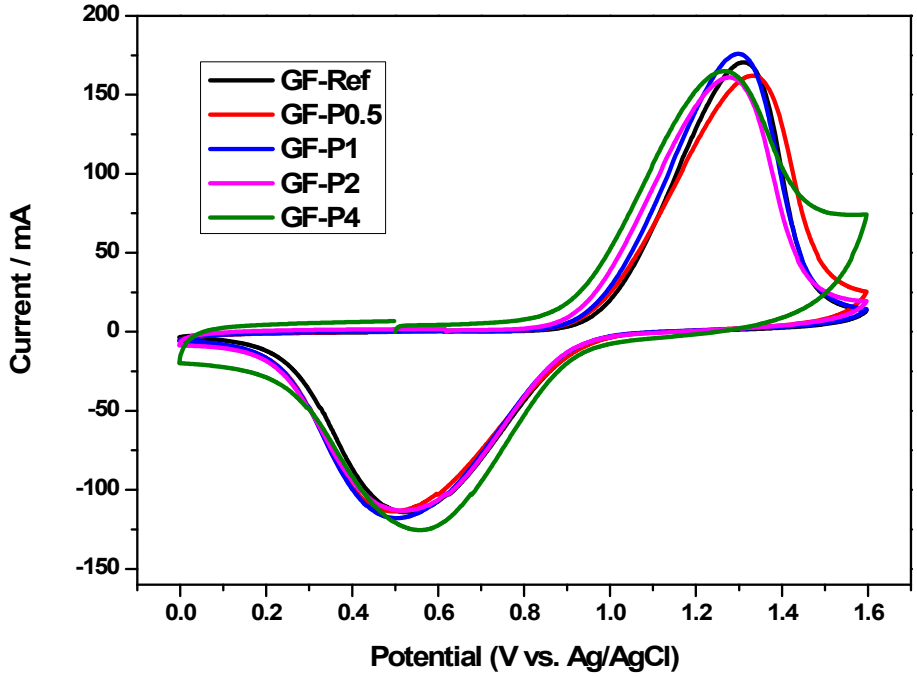

Figure 5.6 Cyclic voltammograms of GF-Ref and PAN coating graphite felts with different loading in 0.05M $VOSO_4$ + 3.0M H_2SO_4 electrolyte at a scan rate of 30 mV s^{-1} with potential window of 0.0 V to 1.6 V vs. Ag/AgCl, i.e. for the V^{4+}/V^{5+} redox reactions.

5.2.3 XPS characterization

To verify the effect of PAN coating to improve the electrochemical activity, XPS analysis was carried out for the prepared electrodes. According to the survey XPS spectra as shown in Figure 5.7a, it was difficult to identify nitrogen peaks in the GF-Ref. For the case of PAN coated graphite felt, a nitrogen peak could be observed and the elemental compositions are summarized in Table 5.1. GF-Ref, GF-P4 and GF-P8 showed nitrogen contents of 0.5, 5.2, and 5.4 at%, respectively. These results confirm that the graphite felt was doped with nitrogen through the PAN coating. In addition, even if the amount of PAN coating increased, the nitrogen content of the PAN coated electrode surface does not increase significantly. To investigate the effect of the nitrogen doping on the PAN coated graphite felt, the N 1s spectra were deconvoluted into four peaks, which corresponded to pyridinic N (398.2 eV), pyrrolic N (399.5 eV), quaternary N (401.1 eV) and oxidized N (402.6 eV) [157,160] as shown in Figure 5.7b and c. The contents of N in the PAN-coated graphite felt electrodes are illustrated in Table 5.2. According to Table 5.2, the amount of quaternary N was the highest among various nitrogen

forms in PAN-coated graphite felt, but the composition of the nitrogenous forms of GF-P4 showed different results from that of GF-P8. As the amount of PAN coating increased, the amount of pyridinic N decreased while the amount of pyrrolic N and oxidized N increased. These results indicate that nitrogen atoms were successfully incorporated into the carbon structure. It is known that nitrogen-doped carbon materials improve their electrical conductivity and oxidation stability [150-154]. The strong electronic affinity of the nitrogen atoms causes modification of the electronic properties of carbon atoms, which enhance the electron transfer between the graphite felt electrode and vanadium ions and improve the wettability of the electrolyte [29,34]. Therefore, nitrogenous groups in the electrode surface improve the electrocatalytic activity of the felt for vanadium redox reaction.

Table 5.1 Elemental composition of PAN coating graphite felt electrodes

Sample	Carbon (at. %)	Nitrogen (at. %)	Oxygen (at. %)
GF-Ref	92.7	0.5	6.8
GF-P4	91.5	5.2	3.3
GF-P8	91.2	5.4	3.4

(a)

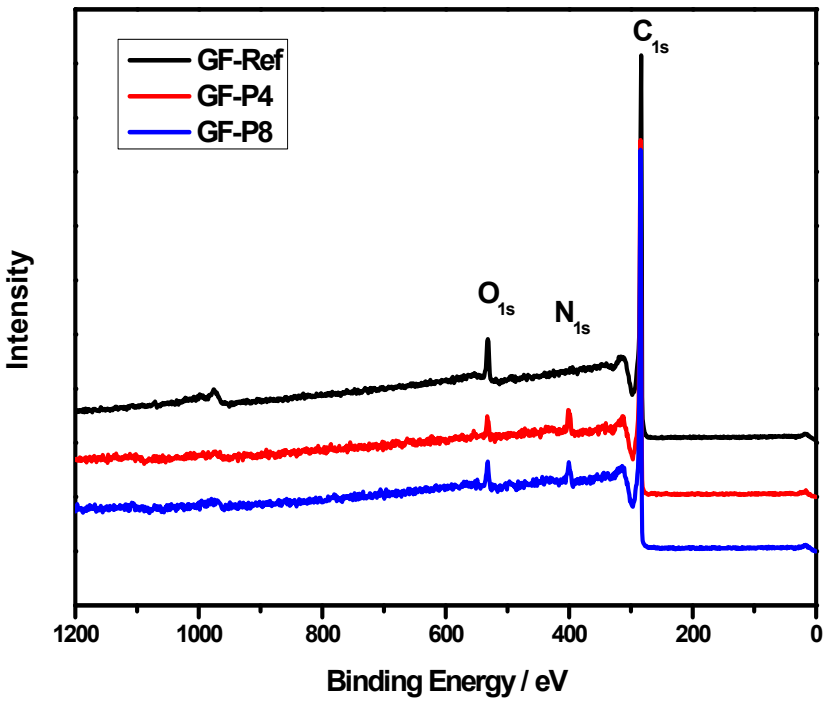
GF-Ref
GF-P4
GF-P8
C1s
O1s
N1s
Intensity
1200
1000
800
600
400
200
0
Binding Energy / eV

(b)

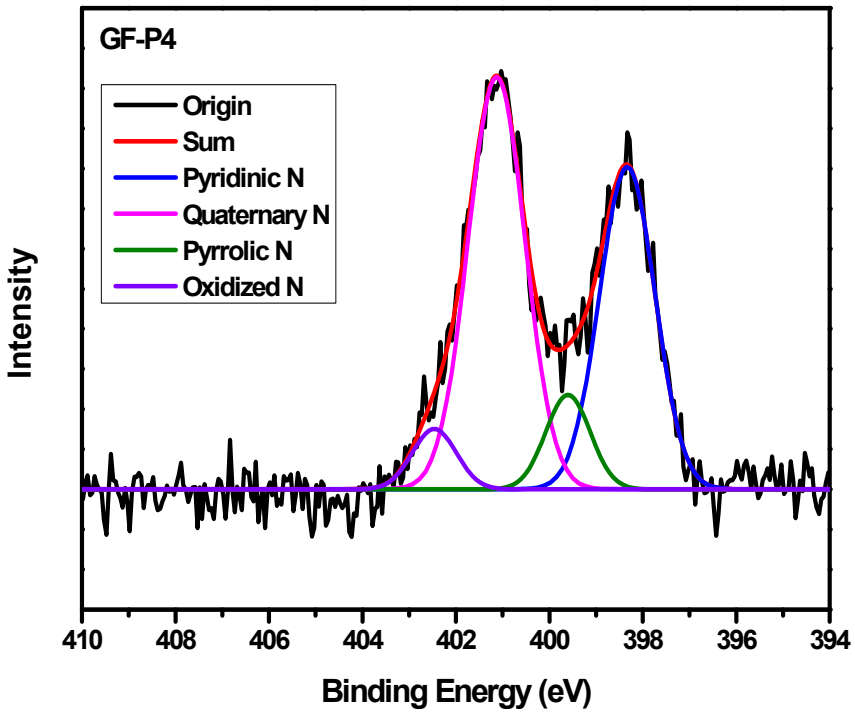
GF-P4
Origin
Sum
Pyridinic N
Quaternary N
Pyrrolic N
Oxidized N
Intensity
410
408
406
404
402
400
398
396
394
Binding Energy (eV)

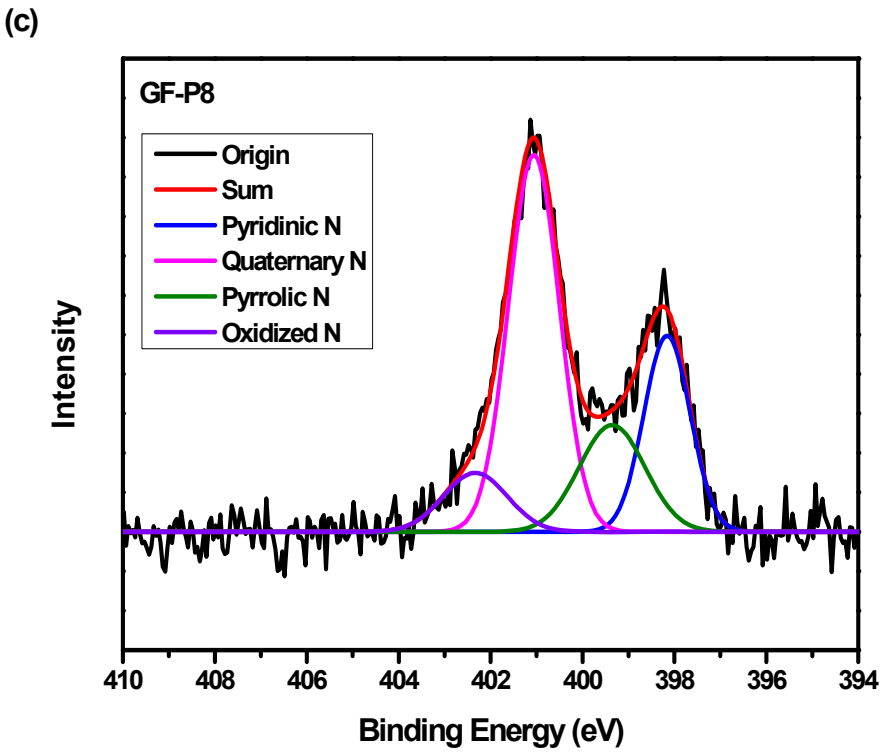

Figure 5.7 (a) Survey XPS spectra of GF-Ref, GF-P4 and GF-P8 (b) N1s XPS spectra of GF-P4 (c) N1s XPS spectra of GF-P8

Table 5.2 The contents of N form in the PAN coating graphite felt electrodes

Sample	Pyridinic N (at. %)	Pyrrolic N (at. %)	Quaternary N (at. %)	Oxidized N (at. %)
GF-P4	37.1	8.7	48.6	5.5
GF-P8	23.3	18.1	49.0	9.6

5.2.4 Charge/discharge test

Charge/discharge experiments were carried out using a VRFB single cell to verify the improved electrochemical activity for the nitrogen doping graphite felt electrodes. The rate performances were measured by varying the current density from 25 to 150 mA cm^{-2}. First, the charge/discharge test was carried out with oxidized PAN-coated graphite felts which had been

coated with 0.5 wt% PAN solution and heated at 280°C for 3 hours under atmosphere in a box furnace, named as O-GF-P0.5. As shown in Figure 5.8, however, the charge/discharge results could not be obtained at the current densities of more than 125 mA cm^{-2}. In the case of coulombic efficiency (CE), the results of the cell using the O-GF-P0.5 sample and the reference cell with GF-Ref are almost similar. In the case of the O-GF-P0.5 sample, it can be confirmed that the CE value is slightly higher than GF-Ref, which is a result when the charging and discharging proceeds relatively fast at low current densities due to the high overpotential. In the case of voltage efficiency (VE) and energy efficiency (EE), efficiencies of the cell using O-GF-P0.5 decrease more than those of the cell using GF-Ref as the current density increases. In particular, at a current density of 100 mA cm^{-2}, the EE of cell using GF-Ref was 79%, whereas the EE of cell with O-GF-P0.5 was only 64%. These results show that the O-GF-P0.5 electrode has lower electrode performance than the GF-Ref electrode, indicating that the oxidation treatment of PAN-coated graphite felt which is heated at 280°C for 3 hours under atmosphere is not suitable for increasing the VRFB performance.

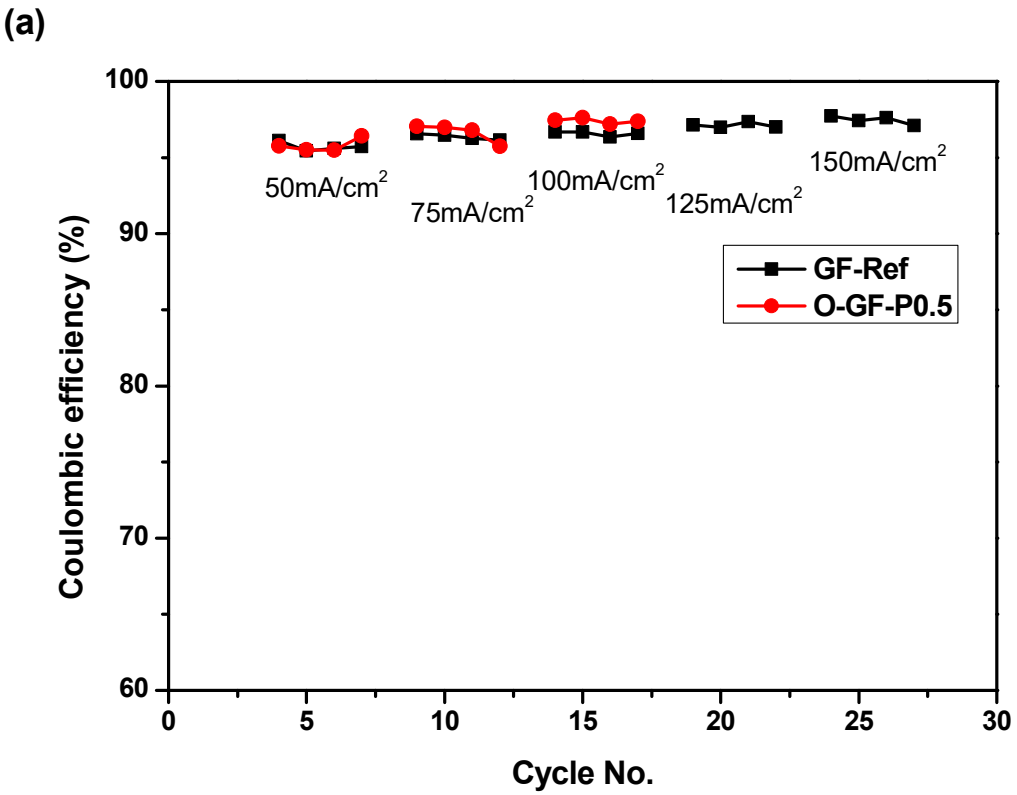

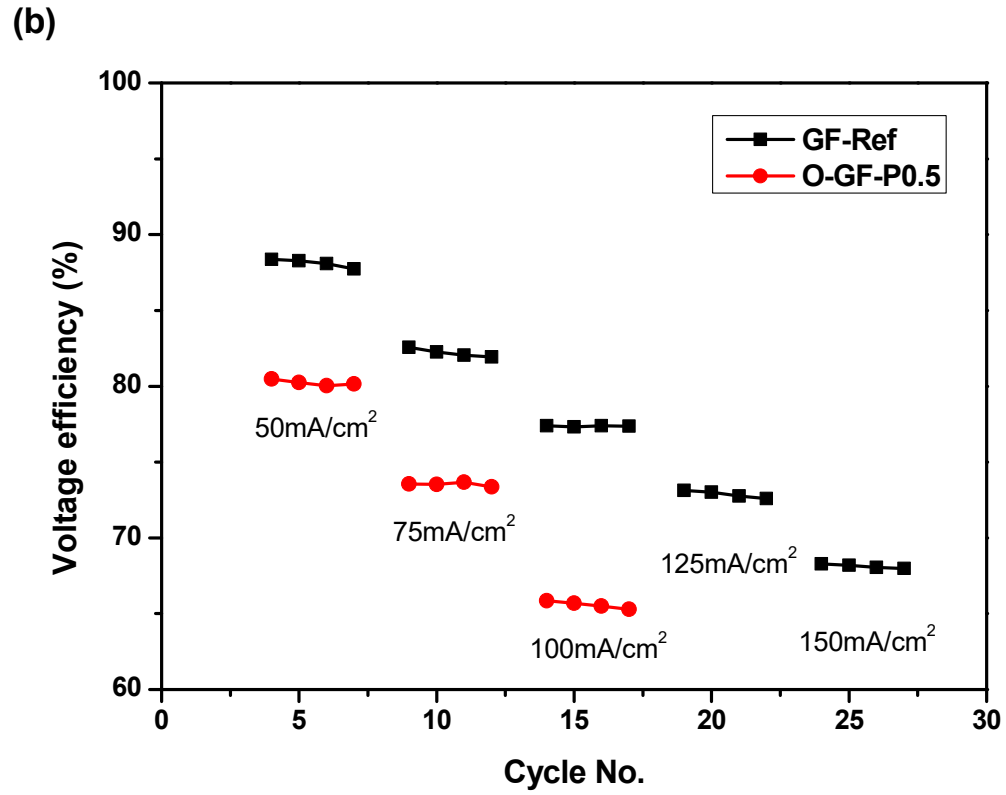

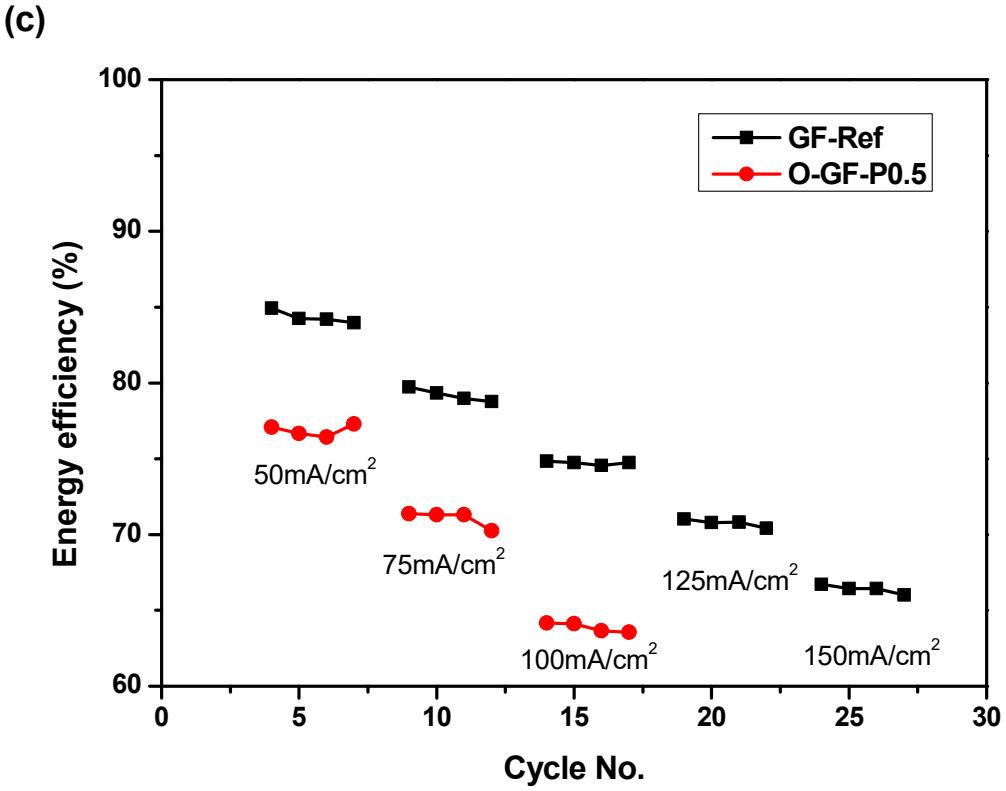

Figure 5.8 Cycling performance of VRFBs employing GF-Ref and O-GF-P0.5 at different current densities; (a) coulombic efficiency, (b) voltage efficiency, and (c) energy efficiency.

Figure 5.9 shows the charge-discharge curves at a constant current density of 100 mA cm^{-2}. When the charge/discharge process was performed with an upper limiting voltage of 1.6 V, the VRFB cell employing the O-GF-P0.5 electrode was only charged and discharged for a very short time and exhibited much lower charge/discharge capacities than the GF-Ref electrode prepared by the conventional heat treatment method. When O-GF-P0.5 was used as the electrode, the discharge capacity decreased to about one fifth, from 293.3 mAh to 58.9 mAh, and the voltage loss at the beginning of discharge process increased by 204 mV compared to GF-Ref at the current density of 100 mA/cm^{-2}.

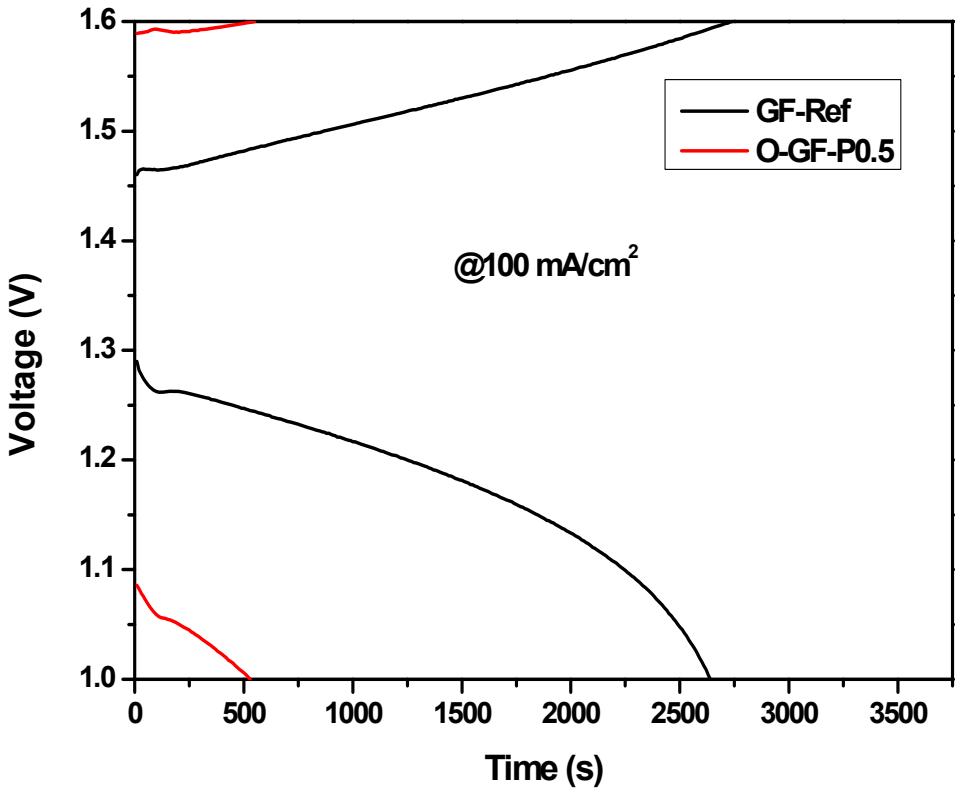

Figure 5.9 Charge/discharge curves for VRFBs employing GF-Ref and O-GF-P0.5 at the current density of 100 mAcm^{-2}.

Second, the charge/discharge tests were carried out with carbonized PAN coating graphite felts which had been coated with 0.5 wt% and 1 wt% PAN solution and heated at 900°C for 1

hour under nitrogen atmosphere, named as C-GF-P0.5 and C-GF-P1, respectively. Figure 5.10 shows the charge/discharge curves at a constant current density of 100 mA cm^{-2}. When the charge/discharge process was performed with an upper limiting voltage of 1.6 V, the VRFB cells employing the C-GF-P0.5 and C-GF-P1 electrodes exhibited lower charge/discharge capacities than the GF-Ref electrode prepared by the conventional heat treatment method. When C-GF-P0.5 and C-GF-P1 were used as the electrodes, the discharge capacities decreased from 293.3 mAh to 256.7 mAh, and the voltage loss at the beginning of discharge process increased by 80 mV, from 1.29 V to 1.21 V, at the current density of 100 mA cm^{-2} compared to GF-Ref.

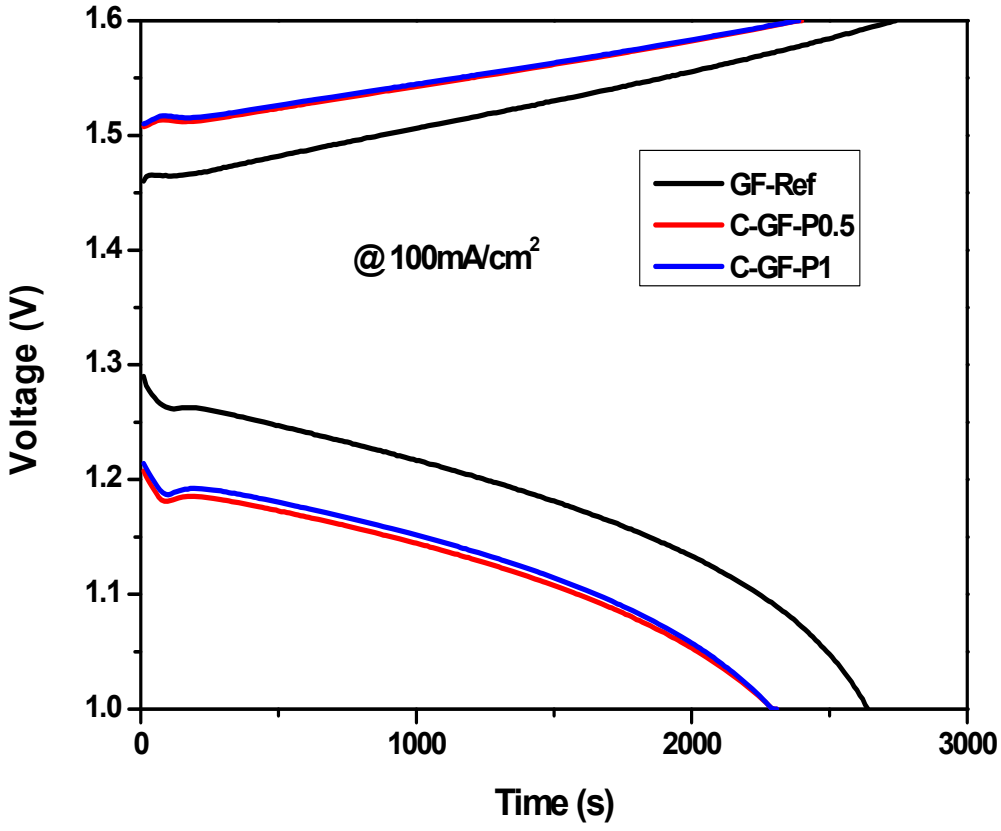

Figure 5.10 Charge/discharge curves for VRFBs employing GF-Ref, C-GF-P0.5 and C-GF-P1 at the current density of 100 mAcm^{-2}.

Figure 5.11 shows the coulombic efficiency (CE), voltage efficiency (VE), and energy efficiency (EE) of the VRFBs at various current densities during the charge-discharge cycles. However, the charge/discharge results could not be obtained at the current densities of 150 mA cm^{-2} because of the high overpotential of carbonized PAN coated graphite felt electrodes. There was no notable difference between the CE values (~96%) of all prepared electrodes. In the case of voltage efficiency (VE) and energy efficiency (EE), efficiencies of the cells using C-GF-P0.5 and C-GF-P1 decrease more than those of the cell using GF-Ref as the current density increases. At a current density of 125 mA cm^{-2}, the EE of cell using GF-Ref was 71%, whereas the EE of cells with C-GF-P0.5 and C-GF-P1 was only 64%. In particular, as confirmed in the 100 mA cm^{-2} charge/discharge curve, no difference in efficiencies was found depending on the concentration of the PAN solution at the overall current densities. These results show that carbonized PAN-coated graphite felt electrodes have lower electrode performance than the GF-Ref electrode, indicating that the carbonization treatment of PAN-coated graphite felt which is heated at 900°C for 1 hours under nitrogen atmosphere is not suitable for increasing VRFB performance.

(a)

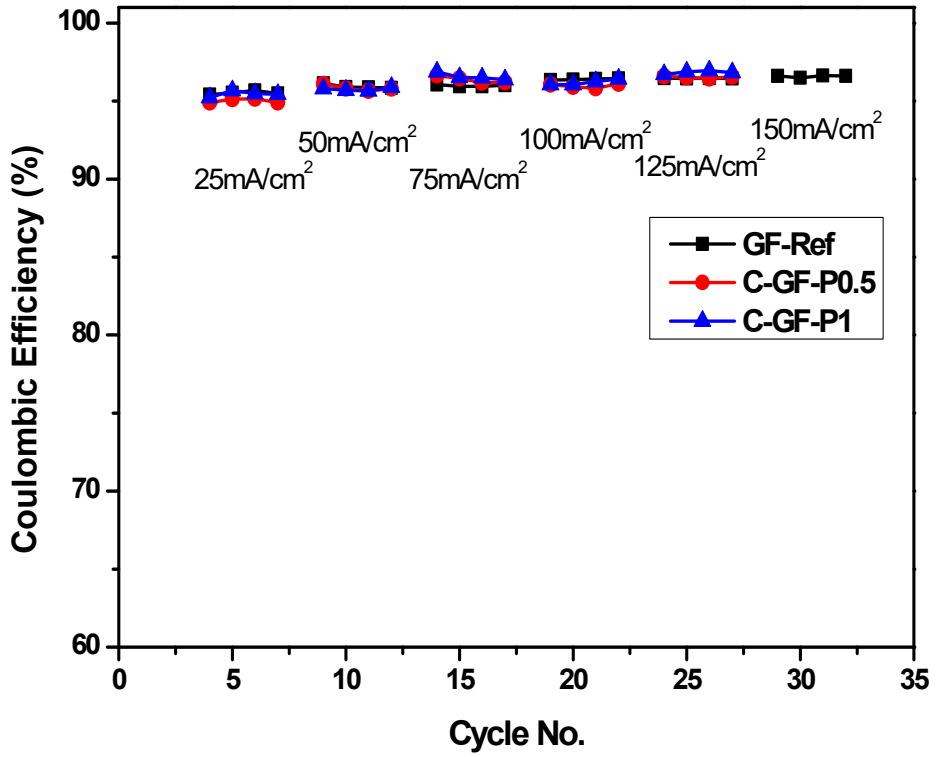
Coulombic Efficiency (%)
Cycle No.
25mA/cm2
50mA/cm2
75mA/cm2
100mA/cm2
125mA/cm2
150mA/cm2
GF-Ref
C-GF-P0.5
C-GF-P1

(b)

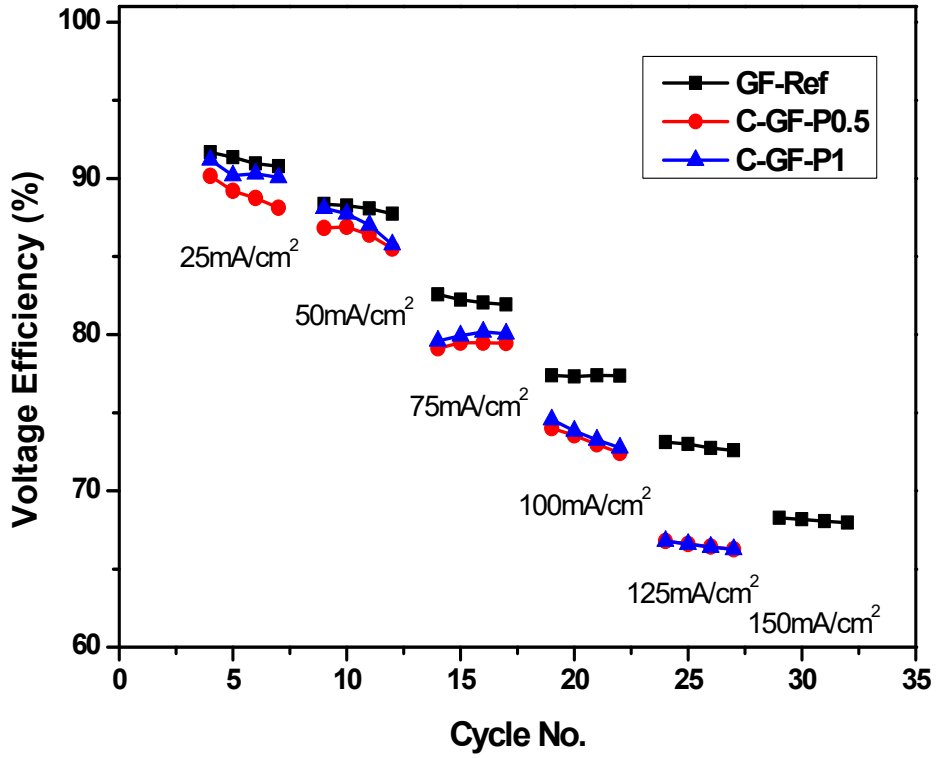
Voltage Efficiency (%)
Cycle No.
25mA/cm2
50mA/cm2
75mA/cm2
100mA/cm2
125mA/cm2
150mA/cm2
GF-Ref
C-GF-P0.5
C-GF-P1

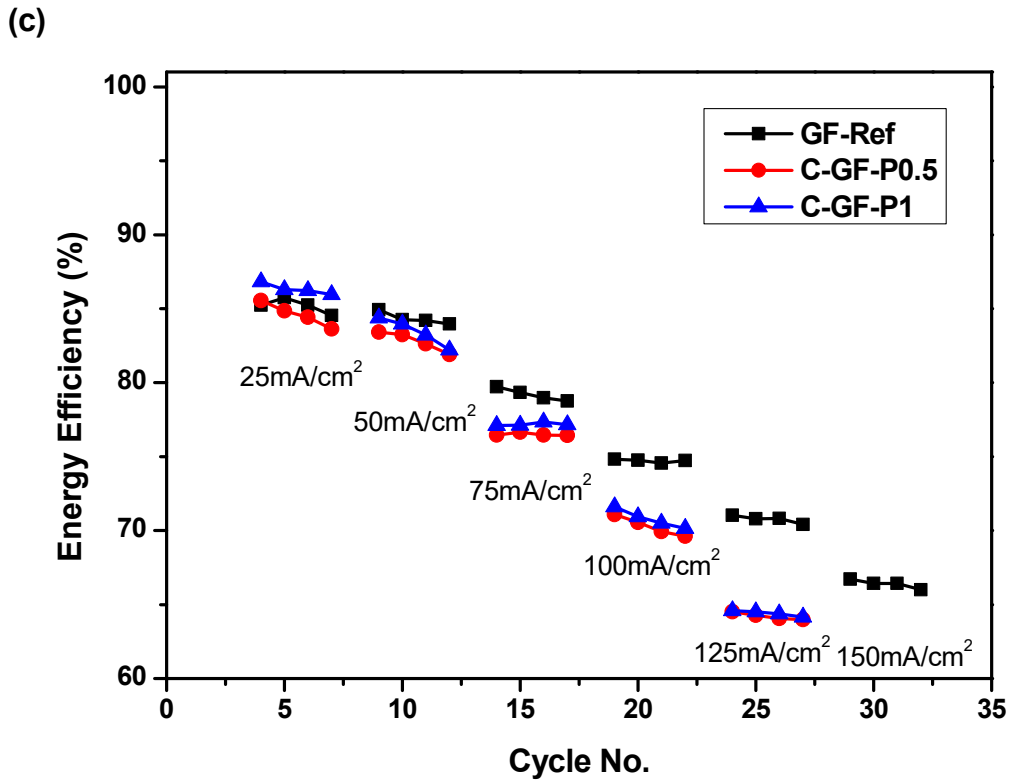

Figure 5.11 Cycling performance of VRFBs employing GF-Ref, C-GF-P0.5 and C-GF-P1 at different current densities; (a) coulombic efficiency, (b) voltage efficiency, and (c) energy efficiency.

Third, the charge/discharge tests were carried out with PAN-coated graphite felt electrodes which had been both oxidized and carbonized at 280°C and at 900°C, respectively. The prepared graphite felt samples were named GF-P0.5 (PAN 0.5 wt%), GF-P1 (PAN 1 wt%), GF-P2 (PAN 2 wt%) and so on according to the concentration of PAN. The rate performances were measured by varying the current density from 25 to 150 mA cm^{-2}. Figure 5.12 shows the charge/discharge curve at a constant current density of 150 mA cm^{-2}. When the charge-discharge process was performed with an upper limiting voltage of 1.6 V, the VRFB cells employing the PAN-coated electrodes exhibited a tendency to increase the charge and discharge capacities as the coating amount of the PAN increased. When GF-P4 which showed the highest charge and discharge capacity was used as the electrode of VRFB, the discharge capacity increased by 87%, from 123.3 mAh to 230 mAh, and the voltage loss at the beginning of discharge process decreased by 89 mV compared to GF-Ref at the current density of 150 mA/cm^{-2}. However, when increasing the concentration of coated PAN up to 8 wt% (GF-P8),

the VRFB cell using GF-P8 showed reduced charge and discharge capacity. In the case of GF-P8, as confirmed in the previous SEM image, excessive PAN coating on the graphite felt decreased the pores of the graphite felt and interfered with mass transport [161], which resulted not only in increasing voltage loss but also in reducing the charge and discharge capacity.

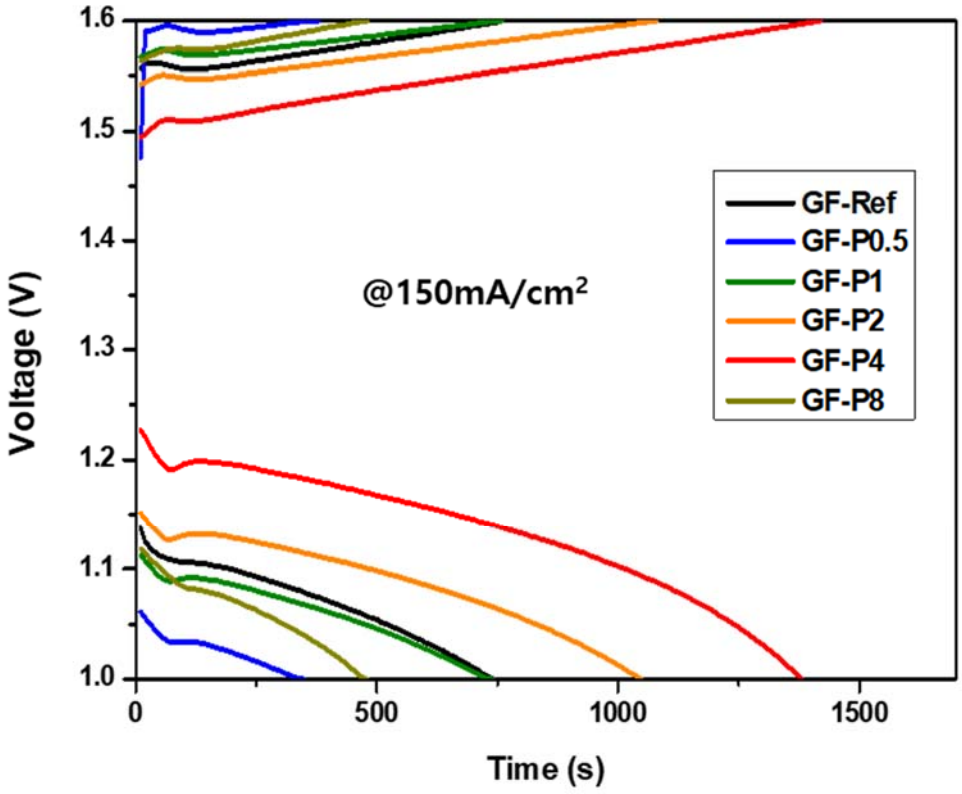

Figure 5.12 Charge/discharge curves for VRFBs employing the graphite felts coated with various amounts of PAN at the current density of 150 mA/cm^{-2}.

Figure 5.13 shows the coulombic efficiency (CE), voltage efficiency (VE), and energy efficiency (EE) of the VRFBs at various current densities during the charge/discharge cycles. In the case of the CE result, the difference between the prepared samples was not noticeable, and it could be confirmed that they were maintained constant at the overall current densities. However, the VE of cells with PAN-coated electrodes increased from 64% to 73% (GF-Ref, 68%) at 150 mA cm^{-2} as the amount of PAN coating increases, indicating that electrodes coated with sufficient amounts of PAN have improved the electrochemical activity of the graphite felt for the vanadium redox reaction. Finally, the cells with the optimized amount of PAN-coated electrodes (GF-P4) showed about 5% higher energy efficiencies, from 66% to 71%, than the cell using GF-Ref at 150 mA cm^{-2}.

(a)

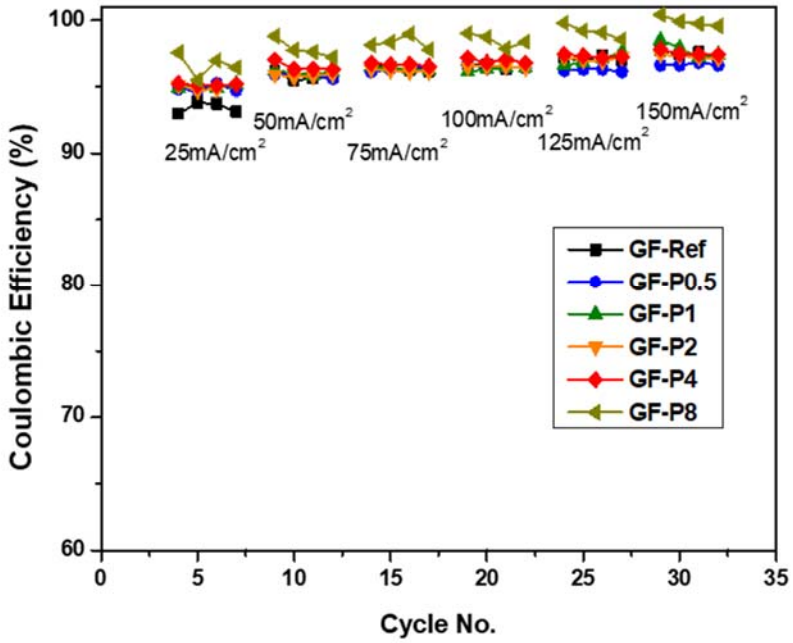

(b)

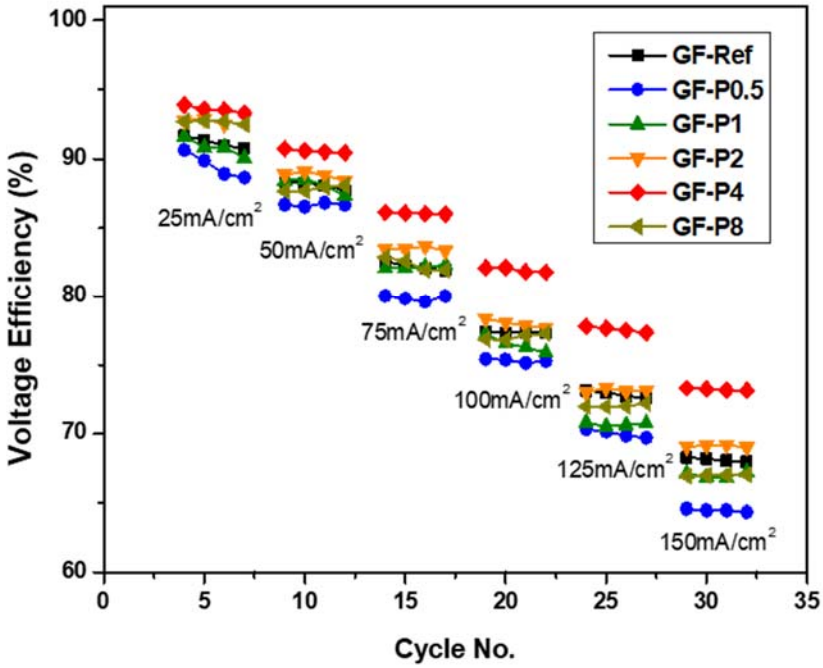
Voltage Efficiency (%)
Cycle No.
GF-Ref
GF-P0.5
GF-P1
GF-P2
GF-P4
GF-P8
25mA/cm2
50mA/cm2
75mA/cm2
100mA/cm2
125mA/cm2
150mA/cm2

(c)

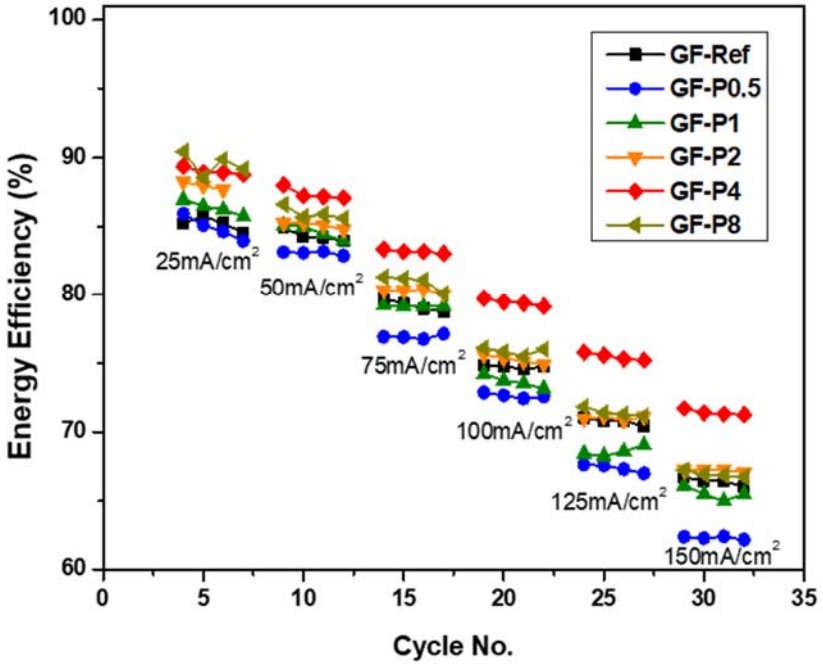
Energy Efficiency (%)
Cycle No.
GF-Ref
GF-P0.5
GF-P1
GF-P2
GF-P4
GF-P8
25mA/cm2
50mA/cm2
75mA/cm2
100mA/cm2
125mA/cm2
150mA/cm2

Figure 5.13 Cycling performance of VRFBs employing the graphite felts coated with various amounts of PAN at different current densities; (a) coulombic efficiency, (b) voltage efficiency, and (c) energy efficiency.

Figure 5.14 shows the efficiencies and discharge capacities for the cells with GF-P4 and GF-Ref during 100 charge/discharge cycles at 100 mA cm^{-2}. In CE results, no obvious difference was observed for 100 cycles. As shown in Figure [W3] 5.14 (b), GF-P4 presents higher VE (from 81% to 75%) than GF-Ref (from 77% to 71%) during 100 cycles. Although the EE of cell with GF-P4 decreased after 100 cycles, it showed stable higher EE than that of GF-Ref during the charge / discharge test. As shown in Figure 5.14 (d), since the VE and EE of the cell with GF-P4 were higher than that of GF-Ref, it exhibited higher discharge capacity during the 100 cycle charge and discharge test. After 100 charge-discharge cycles, the discharge capacity of the cell with GF-P4 was maintained at 77.5%, while the discharge capacity of GF-Ref was reduced to 64.8% from the initial discharge capacity. These results indicate that the PAN coating not only enhances the electrochemical activity but also remains stable during the charge / discharge test.

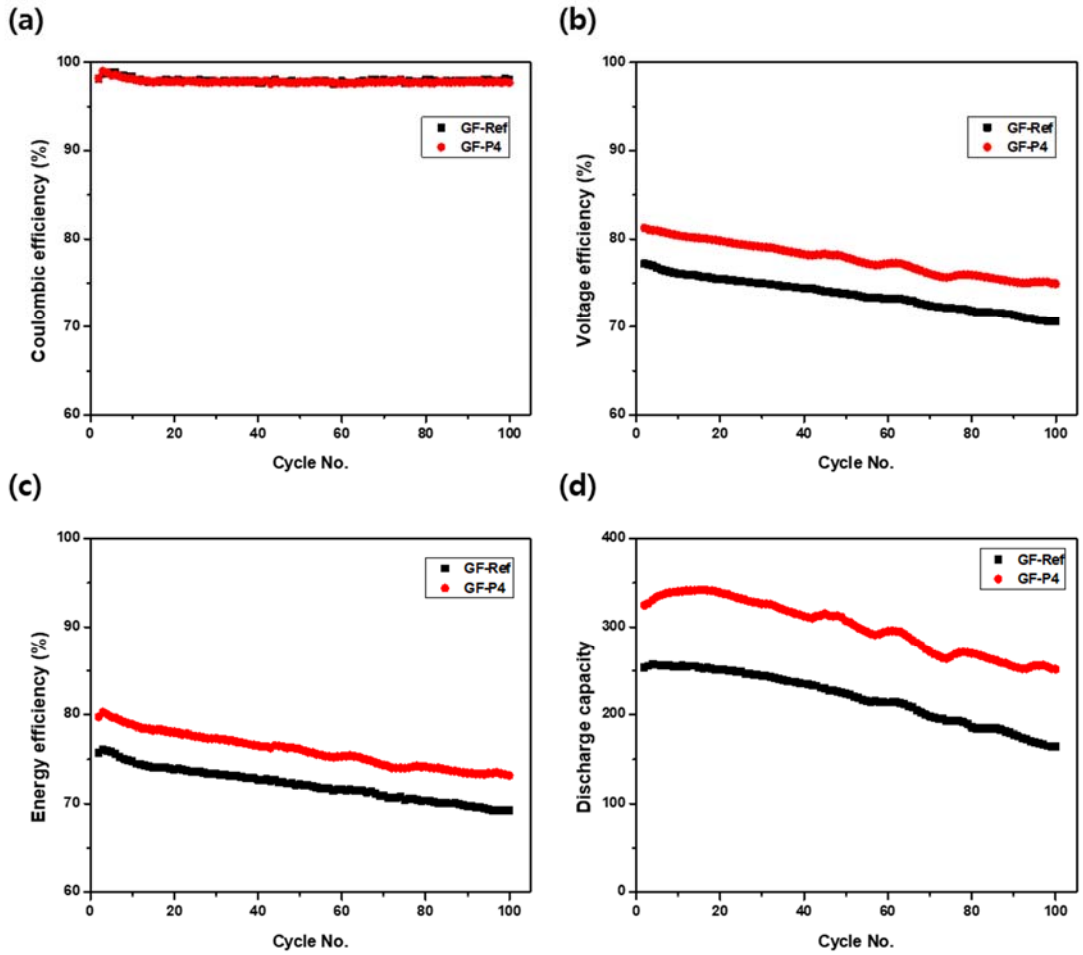

Figure 5.14 Cycling stability of VRFBs with GF-Ref and GF-P4 at the current density of 100 $mAcm^{-2}$; (a) coulombic efficiency, (b) voltage efficiency, (c) energy efficiency, and (d) discharge capacity.

5.2.5 Conclusion

In order to fabricate nitrogen-doped graphite felt electrodes by coating polyacrylonitrile (PAN), two steps of thermal treatment were performed. The graphite felt coated with PAN was heated at 280°C for 3 hours under ambient atmosphere and then carbonized at 900°C for 1 hour under nitrogen atmosphere. According to the experimental results, it was found that the surface of the graphite felt was successfully coated with a nitrogen-containing carbon material. From the results of CV, it was confirmed that the electrochemical activity and reversibility increased with increasing PAN content. The charge-discharge test results showed that PAN-coated graphite felt had higher performance than GF-Ref through PAN coating amount optimization. When 4 wt% PAN solution coated graphite felt (GF-P4) which showed the highest charge and

discharge capacity was used as the electrode of VRFB, the discharge capacity increased by 87%, from 123.3 mAh to 230 mAh. The cell with the optimized amount of PAN coated electrodes (GF-P4) showed about 5% higher energy efficiencies, from 66% to 71%, than the cell using GF-Ref at 150 mA cm^{-2}. In addition, the capacity retention and energy efficiency of the cell with GF-P4 were higher than those of GF-Ref after 100 charge/discharge cycle test, which indicates that the PAN coating not only enhances the electrochemical activity but also remains stable during the charge / discharge test.

6. Optimization of local porosity in the electrode as an advanced channel for all-vanadium redox flow battery

In the previous works, the modifications of the electrode surface by introducing nitrogen-doped carbon materials were performed to improve the electrochemical properties of the surface of the electrode, leading to enhance the performance of VRFBs. On the other hand, the appropriate distribution of electrolyte by controlling the electrode structure and the flow field of bipolar plate is also important, because it is related to the reactant supply and the product removal near the electrode surface. In this chapter, optimization of local porosity of the graphite felt electrode was carried out to improve the power density of VRFBs. Three porous electrodes were considered: uniform porosity, low porosity at the electrolyte inlet, and low porosity at the electrolyte outlet. Because the theoretical operating voltage of VRFBs is lower than other commercial rechargeable batteries, we tried to increase the power density of VRFBs by improving the energy efficiency in the high current density region through optimization of the local porosity of the electrode. First, the electrolyte flow field of VRFB with different electrode design was analyzed numerically. Second, the relationship between electrode porosity and current density was identified by examining the variation of charge/discharge curves and energy efficiencies of the VRFB with varying current densities. In addition, the effect of flow rate on VRFB performance under various electrode design was investigated in high current density region. Finally, we proposed an empirical equation for the optimal distribution of local porosity according to current densities.

6.1 Experimental

In this study, we developed a two-dimensional simulation model to analyze the flow field of the electrolyte in three different porous electrodes. Furthermore, the performance of VRFBs was experimentally measured for the porous electrodes at various current densities.

6.1.1 Electrode designs

In VRFBs, the electrode acts as the site for the electrochemical reaction. Therefore, previous studies focused on treating the electrode surface to increase the surface area. At the high current density region, however, the supply of reactants and the removal of products become

the most important factor for electrochemical reaction. Therefore, we tried to improve the mass transport of electrolyte in the electrode by controlling local porosity of the electrode. That is, we studied the role of the electrode as a channel of the electrolyte to enhance the power density of VRFB. Three different electrode designs as shown in Figure 6.1 were considered. An electrode with uniform porosity (UP) was prepared as reference. Then we prepared an electrode with low porosity at the inlet of electrolyte (LPI) by adding a piece of carbon felt there. A third electrode with low porosity at the electrolyte outlet (LPO) was also prepared similarly.

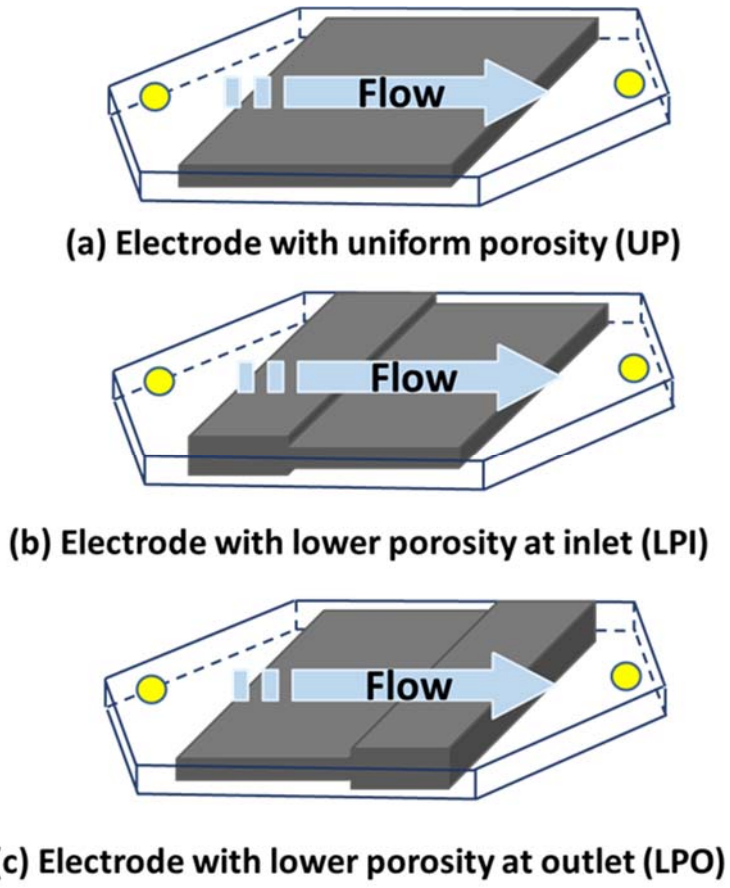

Figure 6.1 Different channel designs in porous electrodes.

6.1.2 Single cell test

An experimental setup was designed to investigate the performance of VRFBs with different electrodes. A single cell assembly of VRFBs is presented in Figure 6.2(a). A cell with an active area of 5 cm × 5 cm was used in this study. The positive and negative electrode chambers were constructed of PVC frame, and a Nafion® 115 membrane sandwiched by carbon felt divided each chamber.

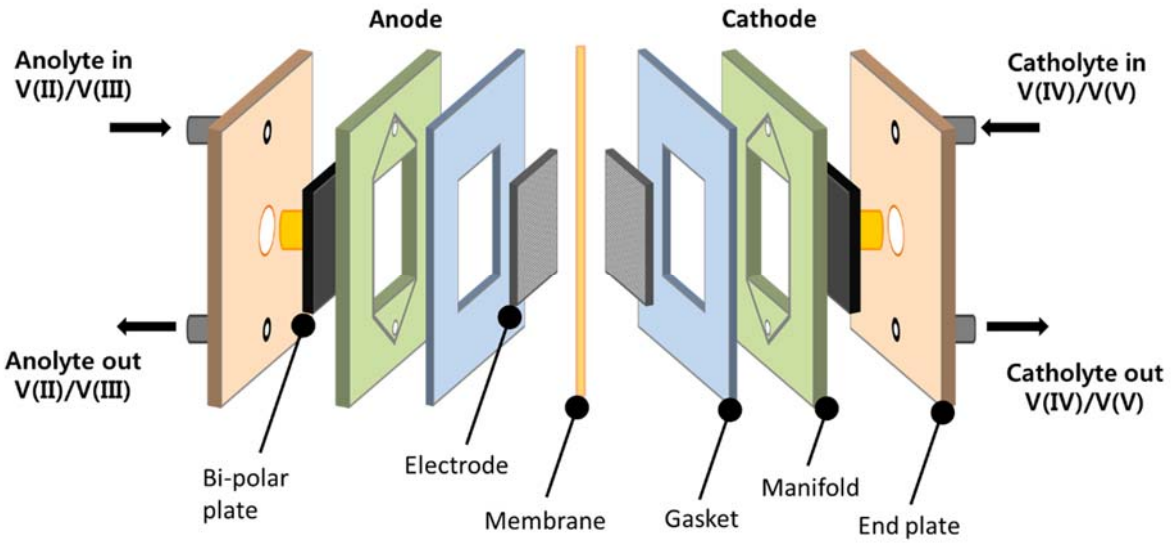

(a) Schematic diagram of all-vanadium flow battery single cell assembly structure

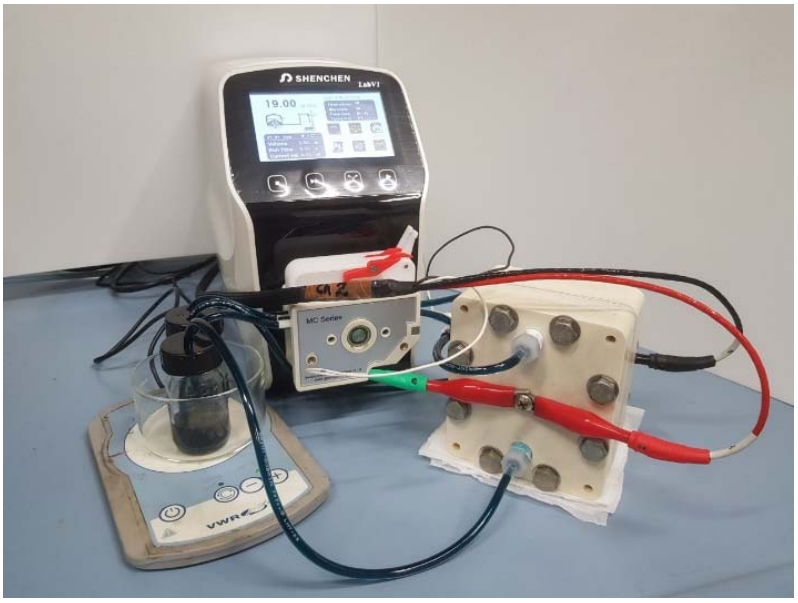

(b) Picture of experimental setup

Figure 6.2 Images of all-vanadium redox flow battery experiment

Carbon felt (SGL group, GFD4.6 EA) was used as the electrode material to provide reaction sites and channel for the electrolyte. The carbon felts were soaked in 3 M H_2SO_4 for 24 h, dried in a hood at 30 °C, and then heated at 400 °C for 30 h to functionalize their surface. We prepared 3 different types of electrodes. The porosity of the UP electrode (50 mm × 50 mm × 4.6 mm) is 0.94. This electrode was compressed to 3 mm-thick and introduced to the single cell. Next, we prepared the LPI electrode by adding another piece of carbon felt (50 mm × 15 mm × 2.3 mm) at the electrolyte inlet of the UP electrode, and also compressed it to 3 mm before use. This way, the electrolyte inlet in the VRFBs is more compressed (i.e., lower porosity). Lastly, we prepared the LPO electrode that has a lower porosity at the outlet, by adding a piece of carbon felt with a thickness of 2.3 mm to the UP electrode before compression. Graphite bi-polar plate and copper current collector were connected to the carbon felt. The electrolyte contained 1.6 M V^{3+} and 1.6 M V^{4+} dissolved in 3 M H_2SO_4 (30 mL).

The experimental setup is shown in Figure 6.2(b). We conducted charge/discharge cycle tests to examine the effect of electrode design with locally controlled porosity on the performance of VRFBs, by varying the electrolyte flow rate from 13 to 25 mL/min and the current density from 50 to 150 mA/cm^2. The cut-off voltages of charging and discharging (1.6 and 1.0 V, respectively) were controlled by a potentiostat provided by Wonatech. The performance of VRFBs was evaluated in terms of the Coulomb, energy, and voltage efficiencies (CE, EE, and VE, respectively) expressed as follows.

$$CE = \frac{Discharge\ capacity(Ah)}{Charge\ capacity(Ah)} \times 100\% \qquad (6-1)$$

$$EE = \frac{Discharge\ energy(Wh)}{Charge\ energy(Wh)} \times 100\% \qquad (6-2)$$

$$VE = \frac{EE}{CE} \times 100\% \qquad (6-3)$$

6.1.3 Flow field modeling

Although vanadium ions are consumed and produced during the reaction, the volume change due to these reactions does not affect the total amount of electrolyte and is therefore ignored in this study. Then, transport of electrolyte in the porous electrode can be modeled by adding a sink term to the Navier-Stokes equations [162-164].

$$\frac{\partial}{\partial t}(\varepsilon\rho u_i) + u_j \frac{\partial}{\partial x_j}(\rho u_i) = -\frac{\partial p}{\partial x_i} + \mu \frac{\partial \tau_{ij}}{\partial x_j} + S_i \quad (6-4)$$

Here, u is the local velocity, ε is the porosity of electrode, and ρ is the density of electrolyte. μ is the dynamic viscosity, and τ is the shear stress acting on the electrolyte. Subscripts i and j represent the x and y components, respectively. For the pressure gradient within the porous media, the first term in the right-hand side of eq. (6−4) is expressed as the Darcy-Forchheimer equation, which is the Darcy's law plus the viscous effects of the fluid:

$$-\frac{\partial p}{\partial x_i} = (\frac{\mu}{k} + \beta\rho|u|)u \quad (6-5)$$

Here, k is the permeability of the porous electrode, and β is the non-Darcy coefficient. The sink term, S_i, is introduced to describe the viscosity and inertial loss, as shown below.

$$S_i = (\mu d + f\frac{1}{2}\rho|u|)u \quad (6-6)$$

Here, d and f are the porosity parameters and expressed as follows

$$d = \frac{1}{k} \quad (6-7)$$

$$f = 2\beta \quad (6-8)$$

By considering conservation of mass in eq. (6−9), we can analyze the electrolyte flow field within the porous electrode.

$$\frac{\partial \rho}{\partial t} + \frac{\partial \rho u_i}{\partial x_j} = 0 \quad (6-9)$$

All parameter values associated with the simulation are listed in Table 6.1. In this study, the

open source software, OpenFOAM version 2.1.2, was used for the two-phase flow simulation within a porous electrode.

Table 6.1 Parameters of the electrode and electrolyte used in this study

Parameters	Value
Thickness of the electrode	3 mm
Porosity of the normal electrode	0.67
Porosity of the compressed electrode	0.33
Viscosity of the electrolyte	4.928×10^{-3} Pa.s
Density of electrolyte	1.84 g/cm^3
Diffusion coefficient of electrolyte	2.12×10^{-9} m^2/s

6.2 Results and discussion

In this study, the performance of VRFBs using different electrode designs was investigated through experiments and numerical analysis. The goal was to understand the effect of local porosity on the flow field of electrolyte and the performance of VRFBs. We especially focused on the improvement of the performance of VRFBs at the high current density region. At the end, we were able to obtain optimum distribution of the local porosity of electrode at the high current density.

6.2.1 Analysis of the flow field of electrolyte in the electrode

The flow fields in the electrode were numerically analyzed shown in Figure 6.3. Here, the dark blue region presented the electrolyte, and white regions represented empty area. The voids can occur when the electrolyte flows from the empty area to porous media. In the void, the electrochemical reaction does not occur, which means the loss of active area. Therefore, when the area of blue region is large, the cell performance is improved, when the area of white region is large, the cell performance is deteriorated. Through the results, we could see that when the electrolyte flows through the UP electrode, the electrolyte is uniformly distributed within the electrode. The uniform distribution of electrolyte appears to be due to the uniform local porosity

of the electrode. Similarly, when the electrolyte flowed through the LPI electrode, few small white regions were observed. A relatively large fraction of the white region is due to the additional electrode layer at the inlet. On the other hand, when we used LPO electrode for the VRFBs cell, many white regions were observed in the electrode. This is due to the extra layer of electrode inserted at the exit. The low porosity region hinders the flow of electrolyte, so the flow becomes disordered, resulting in a many white areas. With increasing void space, the reaction area in the electrode was reduced. Therefore, when we used a LPO electrode the voltage reached the limit voltage sooner, and the charge/discharge process terminated early.

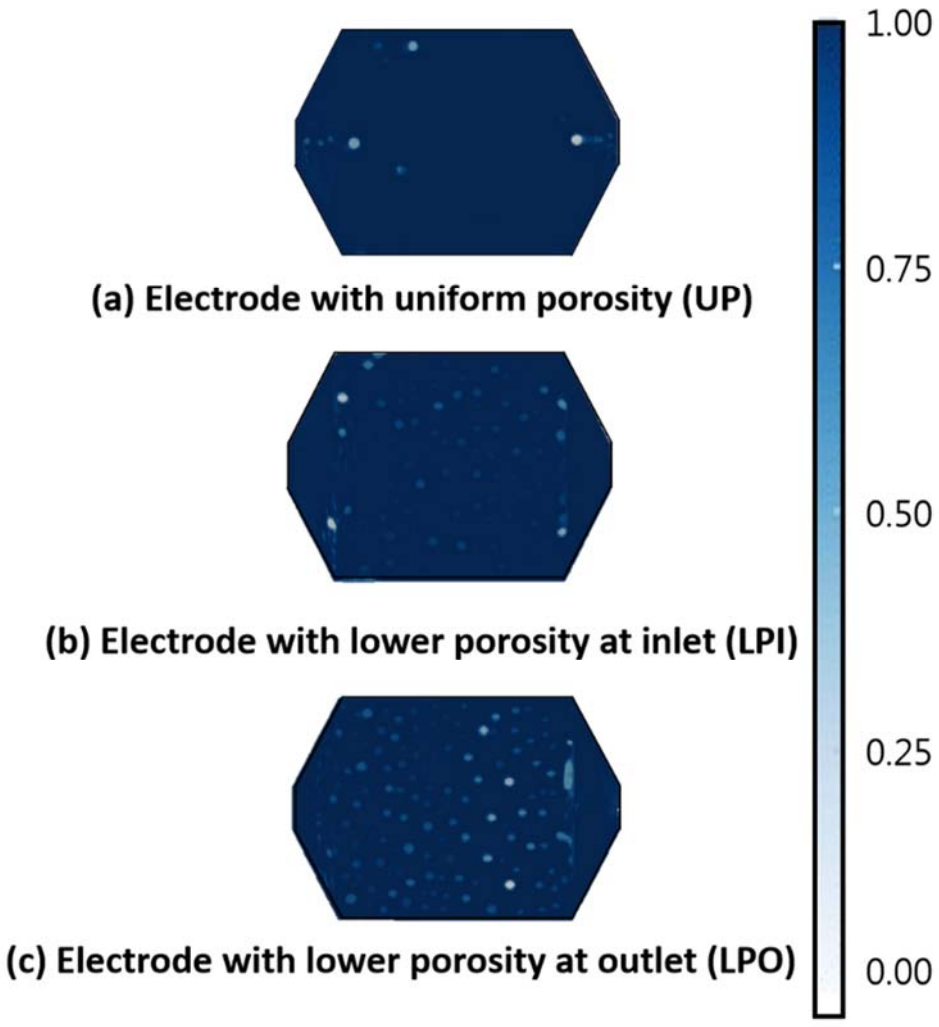

Figure 6.3 Distribution of electrolyte in three different electrodes

Next, we examined the variation of the pressure and velocity vectors of the electrolyte in the electrode that are shown in Figure 6.4. The pressure drop through the porous electrode was relatively low for the UP electrode, being 0.18 bar whereas that for the LPI and LPO electrodes

were 0.27 bar, both. Through this result we can know that more pumping power is consumed when we inserted additional layer of electrode. In addition, the pressure drop was linear within the UP electrode, but nonlinear with the other two with non-uniform porosity. A large pressure drop was observed at the point of porosity change, owing to the high tortuosity. Analysis of the velocity vectors provides further understanding about the electrolyte distribution in the electrode. Except for the entrance region, the flow vectors in the UP electrode were neatly aligned without mixing, while those in the LPI and LPO electrodes were well mixed due to the local non-uniform porosity. The disordered flow could help enhance mass transport of the reactant and product and increase the contact of the electrolyte with the electrode surface, so as to increase the energy efficiency of VRFBs in the high current density region. Through the results we can know that although a high tortuosity hinders the flow rate, it also facilitated the electrochemical reaction by increasing the chance of contact of the electrolyte with the electrode surface.

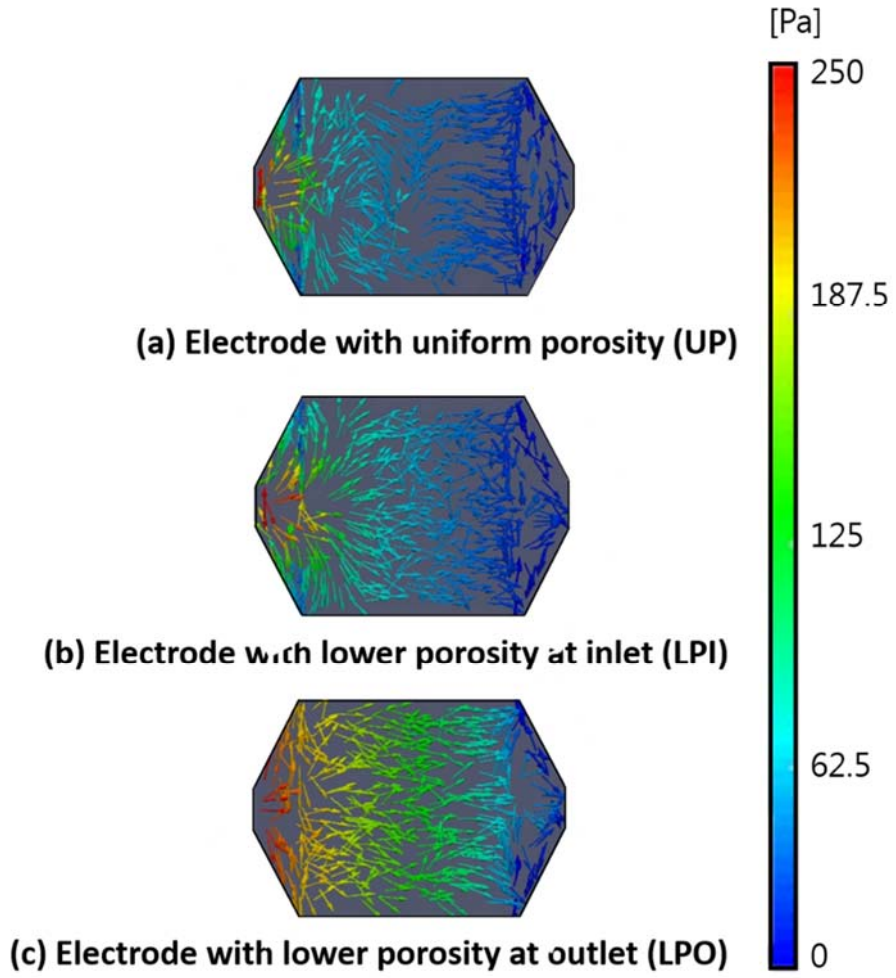

Figure 6.4 pressure and velocity vectors of electrolyte in the different electrode designs

6.2.2 Effect of current densities on the performance of VRFBs

Next, we examined the effect of distribution of local porosity on the performance of VRFBs at various current densities. The charge/discharge results for VRFBs with different electrode designs at the current density of 50 mA/cm^2 and flow rate of 13 mL/min were shown in Figure 6.5. When the charge process starts, the three cells had similar start voltages. However, the operating voltages for the cells with electrodes with lower porosity at the inlet (LPI electrode) and at the outlet (LPO electrode) reached 1.6 V faster than the cells with electrode with uniform porosity (UP electrode). Similarly, the discharge speed was faster for the cells with LPI and LPO electrodes than that of UP electrode. The charge-discharge time is 4040 s for LPO electrode, 5100 s for LPI electrode, and 8300 s for UP electrode.

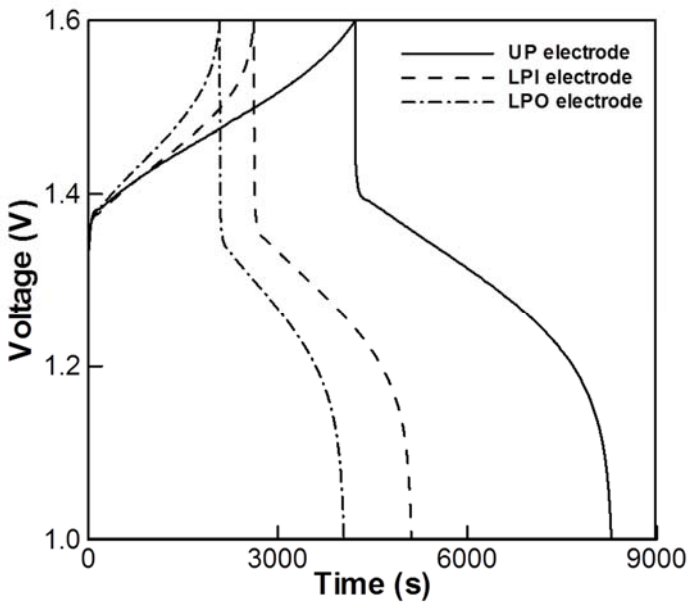

(a) charge-discharge curve

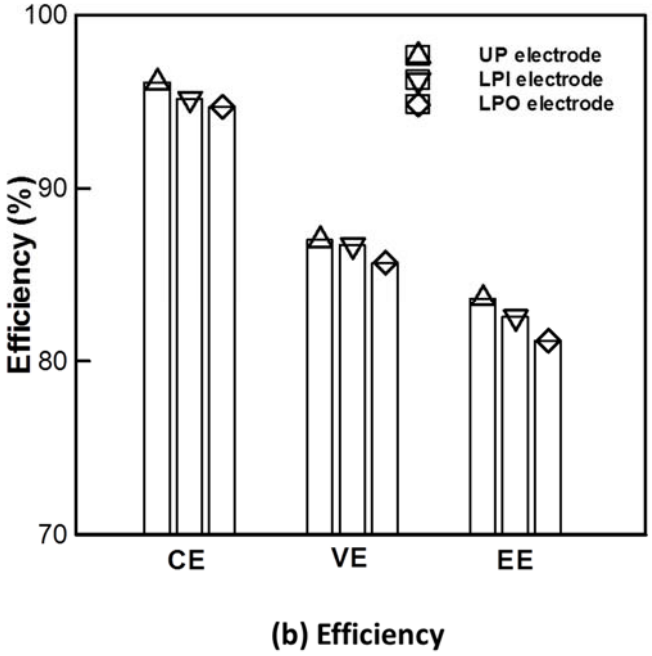

Figure 6.5 Performance of VRFBs using different electrodes at 50 mA/cm^2 and 13 mL/min.

The energy efficiency of VRFBs was maximized when using the UP electrode when the current density was 50 mA/cm^2 (83.6%, 82.5%, and 81.1% for the cells using the UP, LPI, and LPO electrodes, respectively). The high energy efficiency of the cell using the UP electrode originates from the higher Coulomb efficiency compared with other types of electrodes. The Coulomb efficiency of the cell using the UP electrode is 96.1%, but that of LPI and LPO electrode are 95.2% and 94.7%, respectively. The energy density of the cell using the LPI electrode is higher than that of the cell using the LPO electrode because of the relatively high voltage efficiency. The voltage efficiency of the cell using LPI electrode is 86.7%, but that of the cell using LPO electrode is 85.7%. The results are related to the concentration overpotential. At the LPI and LPO electrode, the supply of the reactant and the removal of the product for the electrochemical reaction are insufficient under this operating condition. That is, the concentration overpotential is large for the cell using LPI and LPO electrode at low porosity region. Therefore, the charge/discharge processes of the cell using a LPI or a LPO electrode are terminated earlier than that of the cell using a UP electrode.

Next, we examined the effect of distribution of local porosity on the performance of VRFBs at high current density shown in Figure 6.6. Different from the previous results, the start voltage of the cell using UP electrode turn out to be higher than that of the cell using a LPI or a LPO

electrode. The start voltage of the charge curve is related to the membrane and interfacial resistance of the cell. By adding an extra layer of electrode in the cell, the interfacial resistance between membrane and the electrode decreased, resulting in a reduction of the start voltage of the charge curve of the cell using LPI and LPO electrode. On the other hand, the charge and discharge processes of the cell using LPI and LPO electrode are terminated earlier than the cell using UP electrode as before. The charge/discharge time is 850 s for the cell using a LPO electrode, 1070 s for that using a LPI electrode, and 1155 s for that using an UP electrode. The cell using an UP electrode showed a maximum energy efficiency of 66.6%, and that for the cell using the LPI electrode is 66.4%, and that using the LPO electrode is 65.0%. This result is attributed to the decrease of the current density due to the enlarged reaction area by adding an electrode layer. The results show that the difference of the energy efficiency between the cell using UP electrode and LPI electrode decreases at high current density region. As the current density decreases, the rate of reactant consumption decreases, mitigating concentration overpotential. Therefore, we can expect that the energy efficiency of the cell using a LPI and a LPO electrode can be higher than that of the cell using an UP electrode at high current density region.

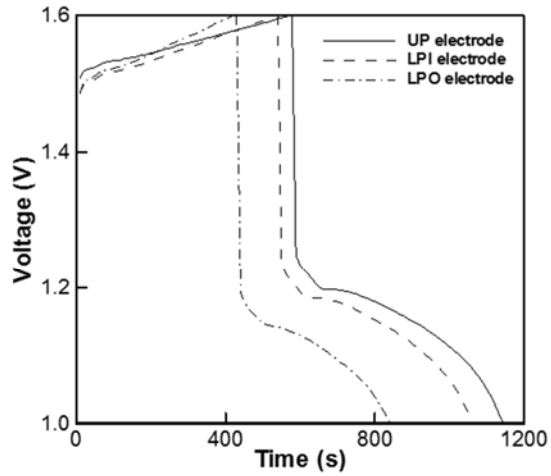

(a) charge-discharge curve

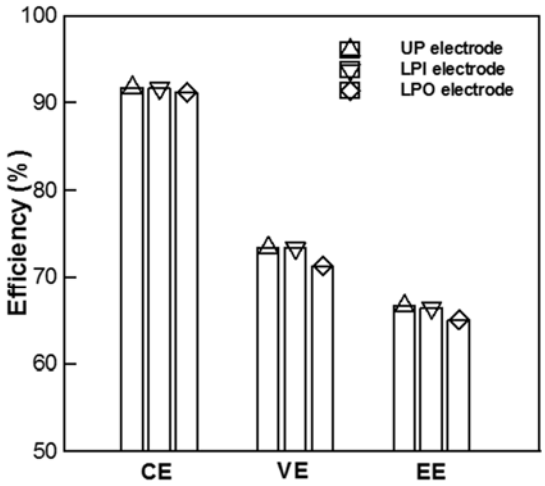

(b) Efficiency

Figure 6.6 Performance of VRFB using different electrodes at 150 mA/cm^2 and 13 mL/min

In Figure 6.7, we examined the variation of energy efficiencies of the cell using three different electrodes at various current densities. The difference in energy efficiency between the cells using UP and LPI electrodes decreased as the current density increases, from 1.2% at 50 mA/cm^2 to 0.2% at 150 mA/cm^2. On the other hand, the difference in energy efficiency between the cells using UP and LPO electrodes decreased as the current density increases, from 2.3% at 50 mA/cm^2 to 0.6% at 150 mA/cm^2. These results showed that increasing the active area at the entrance of electrolyte (LPI electrode) could improve the performance of VRFBs even more

than increasing the active area at the exit of electrolyte (LPO electrode). Since the reactant concentration was higher at the entrance of electrolyte, the former had a stronger effect on promoting the electrochemical reaction. In contrast, when the active area at the electrolyte exit was increased, there was less improvement in the cell performance because of the low concentration of the reactant at the outlet. Therefore, the gap between the energy efficiency between the cells using UP and LPO electrode is larger than that between the cells using UP and LPI electrode.

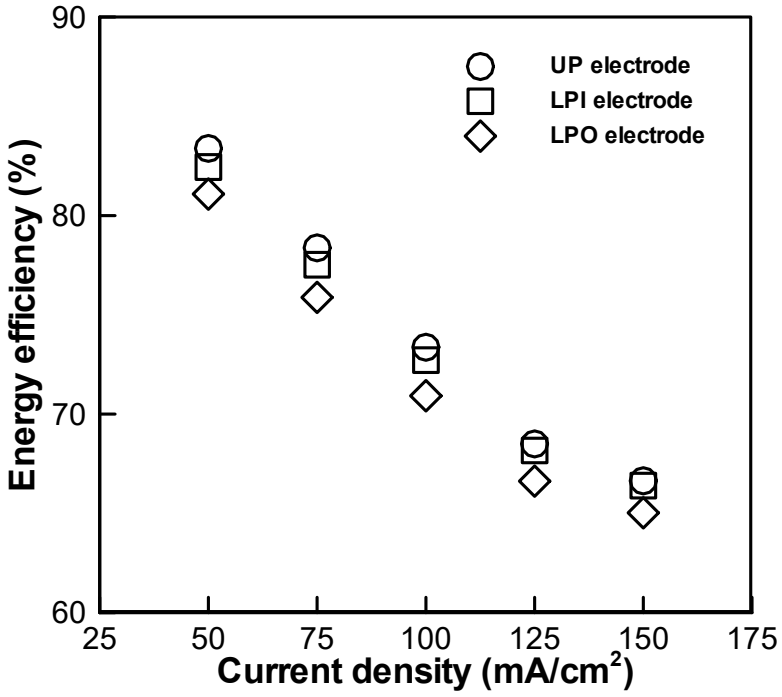

Figure 6.7 Energy efficiency of VRFBs with current density from 50 to 150 mA/cm^2 at a flow rate of 13 mL/min**.**

6.2.3 Effect of flow rate on the performance of VRFBs

In the previous discussion, we have shown that non-uniform porous electrodes can increase the energy efficiency of VRFBs at high current density. Next, we explained the effect of the flow rate of electrolyte on the alleviation of concentration overpotential under high current density.

Figure 6.8 showed the energy efficiencies of charge/discharge cycles at the flow rates of 20 and 25 mL/min. At 20 mL/min, the energy efficiency for the UP electrode was the highest until

the current density reaches 100 mA/cm^2. At the charge/discharge current density of 125 mA/cm^2 or more, however, the cell using LPI electrode had the higher energy efficiency. When the flow rate was 25 mL/min, the cell using LPI electrode had the highest efficiency when the current density was 75 mA/cm^2 or more. The highest energy efficiency of the cell using LPI electrode at high current density is related to well-developed species transport in the electrode.

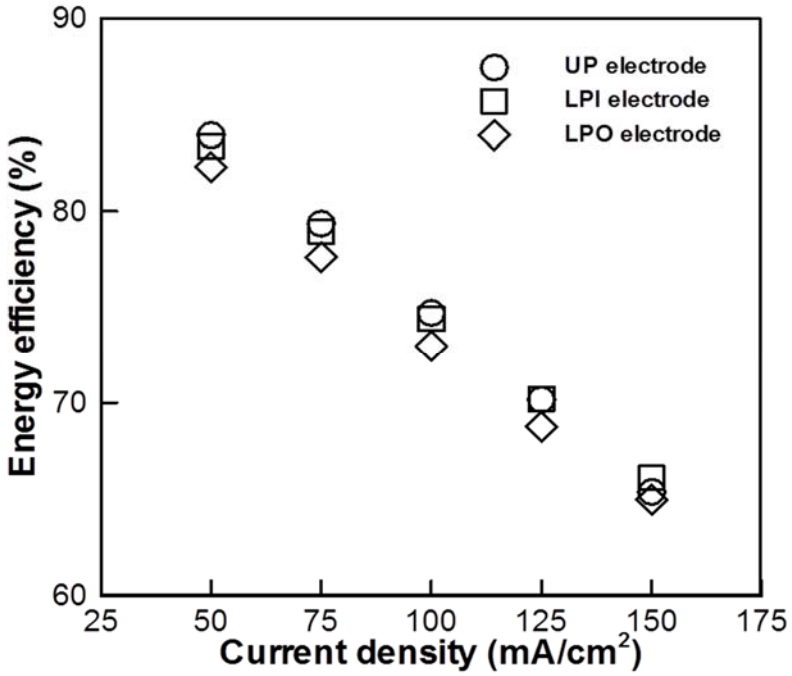

(a) Flow rate of 20 mL/min

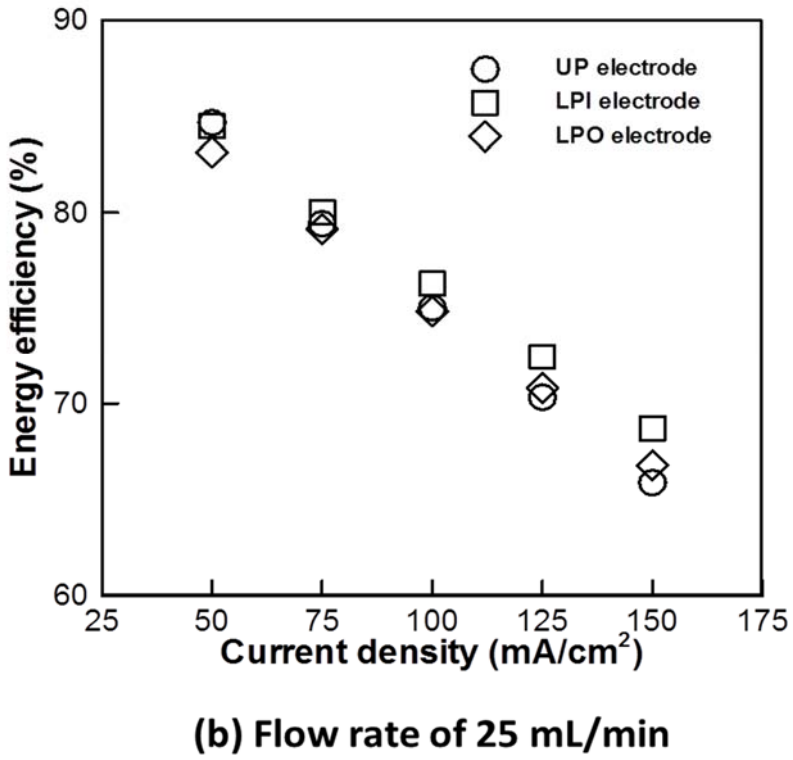

Figure 6.8 Energy efficiency of VRFBs from 50 to 150 mA/cm^2 at the flow rates of (a) 20 and (b) 25 mL/min.

In order to explain the losses occurring in the cell at high current density, we measured i-V curves of VRFBs under various flow rates. Here, the state of charge (SOC) of the cell is maintained as 50% at different operating current densities. The i-V curves of the VRFBs using three different electrodes are presented in Figure 6.9. The discharge voltage of the cell using an UP electrode is 1.3 V, and that of the cell using a LPI electrode is 1.28V at 50 mA/cm^2. As the current density increases, the voltage is almost the same at 125 mA/cm^2, and the discharge voltage of the cell using a LPI electrode become larger than that of the cell using an UP electrode at 150 mA/cm^2 (1.06 V, and 1.08 V for the cell using UP, and LPI electrode, respectively).

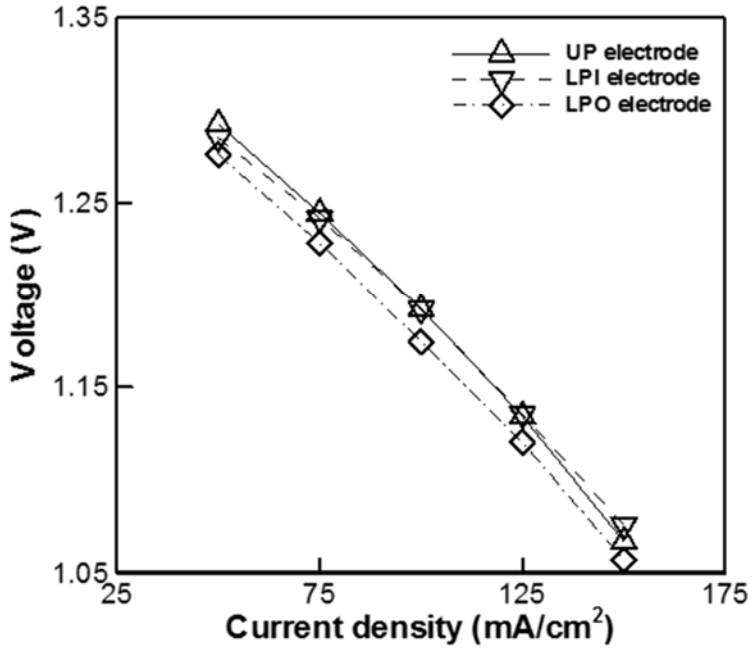

(a) Flow rate of 20 mL/min

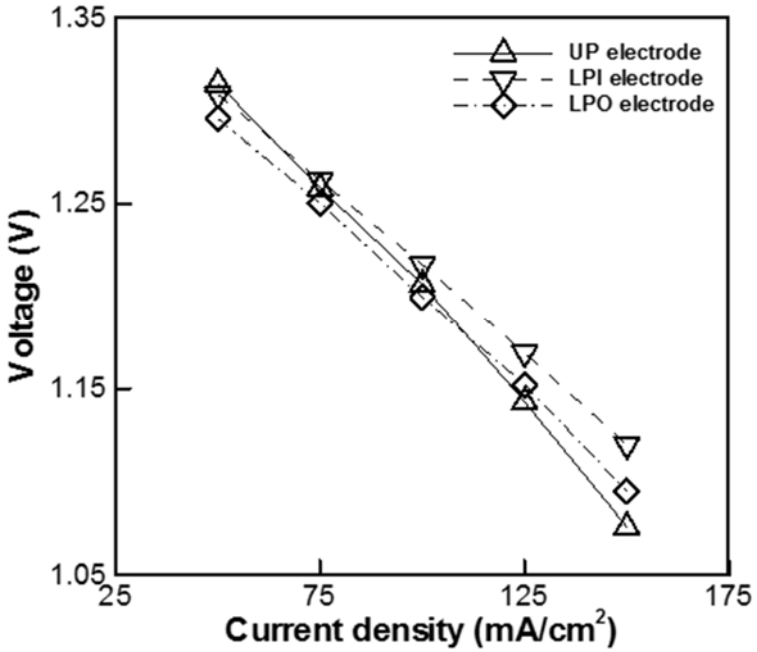

(b) Flow rate of 25 mL/min

Figure 6.9 i-V curve of VRFB from 50 to 150 mA/cm^2 at the flow rate of (a) 20 and (b) 25 mL/min

When the flow rate increases, the energy efficiency of the cell using a LPI electrode shows the highest among the cells using other electrodes when the current density was 75 mA/cm^2 or more, and the energy efficiency differences of the cell using a LPI and a UP electrode become larger at high current density; the energy efficiency of the cell using LPI electrode is 1.12 V, but that of the cell using a UP electrode is 1.07 V. Under low mass flow rate, there is insufficient reactant supply and product removal near electrode surface, inducing severe concentration overpotential. Therefore, the energy efficiency of the cell using a LPI electrode is similar to that of the cells using an UP electrode, despite larger active area. When the flow rate of electrolyte is large, however, the mass transport at the electrode surface is well established, resulting the best performance of the cell using LPI electrode at high current density.

These results suggested that controlling the local porosity of the electrode could have a pronounced effect at high flow rates. In particular, reducing the electrode porosity at the electrolyte inlet could improve the performance of VRFBs more significantly than that at the electrolyte exit.

6.2.4 An optimization of the local porosity distribution of electrode at high current density

Lastly, we examined optimal distribution of local porosity of electrode at high current density region. Here, we proposed an empirical relationship for the optimal distribution of the local porosity with current density. The range of current density is from 75 mA/cm^2 to 150 mA/cm^2, and the flow rate is maintained at 25 mL/min.

We conducted experiments to examine the energy efficiency of the cell by changing the distribution of local porosity. The energy efficiencies of the cell were expressed as function of the length of lower porosity region formed from the inlet and from the outlet shown in Figure 6.10. The maximum energy efficiency of VFB at the current density of 75 mA/cm^2 is 79.8% when the LPI electrode is occupied by 1.6 cm from inlet. Here, there is no LPO region at electrode. The lowest point of 77.2 % is observed when the LPO electrode is formed until 1.5 cm from exit without LPI electrode region. When the current density is 150 mA/cm^2, similar trends is obtained. Here, the maximum energy efficiency is 67.7% and the minimum energy efficiency is 64.6%. Through the results, we can convince that when the lower porosity is formed at the inlet the energy efficiency is increased at high current density. When the LPI electrode fraction amounts to one-third of the total length, the maximum energy efficiency can

be expected. However, when the LPO electrode is introduced to the electrode, it increases the concentration overpotential in the cell, resulting in a deterioration of the VRFB performance. Based on these results, it can be concluded that reducing the electrode porosity at the entrance of the electrolyte exerted more influence on the VRFBs performance than reducing the porosity at the exit.

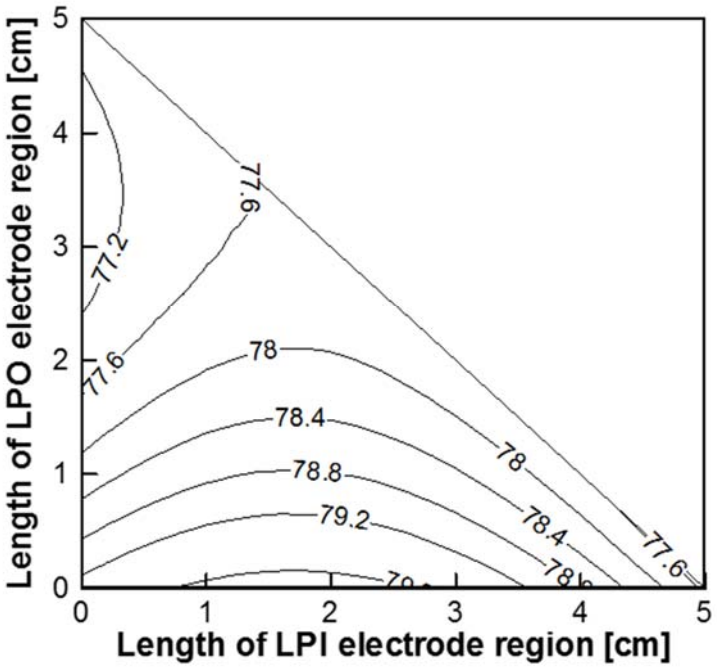

(a) Current density of 75 mA/cm^2

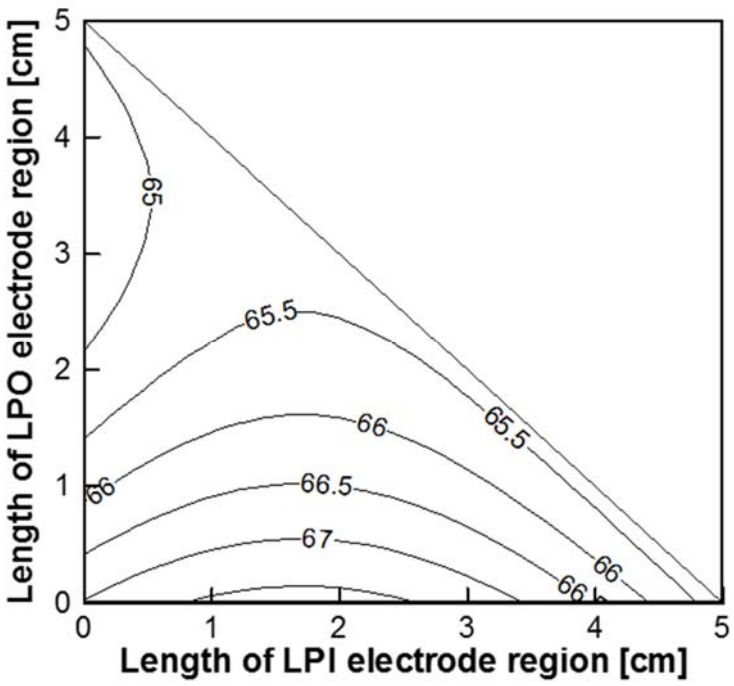

(b) Current density of 150 mA/cm^2

Figure 6.10 Energy efficiency of VRFB at (a) 75 mA/cm^2 and (b) 150 mA/cm^2

Based on the results, we suggest an empirical relationship of the energy efficiency as a function of current density, fraction of LPI and LPO electrode of the total electrode area. The empirical relationship is expressed as follow.

$$aj^2 + bj + cR_i^2 + dR_i + eR_e^2 + fR_e + g = \eta_e \quad (6-10)$$

Here, j is current density, and R_i and R_o are ratio of the length of LPI and LPO electrode to the total length of the electrode shown below.

$$R_i = \frac{L_{LPI}}{L_{total}} \quad (6-11)$$

$$R_o = \frac{L_{LPO}}{L_{total}} \quad (6-13)$$

L_{LPI} is the length of LPI electrode, L_{LPO} is the length of LPO electrode, and L_{total} is the length of whole electrode. The constants of the equation are presented in Table 6.2.

Table 6.2 Constants of empirical equation of energy efficiency

Constant	Value
a	1.62×10^{-4}
b	-0.20
c	-5.70
d	3.87
e	4.93
f	-6.85
g	93.49

To confirm the empirical equation, we measured the performance of the VRFB at 150 mA/cm^2. Figure 6.11 showed the charge/discharge curve and the efficiencies of the VRFB at a current density of 150 mA/cm^2 and a flow rate of 25 mL/min. When the charge process started, the voltages of the cells using an optimal electrode is lower than that using the UP electrode (1.5, and 1.54 V, respectively). Therefore, the voltage efficiencies of the cells with optimal electrodes (71.3%) is higher than that with the UP electrode. Similarly, the energy efficiency was the highest when using the optimal electrode (67.7%, compared to 66.6% for the UP electrode). We can also infer that the charge-discharge capacities were larger for the optimal electrode than the UP electrode, because the charge-discharge time of the former was 47.5% longer than the latter. In the case of the optimal electrode, a higher concentration of reactant (at the inlet) reacted with a larger electrode surface; hence, the charge/discharge capacity was larger. The cell performance using the optimal electrode also benefits from the enhanced mass transport of reactants and products at the exit. These results will help guide the electrode design by varying its local porosity to obtain high power density.

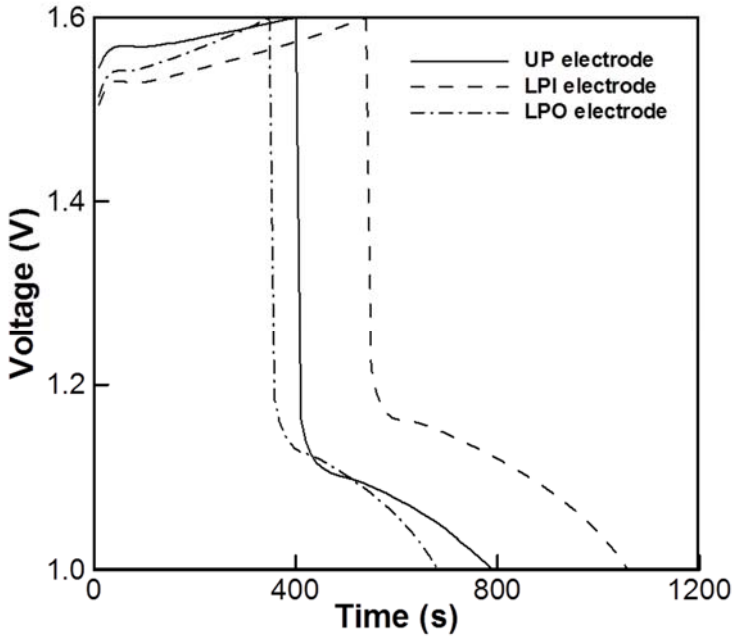

(a) charge-discharge curve

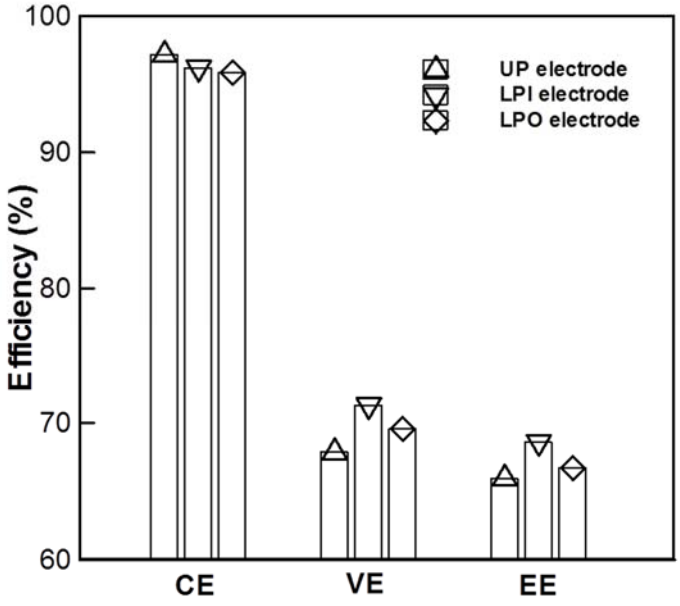

(b) Efficiency

Figure 6.11 Performance of VRFBs using different electrodes at 150 mA/cm^2 and 25 mL/min.

6.2.5 Conclusion

We examined the effect of local porosity of the electrodes on the electrolyte flow field in VRFBs at high current densities. Three different electrode designs were considered: uniform porosity (UP), lower porosity at the inlet of electrolyte (LPI), and lower porosity at the outlet of electrolyte (LPO). The results showed that the energy efficiency is superior with the LPI electrode, because this design provided a larger active area in the region with high reactant concentration, and improves the mass transport of product.

At the current density of 50 mA/cm^2, the cell using UP electrode showed the highest energy efficiency (83.6%), because of high concentration overpotential of the cell using LPI and LPO electrode. At the high current density of 150 mA/cm^2, however, the cell using the LPI and UP electrode showed similar energy efficiency (66.4% and 66.6%, respectively), because this electrode could provide a large active area at the inlet where the concentration of reactant was high. The relatively higher porosity of this electrode at the outlet also helped to supply reactant and remove the product. The advantage of the LPI electrode became more obvious when sufficient electrolyte was supplied. At the higher electrolyte flow rate of 25 mL/min, the energy efficiency of the cell using LPI electrode was 67.2% at 150 mA/cm^2.

Finally, optimization of local porosity is conducted at high current density region. An empirical relationship of energy efficiency is presented in terms of the current density and portion of LPI and LPO electrode region. At 150 mA/cm^2, the maximum performance of VRFBs is obtained when the LPI electrode accounts for one third of whole electrode. The charge-discharge time of this cell was 43.5% longer than those using the UP electrode. The energy efficiency of the cell using optimal electrodes was 67.7%, and the cell using UP electrode is 66.6%. It is expected that the power density of VRFBs can be improved by controlling the local porosity of the electrode. The results of this study confirmed the improvement of performance of VRFBs system at high current density by controlling the porosity of the electrode.

Glossary

ε Porosity

ρ Density (kg m^{-3})

u Velocity (m s^{-1})

P Pressure (bar)

μ Viscosity (Pa·s)

τ Shearing stress (N m^{-2})

S Sink term

κ Permeability (m^2 s^{-1})

β Non-Darcy coefficient

t Time (s)

subscript i x component

subscript j y component

7. Summary

Although vanadium redox flow batteries (VRFBs) have received significant attention as energy storage systems due to their various advantages such as long life time, low cost, high safety, fast response, and design flexibility, there are still many problems to be solved for commercialization. The performance of VRFBs is significantly affected by the electrochemical activity of the electrode because the vanadium ion redox reactions occur at the electrode surface during the charge-discharge cycle. However, the low electrochemical activity, poor wettability and kinetic reversibility of the graphite felt electrode are significant obstacles to the improvement of energy efficiency and rate capability of VRFBs. In this thesis, in order to improve the performance of the electrode used in VRFB, methods of introducing nitrogen doping material on the surface of electrode and local control of the porosity of electrode were studied.

First, nitrogen-doped graphite felts were prepared by a thermal coating process of a nitrogen-containing ionic liquid on the pristine graphite felt for VRFB electrode applications. Ethylmethylimidazolium dicyanamide (EMIM dca) was used as a precursor for the high performance nitrogen-doped graphite felt electrode due to its high nitrogen content. According to the experimental results, via EMIM dca a nitrogen-containing carbon materials has successfully been deposited on the surface of the graphite felt. From the results of CV, EMIM dca coated graphite felts showed higher electrocatalytic activity than the graphite felt with the oxygen functional groups which was prepared by the conventional heat treatment (GF-Ref). The charge-discharge test results showed that EMIM dca coated graphite felts had much higher performance than GF-Ref. Working with an upper limiting voltage of 1.6 V the discharge capacity of the 20 wt% EMIM dca solution coated graphite felt (GF-Ed20) was 24 Ah L^{-1} at the current density of 150 $mAcm^{-2}$, which is three times higher than that of GF-Ref. The cells with GF-Ed20 also showed about 10% higher energy efficiency than the cell using GF-Ref at 150 $mAcm^{-2}$. More specifically, the capacity retention and energy efficiency of the cell with GF-Ed20 were higher than those of GF-Ref after 100 charge/discharge cycle test, which indicates that the EMIM dca coating improved both the electrochemical activity and the stability of the graphite felt electrode.

Second, in order to fabricate nitrogen-doped graphite felt electrodes by coating polyacrylonitrile (PAN), two steps of thermal treatment were performed. The graphite felt coated with PAN was heated at 280°C for 3 hours under ambient atmosphere and then carbonized at 900°C for 1 hour under nitrogen atmosphere. According to the experimental results, it was found that the surface of the graphite felt was successfully coated with a nitrogen-containing carbon material.

From the results of CV, it was confirmed that the electrochemical activity and reversibility increased with increasing PAN content. The charge-discharge test results showed that PAN coated graphite felt had higher performance than GF-Ref through PAN coating amount optimization. When 4 wt% PAN solution coated graphite felt (GF-P4) which showed the highest charge and discharge capacity was used as the electrode of VRFB, the discharge capacity increased by 87%, from 123.3 mAh to 230 mAh. The cell with the optimized amount of PAN coated electrodes (GF-P4) showed about 5% higher energy efficiencies, from 66% to 71%, than the cell using GF-Ref at 150 mA cm^{-2}. In addition, the capacity retention and energy efficiency of the cell with GF-P4 were higher than those of GF-Ref after 100 charge/discharge cycle test, which indicates that the PAN coating not only enhances the electrochemical activity but also remains stable during the charge / discharge test.

Third, we examined the effect of local porosity of the electrodes on the electrolyte flow field in VRFBs at high current densities. Three different electrode designs were considered: uniform porosity (UP), lower porosity at the inlet of electrolyte (LPI), and lower porosity at the outlet of electrolyte (LPO). The results showed that the energy efficiency is superior with the LPI electrode, because this design provided a larger active area in the region with high reactant concentration, and improves the mass transport of product. In addition, optimization of local porosity is conducted at high current density region. An empirical relationship of energy efficiency is presented in terms of the current density and portion of LPI and LPO electrode region. At 150 mA/cm^2, the maximum performance of VRFBs is obtained when the LPI electrode accounts for one third of the whole electrode. The charge-discharge time of this cell was 43.5% longer than those using the UP electrode. The energy efficiency of the cell using optimal electrodes was 67.7%, and the cell using UP electrode is 66.6%. It is expected that the power density of VRFBs can be improved by controlling the local porosity of the electrode. The results of this study confirmed the improvement of performance of VRFBs system at high current density by controlling the porosity of the electrode.

8. Outlook

It was found that the use of nitrogen-doped graphite felt can increase the performance of the VRFB by improving the electrochemical performance of the electrode. As a precursor for nitrogen doping, ethylmethylimidazolium dicyanamide (EMIM dca), an ionic liquid with high nitrogen content, and polyacrylonitrile (PAN), which is frequently used as the main material of carbon / graphite products, were used.

First, even though the use of EMIM dca as a nitrogen doping precursor has been shown to improve the performance and durability of VRFB, the high cost of ionic liquids may be an obstacle, considering commercialization. In addition to reducing the price by mass production of ionic liquids, there is a need for a way to lower the price of the ionic liquid itself.

Second, in this thesis, the performance of VRFB electrodes was improved by controlling the content of PAN coated on the graphite felt, however, it is important to remember that various changes can be made during the heat treatment as shown in previous reports on PAN heat treatment. Therefore, if the PAN coating is made more uniform and the heat treatment process is optimized, the electrode performance can be further improved. In addition, since the PAN contains nitrogen in the polymer, if the process for preparing the graphite felt is controlled, it may be possible to prepare a graphite felt having a nitrogen doping effect by itself without additional nitrogen doping process.

In this study, we did not consider the process of generating oxygen functional groups, however, if we develop a facile method that can prepare oxygen functional groups on the surface of graphite felts and introduce nitrogen-doping effects at the same time, we will be able to improve the performance of VRFB electrodes.

Furthermore, the study controlling the porosity of graphite felt seems to have more possibility for further improvement of VRFB performance. As many studies have been conducted in the field of flow path design in the case of polymer electrolyte membrane fuel cells (PEMFC) having a similar cell structure, various studies in VRFB applications can be made using the porosity of graphite felt. In addition, it is expected that the performance of VRFBs can be further increased when applied simultaneously with the study of introducing functional groups on the surface of the graphite felt.

9. Appendix

9.1 List of figures

9.2 List of tables

9.3 Acknowledgements

This PhD research work would not have been completed without the support, guidance and efforts of many people.

First of all, I would like to thank my supervisor, Prof. Dr. Dr. h.c. Rolf Hempelmann for giving me the great opportunity to start my PhD research in Germany and for his appreciated guidance and support. With his active helps on ideas as well as technical issues, the scientific results of this thesis could be produced.

I also appreciate Prof. Dr. Kaspar Hegetschweiler, who serves as my scientific advisor, for his valuable comments in my annual presentations.

Special thanks to Dr. Sangwon Kim for helping me adapt to German life and for his kind supports in KIST-Europe laboratory. I gratefully thank Prof. Dong Kyu Kim for for his generous assistance in conducting the research together. With his help the experimental results became more valuable. I am also grateful to Dr. Jaeho Lee and Dr. Ruiyong Chen for their kind suggestion and advices about research and German life.

Furthermore, I would like to thank my colleagues in Prof. Hempelmann's group and KIST Europe. Thanks to Dr. Yonglai Zhang, Galina Skorikova, and Zhifeng Huang for their kind help.

I really appreciate Dr. Young Jun Kim and Eun Ju Jang for their warm consideration and help throughout the entire German life. I was so lucky to know them in Germany and I will never forget their help.

This work was financially supported by 'GO KRICT' project from Korea Reseach Institute of Chemical Technology (KRICT). I wish to thank my group leader Dr. Young Taik Hong for organizing the project and his advice.

This PhD research work would not have been possible without the unrelenting support and the backing of my family. I sincerely thank my parents, my wife and my children for their love, encouragement, and understanding.

9.4 References

[1] B. Dunn, H. Kamath, and J.-M. Tarascon, Electrical energy storage for the grid: a battery of choices, Science, 334 (2011) 928-935. https://doi.org/10.1126/science.1212741.

[2] J. E. Halls, A. Hawthornthwaite, R. J. Hepworth, N. A. Roberts, K. J. Wright, Y. Zhou, S. J. Haswell, S. K. Haywood, S. M. Kelly, N. S. Lawrence, and J. D. Wadhawan, Empowering the smart grid: can redox batteries be matched to renewable energy systems for energy storage?, Energy & Environmental Science, 6 (2013) 1026-1041. https://doi.org/10.1039/c3ee23708g.

[3] C. Ding, H. Zhang, X. Li, T. Liu, and F. Xing, Vanadium Flow Battery for Energy Storage: Prospects and Challenges, The Journal of Physical Chemistry Letters, 4 (2013) 1281-1294. https://doi.org/10.1021/jz4001032.

[4] E. Sum and M. Skyllas-Kazacos, A study of the V(II)/V(III) redox couple for redox flow cell applications, J. Power Sources, 15 (1985) 179-190. https://doi.org/10.1016/0378-7753(85)80071-9.

[5] E. Sum, M. Rychcik and M. Skyllas-Kazacos, Investigation of the V(V)/V(IV) system for use in the positive half-cell of a redox battery, J. Power Sources, 16 (1985) 85-95. https://doi.org/10.1016/0378-7753(85)80082-3

[6] M. Skyllas-Kazacos, M. Rychcik, R. G. Robins, A. G. Fane, and M. A. Green, New All-Vanadium Redox Flow Cell, Journal of The Electrochemical Society, 133 (1986) 1057-1058. https://doi.org/10.1149/1.2108706

[7] C. Ponce de Leon, A. Frıas-Ferrer, J. Gonzalez-Garcıa, D. A. Szanto, and F. C. Walsh, Redox flow cells for energy conversion, Journal of Power Sources, 160, (2006) 716-732. https://doi.org/10.1016/j.jpowsour.2006.02.095

[8] B. Sun and M. Skyllas-Kazacos, Modification of graphite electrode materials for vanadium redox flow battery application—I. Thermal treatment, Electrochim. Acta, 37 (1992) 1253-1260. https://doi.org/10.1016/0013-4686(92)85064-R

[9] K. J. Kim, Y.-J. Kim, J.-H. Kim and M.-S. Park, The effects of surface modification on carbon felt electrodes for use in vanadium redox flow batteries, Mater. Chem. Phys., 131 (2011) 547-553. https://doi.org/10.1016/j.matchemphys.2011.10.022

[10] Z. Gonzalez, C. Botas, P. Alvarez, S. Roldan, C. Blanco, R. Santamarıa, M. Granda and R. Menendez, Thermally reduced graphite oxide as positive electrode in Vanadium Redox Flow Batteries, Carbon, 50 (2012) 828–834. https://doi.org/10.1016/j.carbon.2011.09.041

[11] H. Kaneko, K. Nozaki, Y. Wada, T. Aoki, A. Negishi, and M. Kamimoto, Vanadium redox reactions and carbon electrodes for vanadium redox flow battery, Electrochimica Acta 36 (1991) 1191-1196. https://doi.org/10.1016/0013-4686(91)85108-J

[12] B. Sun and M. Skyllas-Kazakos, Chemical modification and electrochemical behaviour of graphite fibre in acidic vanadium solution, Electrochimica Acta, 36 (1991) 513-517. https://doi.org/10.1016/0013-4686(91)85135-T
[13] B. Sun and M. Skyllas-Kazacos, Chemical modification of graphite electrode materials for vanadium redox flow battery application—part II. Acid treatments, Electrochimica Acta, 37 (1992) 2459-2465. https://doi.org/10.1016/0013-4686(92)87084-D
[14] W.G. Zhang, J.Y. Xi, Z.H. Li, H.P. Zhou, L. Liu, Z.H. Wu, et al., Electrochemical activation of graphite felt electrode for VO2+ /VO2+ redox couple application, Electrochim. Acta, 89 (2013) 429-435. https://doi.org/10.1016/j.electacta.2012.11.072
[15] B. Li, M. Gu, Z.M. Nie, Y.Y. Shao, Q.T. Luo, X.L. Wei, et al., Bismuth nanoparticle decorating graphite felt as a high-performance electrode for an all-vanadium redox flow battery, Nano Lett., 13 (2013) 1330-1335. https://doi.org/10.1021/nl400223v
[16] K.J. Kim, M.S. Park, Y.J. Kim, J.H. Kim, S.X. Dou, M. Skyllas-Kazacos, A technology review of electrodes and reaction mechanisms in vanadium redox flow batteries, J. Mater. Chem. A, 3 (2015) 16913-16933. https://doi.org/10.1039/c5ta02613j
[17] W.H. Wang, X.D. Wang, Investigation of Ir-modified carbon felt as the positive electrode of an all-vanadium redox flow battery, Electrochim. Acta, 52 (2007) 6755-6762. https://doi.org/10.1016/j.electacta.2007.04.121
[18] R.H. Huang, C.H. Sun, T.M. Tseng, W.K. Chao, K.L. Hsueh, F.S. Shieu, Investigation of active electrodes modified with platinum/multiwalled carbon nanotube for vanadium redox flow battery, J. Electrochem. Soc., 159 (2012) A1579-A1586. https://doi.org/10.1149/2.003210jes
[19] C. Flox, J. Rubio-Garcia, R. Nafria, R. Zamani, M. Skoumal, T. Andreu, et al., Active nano-CuPt3 electrocatalyst supported on graphene for enhancing reactions at the cathode in all-vanadium redox flow batteries, Carbon, 50 (2012) 2372-2374. https://doi.org/10.1016/j.carbon.2012.01.060
[20] C.A. Yao, H.M. Zhang, T. Liu, X.F. Li, Z.H. Liu, Carbon paper coated with supported tungsten trioxide as novel electrode for all-vanadium flow battery, J. Power Sources, 218 (2012) 455-461. https://doi.org/10.1016/j.jpowsour.2012.06.072
[21] K.J. Kim, M.S. Park, J.H. Kim, U. Hwang, N.J. Lee, G. Jeong, et al., Novel catalytic effects of Mn_3O_4 for all vanadium redox flow batteries, Chem. Commun., 48 (2012) 5455-5457. https://doi.org/10.1039/C2CC31433A
[22] B. Li, M. Gu, Z.M. Nie, X.L. Wei, C.M. Wang, V. Sprenkle, W. Wang, Nanorod niobium oxide as powerful catalysts for an all vanadium redox flow battery, Nano Lett., 14 (2014) 158-165. https://doi.org/10.1021/nl403674a

[23] H.P. Zhou, J.Y. Xi, Z.H. Li, Z.Y. Zhang, L.H. Yu, L. Liu, et al., CeO_2 decorated graphite felt as a high-performance electrode for vanadium redox flow batteries, RSC Adv., 4 (2014) 61912-61918. https://doi.org/10.1039/C4RA12339E
[24] X. Wu, H. Xu, L. Lu, H. Zhao, J. Fu, Y. Shen, P. Xu, and Y. Dong, PbO_2-modified graphite felt as the positive electrode for an all-vanadium redox flow battery, Journal of Power Sources, 250 (2014) 274-278. https://doi.org/10.1016/j.jpowsour.2013.11.021
[25] Y. Shen, H. Xu, P. Xu, X. Wu, Y. Dong, and L. Lu, Electrochemical catalytic activity of tungsten trioxide modified graphite felt toward VO_{2+}/VO_2^+ redox reaction, Electrochimica Acta, 132 (2014) 37-41. https://doi.org/10.1016/j.electacta.2014.03.107
[26] H. Lee and H. Kim, Development of nitrogen-doped carbons using the hydrothermal method as electrode materials for vanadium redox flow batteries, J. Appl. Electrochem., 43 (2013) 553–557. https://doi.org/10.1007/s10800-013-0539-0
[27] L. Shi, S. Liu, Z. He and J. Shen, Nitrogen-Doped Graphene: Effects of nitrogen species on the properties of the vanadium redox flow battery, Electrochim. Acta, 138 (2014) 93–100. https://doi.org/10.1016/j.electacta.2014.06.099
[28] Y. Shao, X. Wang, M. Engelhard, C. Wang, S. Dai, J. Liu, Z. Yang, Y. Lin, Nitrogen-doped mesoporous carbon for energy storage in vanadium redox flow batteries, J. Power Sources. 195 (2010) 4375–4379. https://doi.org/10.1016/j.jpowsour.2010.01.015.
[29] Wu, T., Huang, K. L., Liu, S. Q., Zhung, S. X., Fang, D., Li, S., Lu, D., and Su, A. Q., Hydrothermal ammoniated treatment of PAN-graphite felt for vanadium redox flow battery, J. Solid State Electrochem., 16 (2012) 579–585. https://doi.org/10.1007/s10008-011-1383-y
[30] Wang, S. G., Zhao, X. S., Cochell, T., and Manthiram, A., Nitrogen-doped carbon nanotube/graphite Felts as advanced electrode materials for vanadium redox flow batteries, J. Phys. Chem. Lett., 3 (2012) 2164–2167. https://doi.org/10.1021/jz3008744
[31] Jin, J. T., Fu, X. G., Liu, Q., Liu, Y. R., Wei, Z. Y., Niu, K. X., and Zhang, J. Y., Identifying the active site in nitrogen-doped graphene for the VO2+/VO2+ redox reaction, ACS Nano, 7 (2013) 4764–4773. https://doi.org/10.1021/nn3046709
[32] S. Park and H. Kim, Fabrication of nitrogen-doped graphite felts as positive electrodes using polypyrrole as a coating agent in vanadium redox flow batteries, J. Mater. Chem. A, 3 (2015) 12276-12283. https://doi.org/10.1039/c5ta02674a
[33] H. J. Lee and H. Kim, Graphite Felt Coated with Dopamine-Derived Nitrogen-Doped Carbon as a Positive Electrode for a Vanadium Redox Flow Battery, Journal of The Electrochemical Society, 162 (2015) A1675-A1681. https://doi.org/10.1149/2.0081509jes
[34] H. J. Lee, D. Kil, and H. Kim, Synthesis of Activated Graphite Felt Using Consecutive Post-Treatments for Vanadium Redox Flow Batteries, Journal of The Electrochemical Society, 163 (2016) A2586-A2591. https://doi.org/10.1149/2.0531613jes

[35] T.C. Chang, J.P. Zhang, Y.K. Fuh, Electrical, mechanical and morphological properties of compressed carbon felt electrodes in vanadium redox flow battery, J. Power Sources. 245 (2014) 66–75. https://doi.org/10.1016/j.jpowsour.2013.06.018.
[36] D.S. Aaron, Q. Liu, Z. Tang, G.M. Grim, A.B. Papandrew, A. Turhan, T.A. Zawodzinski, M.M. Mench, Dramatic performance gains in vanadium redox flow batteries through modified cell architecture, J. Power Sources. 206 (2012) 450–453. https://doi.org/10.1016/j.jpowsour.2011.12.026.
[37] R. Badrinarayanan, K.J. Tseng, B.H. Soong, Z. Wei, Modelling and control of vanadium redox flow battery for profile based charging applications, Energy. 141 (2017) 1479–1488. https://doi.org/10.1016/j.energy.2017.11.082.
[38] C. Yin, Y. Gao, S. Guo, H. Tang, A coupled three dimensional model of vanadium redox flow battery for flow field designs, Energy. 74 (2014) 886–895. https://doi.org/10.1016/j.energy.2014.07.066.
[39] K. Oh, H. Yoo, J. Ko, S. Won, H. Ju, Three-dimensional, transient, nonisothermal model of all-vanadium redox flow batteries, Energy. 81 (2015) 3–14. https://doi.org/10.1016/j.energy.2014.05.020.
[40] A. Bhattarai, N. Wai, R. Schweiss, A. Whitehead, T.M. Lim, H.H. Hng, Advanced porous electrodes with flow channels for vanadium redox flow battery, J. Power Sources. 341 (2017) 83–90. https://doi.org/10.1016/j.jpowsour.2016.11.113.
[41] J. P. Paraknowitsch, J. Zhang, D. Su, A. Thomas, and M. Antonietti, Ionic liquids as precursors for nitrogen-doped graphite carbon, Adv. Mater., 22 (2010) 87-92. https://doi.org/10.1002/adma.200900965
[42] J. P. Paraknowitsch, A. Thomas, and M. Antonietti, A detailed view on the polycondensation of ionic liquid monomers towards nitrogen doped carbon materials, J. Mater. Chem., 20 (2010) 6746-6758. https://doi.org/10.1039/c0jm00869a
[43] E. Oh, R. Hempelmann, V. Nica, I. Radev, H. Natter, New catalyst supports prepared by surface modification of graphene and carbon nanotube structures with nitrogen containing carbon coatings, J. Power Sources, 341 (2017) 240-249. https://doi.org/10.1016/j.jpowsour.2016.11.116
[44] E. Oh, R. Hempelmann, V. Nica, I. Radev, H. Natter, Coating procedure for chemical and morphological functionalization of multilayer-graphene foams, Carbon, 121 (2017) 170-180. https://doi.org/10.1016/j.carbon.2017.05.058
[45] B.A. Newcomb, Processing, structure, and properties of carbon fibers, Compos. Part A Appl. Sci. Manuf. 91 (2016) 262–282. https://doi.org/10.1016/j.compositesa.2016.10.018.
[46] L. Li, S. Kim, W. Wang, M. Vijayakumar, Z. Nie, B. Chen, J. Zhang, G. Xia, J. Hu, G. Graff, J. Liu, Z. Yang, A stable vanadium redox-flow battery with high energy density for

large-scale energy storage, Adv. Energy Mater. 1 (2011) 394–400. https://doi.org/10.1002/aenm.201100008.
[47] V. Aravindan, J. Sundaramurthy, P. Suresh Kumar, Y.S. Lee, S. Ramakrishna, S. Madhavi, Electrospun nanofibers: A prospective electro-active material for constructing high performance Li-ion batteries, Chem. Commun. 51 (2015) 2225–2234. https://doi.org/10.1039/c4cc07824a.
[48] V. Aravindan, Y.S. Lee, S. Madhavi, Research Progress on Negative Electrodes for Practical Li-Ion Batteries: Beyond Carbonaceous Anodes, Adv. Energy Mater. 5 (2015). https://doi.org/10.1002/aenm.201402225.
[49] M. Ulaganathan, V. Aravindan, Q. Yan, S. Madhavi, M. Skyllas-Kazacos, T.M. Lim, Recent Advancements in All-Vanadium Redox Flow Batteries, Adv. Mater. Interfaces. 3 (2016) 1–22. https://doi.org/10.1002/admi.201500309.
[50] A. Z. Weber, M.M. Mench, J.P. Meyers, P.N. Ross, J.T. Gostick, Q. Liu, Redox flow batteries: A review, J. Appl. Electrochem. 41 (2011) 1137–1164. https://doi.org/10.1007/s10800-011-0348-2.
[51] L. H. Thaller, US3996064, 1976
[52] M. Lopez-Atalaya, G. Codina, J.R. Perez, J.L. Vazquez, A. Aldaz, Optimization studies on a Fe/Cr redox flow battery, J. Power Sources. 39 (1992) 147–154. https://doi.org/10.1016/0378-7753(92)80133-V.
[53] M. Skyllas-Kazacos, M. Rychcik, R. Robin, US4786567A, 1988
[54] M. Rychcik, M. Skyllas-Kazacos, Characteristics of a new all-vanadium redox flow battery, J. Power Sources. 22 (1988) 59–67. https://doi.org/10.1016/0378-7753(88)80005-3.
[55] M. Skyllas-Kazacos, F. Grossmith, Efficient Vanadium Redox Flow Cell, J. Electrochem. Soc. 134 (1987) 2950–2953. https://doi.org/10.1149/1.2100321.
[56] R. L. Clarke, B. J. Dougherty, S. Harrison, P. J. Millington, S. Mohanta, US0202925A1, 2004
[57] H.F. Gibbard, Physical chemistry of the zinc-bromine battery: I. Activity coefficients of aqueous zinc bromide, J. Solution Chem. 10 (1981) 611–620. https://doi.org/10.1007/BF00650737.
[58] Q. Lai, H. Zhang, X. Li, L. Zhang, Y. Cheng, A novel single flow zinc-bromine battery with improved energy density, J. Power Sources. 235 (2013) 1–4. https://doi.org/10.1016/j.jpowsour.2013.01.193.
[59] W. Wang, S. Kim, B. Chen, Z. Nie, J. Zhang, G.G. Xia, L. Li, Z. Yang, A new redox flow battery using Fe/V redox couples in chloride supporting electrolyte, Energy Environ. Sci. 4 (2011) 4068–4073. https://doi.org/10.1039/c0ee00765j.

[60] M. Skyllas-Kazacos, G. Kazacos, G. Poon, and H. Verseema, Recent advances with UNSW vanadium-based redox flow batteries, Int. J. Energy. Res. 34 (2010) 182–189. https://doi.org/10.1002/er.1658.
[61] R. Zito, US5612148 A 1997.
[62] P. J. Morrissey, P. J. Mitchell, S. E. Male, US20130084482, 2005.
[63] F.Q. Xue, Y.L. Wang, W.H. Wang, X.D. Wang, Investigation on the electrode process of the Mn(II)/Mn(III) couple in redox flow battery, Electrochim. Acta. 53 (2008) 6636–6642. https://doi.org/10.1016/j.electacta.2008.04.040.
[64] F.C. Walsh, C. Poncedeléon, L. Berlouis, G. Nikiforidis, L.F. Arenas-Martínez, D. Hodgson, D. Hall, The development of Zn-Ce hybrid redox flow batteries for energy storage and their continuing challenges, Chempluschem. 80 (2015) 288–311. https://doi.org/10.1002/cplu.201402103.
[65] Z. Na, S. Xu, D. Yin, L. Wang, A cerium-lead redox flow battery system employing supporting electrolyte of methanesulfonic acid, J. Power Sources. 295 (2015) 28–32. https://doi.org/10.1016/j.jpowsour.2015.06.115.
[66] D. Pletcher, R. Wills, A novel flow battery: A lead acid battery based on an electrolyte with soluble lead(II), Phys. Chem. Chem. Phys. 6 (2004) 1779–1785.
[67] D. Pletcher, R. Wills, A novel flow battery - A lead acid battery based on an electrolyte with soluble lead(II): III. The influence of conditions on battery performance, J. Power Sources. 149 (2005) 96–102. https://doi.org/10.1016/j.jpowsour.2005.01.048.
[68] L.W. Hruska, R.F. Savinell, Investigation of Factors Affecting Performance of the Iron-Redox Battery, J. Electrochem. Soc. 128 (1981) 18–25. https://doi.org/10.1149/1.2127366.
[69] B. Li, Z. Nie, M. Vijayakumar, G. Li, J. Liu, V. Sprenkle, W. Wang, Ambipolar zinc-polyiodide electrolyte for a high-energy density aqueous redox flow battery, Nat. Commun. 6 (2015). https://doi.org/10.1038/ncomms7303.
[70] Z. Yang, J. Zhang, M.C.W. Kintner-Meyer, X. Lu, D. Choi, J.P. Lemmon, J. Liu, Electrochemical energy storage for green grid, Chem. Rev. 111 (2011) 3577–3613. https://doi.org/10.1021/cr100290v.
[71] M. Skyllas-Kazacos, M.H. Chakrabarti, S.A. Hajimolana, F.S. Mjalli, M. Saleem, Progress in flow battery research and development, J. Electrochem. Soc. 158 (2011) R55–R79. https://doi.org/10.1149/1.3599565.
[72] S.Eckroad, “Vanadium redox fl ow batteries: An in-depth analysis” (Technical Report EPRI-1014836, Electric Power Research Institute, Palo Alto, CA , 2007).
[73] F. Rahman, M. Skyllas-Kazacos, Vanadium redox battery: Positive half-cell electrolyte studies, J. Power Sources. 189 (2009) 1212–1219. https://doi.org/10.1016/j.jpowsour.2008.12.113.

[74] M. Kazacos, M. Cheng, M. Skyllas-Kazacos, Vanadium redox cell electrolyte optimization studies, J. Appl. Electrochem. 20 (1990) 463–467. https://doi.org/10.1007/BF01076057.
[75] P. Zhao, H. Zhang, H. Zhou, J. Chen, S. Gao, B. Yi, Characteristics and performance of 10 kW class all-vanadium redox-flow battery stack, J. Power Sources. 162 (2006) 1416–1420. https://doi.org/10.1016/j.jpowsour.2006.08.016.
[76] F. Rahman, M. Skyllas-Kazacos, Solubility of vanadyl sulfate in concentrated sulfuric acid solutions, J. Power Sources. 72 (1998) 105–110. https://doi.org/10.1016/S0378-7753(97)02692-X.
[77] M. Lopez-Atalaya, G. Codina, J.R. Perez, J.L. Vazquez, A. Aldaz, M.A. Climent, Behaviour of the Cr(III)/Cr(II) reaction on goldgraphite electrodes. Application to redox flow storage cell, J. Power Sources. 35 (1991) 225–234. https://doi.org/10.1016/0378-7753(91)80108-A.
[78] C.H. Bae, E.P.L. Roberts, R.A.W. Dryfe, Chromium redox couples for application to redox flow batteries, Electrochim. Acta. 48 (2002) 279–287. https://doi.org/10.1016/S0013-4686(02)00649-7.
[79] R. F. Gahn, N. H. Hagedorn, J. S. Ling, NASA, Lewis Research Center, Cleveland, OH 1983, DOE/NASA/12726-21
[80] D.J. Eustace, Bromine Complexation in Zinc-Bromine Circulating Batteries, J. Electrochem. Soc. 127 (1980) 528–532. https://doi.org/10.1149/1.2129706.
[81] K. Cedzynska, Properties Electrolyte, Electrochim. Acta. 40 (1995) 971–976.
[82] K.J. Cathro, K. Cedzynska, D.C. Constable, Preparation and performance of plastic-bonded-carbon bromine electrodes, J. Power Sources. 19 (1987) 337–356. https://doi.org/10.1016/0378-7753(87)87009-X.
[83] S. Licht, J. Davis, Disproportionation of aqueous sulfur and sulfide: Kinetics of polysulfide decomposition, J. Phys. Chem. B. 101 (1997) 2540–2545. https://doi.org/10.1021/jp962661h.
[84] M. Bartolozzi, Development of redox flow batteries. A historical bibliography, J. Power Sources. 27 (1989) 219–234. https://doi.org/10.1016/0378-7753(89)80037-0.
[85] S. Zhong, M. Skyllas-Kazacos, Electrochemical behaviour of vanadium(V)/vanadium(IV) redox couple at graphite electrodes, J. Power Sources. 39 (1992) 1–9. https://doi.org/10.1016/0378-7753(92)85001-Q.
[86] S. Zhong, M. Kazacos, R.P. Burford, M. Skyllas-Kazacos, Fabrication and activation studies of conducting plastic composite electrodes for redox cells, J. Power Sources. 36 (1991) 29–43. https://doi.org/10.1016/0378-7753(91)80042-V.
[87] M. Kazacos, M. Skyllas-Kazacos, Performance Characteristics of Carbon Plastic Electrodes in the All-Vanadium Redox Cell, J. Electrochem. Soc. 136 (1989) 2759–2760. https://doi.org/10.1149/1.2097588.

[88] V. Haddadi-Asl, M. Kazacos, M. Skyllas-Kazacos, Conductive carbon-polypropylene composite electrodes for vanadium redox battery, J. Appl. Electrochem. 25 (1995) 29–33. https://doi.org/10.1007/BF00251261.

[89] V. Haddadi-Asl, M. Kazacos, M. Skyllas-Kazacos, Carbon–polymer composite electrodes for redox cells, J. Appl. Polym. Sci. 57 (1995) 1455–1463. https://doi.org/10.1002/app.1995.070571205.

[90] G.J.W. Radford, J. Cox, R.G.A. Wills, F.C. Walsh, Electrochemical characterisation of activated carbon particles used in redox flow battery electrodes, J. Power Sources. 185 (2008) 1499–1504. https://doi.org/10.1016/j.jpowsour.2008.08.020.

[91] M. Inoue, Y. Tsuzuki, Y. Iizuka, M. Shimada, Carbon Fiber Electrode for Redox Flow Battery, J. Electrochem. Soc. 134 (1987) 756–757. https://doi.org/10.1149/1.2100549.

[92] J. Xi, Z. Wu, X. Qiu, L. Chen, Nafion/SiO2 hybrid membrane for vanadium redox flow battery, J. Power Sources. 166 (2007) 531–536. https://doi.org/10.1016/j.jpowsour.2007.01.069.

[93] F. Mohammadi, P. Timbrell, S. Zhong, C. Padeste, M. Skyllas-Kazacos, Overcharge in the vanadium redox battery and changes in electrical resistivity and surface functionality of graphite-felt electrodes, J. Power Sources. 52 (1994) 61–68. https://doi.org/10.1016/0378-7753(94)01938-X.

[94] M. Rychcik, M. Skyllas-Kazacos, Evaluation of electrode materials for vanadium redox cell, J. Power Sources. 19 (1987) 45–54. https://doi.org/10.1016/0378-7753(87)80006-X.

[95] S. Zhong, C. Padeste, M. Kazacos, M. Skyllas-Kazacos, Comparison of the physical, chemical and electrochemical properties of rayon- and polyacrylonitrile-based graphite felt electrodes, J. Power Sources. 45 (1993) 29–41. https://doi.org/10.1016/0378-7753(93)80006-B.

[96] W.W. Li, Y.Q. Chu, C.A. Ma, Highly hydroxylated graphite felts used as electrodes for a vanadium redox flow battery, Adv. Mater. Res. 936 (2014) 471–475. https://doi.org/10.4028/www.scientific.net/AMR.936.471.

[97] X. gang LI, K. long HUANG, S. qin LIU, N. TAN, L. quan CHEN, Characteristics of graphite felt electrode electrochemically oxidized for vanadium redox battery application, Trans. Nonferrous Met. Soc. China (English Ed. 17 (2007) 195–199. https://doi.org/10.1016/S1003-6326(07)60071-5.

[98] N. Tan, K.L. Huang, S.Q. Liu, X.G. Li, Z.F. Chang, Activation mechanism study of electrochemical treated graphite felt for vanadium redox cell by electrochemical impedance spectrum, Acta Chim. Sin. 64 (2006) 584–588.

[99] S. Jeong, S. Kim, Y. Kwon, Performance enhancement in vanadium redox flow battery using platinum-based electrocatalyst synthesized by polyol process, Electrochim. Acta. 114 (2013) 439–447. https://doi.org/10.1016/j.electacta.2013.10.011.

[100] Z. González, A. Sánchez, C. Blanco, M. Granda, R. Menéndez, R. Santamaría, Enhanced performance of a Bi-modified graphite felt as the positive electrode of a vanadium redox flow battery, Electrochem. Commun. 13 (2011) 1379–1382. https://doi.org/10.1016/j.elecom.2011.08.017.
[101] D.J. Suárez, Z. González, C. Blanco, M. Granda, R. Menéndez, R. Santamaría, Graphite felt modified with bismuth nanoparticles as negative electrode in a vanadium redox flow battery, ChemSusChem. 7 (2014) 914–918. https://doi.org/10.1002/cssc.201301045.
[102] T.M. Tseng, R.H. Huang, C.Y. Huang, F.S. Shieu, K.L. Hsueh, Improvement of Titanium Dioxide Addition on Carbon Black Composite for Negative Electrode in Vanadium Redox Flow Battery, J. Electrochem. Soc. 160 (2013) A1269–A1275. https://doi.org/10.1149/2.082308jes.
[103] X. Wang, W. Li, Z. Chen, M. Waje, Y. Yan, Durability investigation of carbon nanotube as catalyst support for proton exchange membrane fuel cell, J. Power Sources. 158 (2006) 154–159. https://doi.org/10.1016/j.jpowsour.2005.09.039.
[104] N. Jha, A. Leela Mohana Reddy, M.M. Shaijumon, N. Rajalakshmi, S. Ramaprabhu, Pt-Ru/multi-walled carbon nanotubes as electrocatalysts for direct methanol fuel cell, Int. J. Hydrogen Energy. 33 (2008) 427–433. https://doi.org/10.1016/j.ijhydene.2007.07.064.
[105] A.L. Mohana Reddy, N. Rajalakshmi, S. Ramaprabhu, Cobalt-polypyrrole-multiwalled carbon nanotube catalysts for hydrogen and alcohol fuel cells, Carbon N. Y. 46 (2008) 2–11. https://doi.org/10.1016/j.carbon.2007.10.021.
[106] M.S. Saha, R. Li, X. Sun, High loading and monodispersed Pt nanoparticles on multiwalled carbon nanotubes for high performance proton exchange membrane fuel cells, J. Power Sources. 177 (2008) 314–322. https://doi.org/10.1016/j.jpowsour.2007.11.036.
[107] H.Q. Zhu, Y.M. Zhang, L. Yue, W.S. Li, G.L. Li, D. Shu, H.Y. Chen, Graphite-carbon nanotube composite electrodes for all vanadium redox flow battery, J. Power Sources. 184 (2008) 637–640. https://doi.org/10.1016/j.jpowsour.2008.04.016.
[108] W. Li, J. Liu, C. Yan, Multi-walled carbon nanotubes used as an electrode reaction catalyst for VO2+/VO2+ for a vanadium redox flow battery, Carbon N. Y. 49 (2011) 3463–3470. https://doi.org/10.1016/j.carbon.2011.04.045.
[109] G. Wei, C. Jia, J. Liu, C. Yan, Carbon felt supported carbon nanotubes catalysts composite electrode for vanadium redox flow battery application, J. Power Sources. 220 (2012) 185–192. https://doi.org/10.1016/j.jpowsour.2012.07.081.
[110] W. Li, J. Liu, C. Yan, The electrochemical catalytic activity of single-walled carbon nanotubes towards VO 2+/VO 2+ and V 3+/V 2+ redox pairs for an all vanadium redox flow battery, Electrochim. Acta. 79 (2012) 102–108. https://doi.org/10.1016/j.electacta.2012.06.109.
[111] W. Li, J. Liu, C. Yan, Modified multiwalled carbon nanotubes as an electrode reaction catalyst for an all vanadium redox flow battery, J. Solid State Electrochem. 17 (2013) 1369–1376. https://doi.org/10.1007/s10008-013-2006-6.

[112] S. Maldonado, K.J. Stevenson, Influence of nitrogen doping on oxygen reduction electrocatalysis at carbon nanofiber electrodes, J. Phys. Chem. B. 109 (2005) 4707–4716. https://doi.org/10.1021/jp044442z.

[113] Y. Shao, J. Sui, G. Yin, Y. Gao, Nitrogen-doped carbon nanostructures and their composites as catalytic materials for proton exchange membrane fuel cell, Appl. Catal. B Environ. 79 (2008) 89–99. https://doi.org/10.1016/j.apcatb.2007.09.047.

[114] K. Gong, F. Du, Z. Xia, M. Durstock, L Dai, Nitrogen-doped carbon nanotube arrays with high electrocatalytic activity for oxygen reduction, Science, 323 (2009) 760–764. https://doi.org/10.1126/science.1168049

[115] R.A. Sidik, A.B. Anderson, N.P. Subramanian, S.P. Kumaraguru, B.N. Popov, O2 reduction on graphite and nitrogen-doped graphite: Experiment and theory, J. Phys. Chem. B. 110 (2006) 1787–1793. https://doi.org/10.1021/jp055150g.

[116] G. Wu, D. Li, C. Dai, D. Wang, N. Li, Well-dispersed high-loading Pt nanoparticles supported by shell-core nanostructured carbon for methanol electrooxidation, Langmuir. 24 (2008) 3566–3575. https://doi.org/10.1021/la7029278.

[117] M.S. Saha, R. Li, X. Sun, S. Ye, 3-D composite electrodes for high performance PEM fuel cells composed of Pt supported on nitrogen-doped carbon nanotubes grown on carbon paper, Electrochem. Commun. 11 (2009) 438–441. https://doi.org/10.1016/j.elecom.2008.12.013.

[118] L. Shi, Q. Gao, Y. Wu, High performance oxide functionalized nitrogen-doped mesocellular carbon foam for biosensor construction, Electroanalysis. 21 (2009) 715–722. https://doi.org/10.1002/elan.200804469.

[119] M. Park, J. Ryu, Y. Kim, J. Cho, Corn protein-derived nitrogen-doped carbon materials with oxygen-rich functional groups: A highly efficient electrocatalyst for all-vanadium redox flow batteries, Energy Environ. Sci. 7 (2014) 3727–3735. https://doi.org/10.1039/c4ee02123a.

[120] M. Ulaganathan, A. Jain, V. Aravindan, S. Jayaraman, W.C. Ling, T.M. Lim, M.P. Srinivasan, Q. Yan, S. Madhavi, Bio-mass derived mesoporous carbon as superior electrode in all vanadium redox flow battery with multicouple reactions, J. Power Sources. 274 (2015) 846–850. https://doi.org/10.1016/j.jpowsour.2014.10.176.

[121] J.J. Park, J.H. Park, O.O. Park, J.H. Yang, Highly porous graphenated graphite felt electrodes with catalytic defects for high-performance vanadium redox flow batteries produced via NiO/Ni redox reactions, Carbon N. Y. 110 (2016) 17–26. https://doi.org/10.1016/j.carbon.2016.08.094.

[122] Z. González, C. Flox, C. Blanco, M. Granda, J.R. Morante, R. Menéndez, R. Santamaría, Outstanding electrochemical performance of a graphene-modified graphite felt for vanadium redox flow battery application, J. Power Sources. 338 (2017) 155–162. https://doi.org/10.1016/j.jpowsour.2016.10.069.

[123] A. Di Blasi, C. Busaccaa, O. Di Blasia, N. Briguglio, G. Squadrito, V. Antonuccia, Synthesis of flexible electrodes based on electrospun carbon nanofibers with Mn3O4nanoparticles for vanadium redox flow battery application, Appl. Energy. 190 (2017) 165–171. https://doi.org/10.1016/j.apenergy.2016.12.129.

[124] C. Busacca, O. Di Blasi, N. Briguglio, M. Ferraro, V. Antonucci, A. Di Blasi, Electrochemical performance investigation of electrospun urchin-like V2O3-CNF composite nanostructure for vanadium redox flow battery, Electrochim. Acta. 230 (2017) 174–180. https://doi.org/10.1016/j.electacta.2017.01.193.

[125] W. Wang, Q. Luo, B. Li, X. Wei, L. Li, Z. Yang, Recent progress in redox flow battery research and development, Adv. Funct. Mater. 23 (2013) 970–986. https://doi.org/10.1002/adfm.201200694.

[126] T. Mohammadi, M. Skyllas Kazacos, Evaluation of the chemical stability of some membranes in vanadium solution, J. Appl. Electrochem. 27 (1997) 153–160. https://doi.org/10.1023/A:1018495722379.

[127] X. Teng, Y. Zhao, J. Xi, Z. Wu, X. Qiu, L. Chen, Nafion/organically modified silicate hybrids membrane for vanadium redox flow battery, J. Power Sources. 189 (2009) 1240–1246. https://doi.org/10.1016/j.jpowsour.2008.12.040.

[128] S. Sang, Q. Wu, K. Huang, Preparation of zirconium phosphate (ZrP)/Nafion1135 composite membrane and H+/VO2+ transfer property investigation, J. Memb. Sci. 305 (2007) 118–124. https://doi.org/10.1016/j.memsci.2007.07.041.

[129] X. Teng, Y. Zhao, J. Xi, Z. Wu, X. Qiu, L. Chen, Nafion/organic silica modified TiO2 composite membrane for vanadium redox flow battery via in situ sol-gel reactions, J. Memb. Sci. 341 (2009) 149–154. https://doi.org/10.1016/j.memsci.2009.05.051.

[130] S. Kim, J. Yan, B. Schwenzer, J. Zhang, L. Li, J. Liu, Z. Yang, M.A. Hickner, Cycling performance and efficiency of sulfonated poly(sulfone) membranes in vanadium redox flow batteries, Electrochem. Commun. 12 (2010) 1650–1653. https://doi.org/10.1016/j.elecom.2010.09.018.

[131] D. Chen, S. Wang, M. Xiao, Y. Meng, Synthesis and characterization of novel sulfonated poly(arylene thioether) ionomers for vanadium redox flow battery applications, Energy Environ. Sci. 3 (2010) 622–628. https://doi.org/10.1039/b917117g.

[132] D. Chen, S. Wang, M. Xiao, Y. Meng, Preparation and properties of sulfonated poly(fluorenyl ether ketone) membrane for vanadium redox flow battery application, J. Power Sources. 195 (2010) 2089–2095. https://doi.org/10.1016/j.jpowsour.2009.11.010.

[133] D. Chen, S. Wang, M. Xiao, D. Han, Y. Meng, Sulfonated poly (fluorenyl ether ketone) membrane with embedded silica rich layer and enhanced proton selectivity for vanadium redox flow battery, J. Power Sources. 195 (2010) 7701–7708. https://doi.org/10.1016/j.jpowsour.2010.05.026.

[134] D. Chen, S. Wang, M. Xiao, Y. Meng, Synthesis and properties of novel sulfonated poly(arylene ether sulfone) ionomers for vanadium redox flow battery, Energy Convers. Manag. 51 (2010) 2816–2824. https://doi.org/10.1016/j.enconman.2010.06.019.
[135] D. Chen, S. Wang, M. Xiao, D. Han, Y. Meng, Synthesis of sulfonated poly(fluorenyl ether thioether ketone)s with bulky-block structure and its application in vanadium redox flow battery, Polymer (Guildf). 52 (2011) 5312–5319. https://doi.org/10.1016/j.polymer.2011.09.021.
[136] Z. Mai, H. Zhang, X. Li, C. Bi, H. Dai, Sulfonated poly(tetramethydiphenyl ether ether ketone) membranes for vanadium redox flow battery application, J. Power Sources. 196 (2011) 482–487. https://doi.org/10.1016/j.jpowsour.2010.07.028.
[137] G.J. Hwang, H. Ohya, Crosslinking of anion exchange membrane by accelerated electron radiation as a separator for the all-vanadium redox flow battery, J. Memb. Sci. 132 (1997) 55–61. https://doi.org/10.1016/S0376-7388(97)00040-9.
[138] M. Mitsutaka, S. Kanji, N. Masato, F. Kouichi and S. Sumie, EP790658 (Europe), or DE69703399 (Germany), or ES2153611 (Spain) 1997.
[139] S. Zhang, C. Yin, D. Xing, D. Yang, X. Jian, Preparation of chloromethylated/quaternized poly(phthalazinone ether ketone) anion exchange membrane materials for vanadium redox flow battery applications, J. Memb. Sci. 363 (2010) 243–249. https://doi.org/10.1016/j.memsci.2010.07.046.
[140] D. Xing, S. Zhang, C. Yin, C. Yan, X. Jian, Preparation and characterization of chloromethylated/quanternized poly (phthalazinone ether sulfone) anion exchange membrane, Mater. Sci. Eng. B Solid-State Mater. Adv. Technol. 157 (2009) 1–5. https://doi.org/10.1016/j.mseb.2008.11.019.
[141] D. Chen, M.A. Hickner, E. Agar, E.C. Kumbur, Selective anion exchange membranes for high coulombic efficiency vanadium redox flow batteries, Electrochem. Commun. 26 (2013) 37–40. https://doi.org/10.1016/j.elecom.2012.10.007.
[142] S. Maurya, S.H. Shin, K.W. Sung, S.H. Moon, Anion exchange membrane prepared from simultaneous polymerization and quaternization of 4-vinyl pyridine for non-aqueous vanadium redox flow battery applications, J. Power Sources. 255 (2014) 325–334. https://doi.org/10.1016/j.jpowsour.2014.01.047.
[143] S.C. Chieng, M. Kazacos, M. Skyllas-Kazacos, Preparation and evaluation of composite membrane for vanadium redox battery applications, J. Power Sources. 39 (1992) 11–19. https://doi.org/10.1016/0378-7753(92)85002-R.
[144] T. Mohammadi, M. Skyllas-Kazacos, Use of polyelectrolyte for incorporation of ion-exchange groups in composite membranes for vanadium redox flow battery applications, J. Power Sources. 56 (1995) 91–96. https://doi.org/10.1016/0378-7753(95)80014-8.

[145] S.C. Chieng, M. Kazacos, M. Skyllas-Kazacos, Modification of Daramic, microporous separator, for redox flow battery applications, J. Memb. Sci. 75 (1992) 81–91. https://doi.org/10.1016/0376-7388(92)80008-8.

[146] T. Mohammadi, M. Skyllas-Kazacos, Preparation of sulfonated composite membrane for vanadium redox flow battery applications, J. Memb. Sci. 107 (1995) 35–45. https://doi.org/10.1016/0376-7388(95)00096-U.

[147] T. Mohammadi, M. Skyllas-Kazacos, Characterisation of novel composite membrane for redox flow battery applications, J. Memb. Sci. 98 (1995) 77–87. https://doi.org/10.1016/0376-7388(94)00178-2.

[148] B. Tian, C.W. Yan, F.H. Wang, Proton conducting composite membrane from Daramic/Nafion for vanadium redox flow battery, J. Memb. Sci. 234 (2004) 51–54. https://doi.org/10.1016/j.memsci.2004.01.012.

[149] R. Zhu, Q. Chen, X. Wang, S. Wang, J. Zhu, H. He, Templated synthesis of nitrogen-doped graphene-like carbon materials using spent montmorillonite, RSC Adv., 5 (2015) 7522-7528. https://doi.org/10.1039/C4RA13732A

[150] Q. Yang, W. Xu, A. Tomita, T. Kyotani, Double Coaxial Structure and Dual Physicochemical Properties of Carbon Nanotubes Composed of Stacked Nitrogen-Doped and Undoped Multiwalls, Chem. Mater., 17 (2005) 2940-2945. https://doi.org/10.1021/cm047830m

[151] Y. Zhou, K. Neyerlin, T. S. Olson, S. Pylypenko, J. Bult, H. N. Dinh, T. Gennett, Z. Shao, R. O'Hayre, Enhancement of Pt and Pt-alloy fuel cell catalyst activity and durability via nitrogen-modified carbon supports, Energy Environ. Sci., 3 (2010) 1437-1446. https://doi.org/10.1039/c003710a

[152] Y. Shao, J. Sui, G. Yin, Y. Gao, Nitrogen-doped carbon nanostructures and their composites as catalytic materials for proton exchange membrane fuel cell, Appl., Catal. B, 79 (2006) 89-99. https://doi.org/10.1016/j.apcatb.2007.09.047

[153] R. Czerw, M. Terrones, J. C. Charlier, X. Blase, B. Foley, R. Kamalakaran, N. Grobert, H. Terrones, D. Tekleab, P. M. Ajayan, W. Blau, M. Ruhle, D. L. Carroll, Identification of Electron Donor States in N-Doped Carbon Nanotubes, Nano Lett., 1 (2001) 457-460. https://doi.org/10.1021/nl015549q

[154] A. C. M. Carvalho, M. C. dos Santos, Nitrogen-substituted nanotubes and nanojunctions: Conformation and electronic properties, J. Appl. Phys., 100 (2006) 084305. https://doi.org/10.1063/1.2357646

[155] A.K. Gupta, D.K. Paliwal, P. Bajaj, Acrylic Precursors for Carbon Fibers, J. Macromol. Sci. Part C (1991) 1–89. http://dx.doi.org/10.1080/15321799108021557

[156] X. Huang, Fabrication and properties of carbon fibers, Materials (Basel). 2 (2009) 2369–2403. https://doi.org/10.3390/ma2042369.

[157] C. Cao, X. Zhuang, Y. Su, Y. Zhang, F. Zhang, D. Wu, X. Feng, 2D polyacrylonitrile brush derived nitrogen-doped carbon nanosheets for high-performance electrocatalysts in oxygen reduction reaction, Polym. Chem. 5 (2014) 2057–2064. https://doi.org/10.1039/c3py01581e
[158] C.K. Liu, Y. Feng, H.J. He, J. Zhang, R.J. Sun, M.Y. Chen, Effect of carbonization temperature on properties of aligned electrospun polyacrylonitrile carbon nanofibers, Mater. Des. 85 (2015) 483–486. https://doi.org/10.1016/j.matdes.2015.07.021.
[159] F. Agend, N. Naderi, R. Fareghi-Alamdari, Fabrication and electrical characterization of electrospun polyacylonitrile-derived carbon nanofibers, J. Appl. Polymer Sci.,106 (2007) 255-259. https://doi.org/10.1002/app.26476.
[160] Z. Li, O. Zabihi, J. Wang, Q. Li, J. Wang, W. Lei, M. Naebe, Hydrophilic PAN based carbon nanofibres with improved graphitic structure and enhanced mechanical performance using ethylenediamine functionalized graphene, RSC Adv. 7 (2017) 2621–2628. https://doi.org/10.1039/C6RA24719A.
[161] S.J. Yoon, S. Kim, D.K. Kim, Optimization of local porosity in the electrode as an advanced channel for all-vanadium redox flow battery, Energy. 172 (2019) 26–35. https://doi.org/10.1016/j.energy.2019.01.101.
[162] D.K. Kim, S.J. Yoon, S. Kim, Development of advanced porous electrode to enhance the flow distribution for vanadium flow battery. KSME (2017) 1389-1392
[163] E. Knudsen, P. Albertus, K.T. Cho, A.Z. Weber, A. Kojic, Flow simulation and analysis of high-power flow batteries, J. Power Sources. 299 (2015) 617–628. https://doi.org/10.1016/j.jpowsour.2015.08.041.
[164] S.B. Beale, H.W. Choi, J.G. Pharoah, H.K. Roth, H. Jasak, D.H. Jeon, Open-source computational model of a solid oxide fuel cell, Comput. Phys. Commun. 200 (2016) 15–26. https://doi.org/10.1016/j.cpc.2015.10.007.

9.5 Publications

9.5.1 Journal articles

[1] D.S. Yang, J.Y. Lee, S.W. Jo, **S.J. Yoon**, T.H. Kim, Y.T. Hong, Electrocatalytic activity of nitrogen-doped CNT graphite felt hybrid for all-vanadium redox flow batteries, Int. J. Hydrogen Energy. 43 (2018) 1516–1522. https://doi.org/10.1016/j.ijhydene.2017.11.145.

[2] R. Ye, D. Henkensmeier, **S.J. Yoon**, Z. Huang, D.K. Kim, Z. Chang, S. Kim, R. Chen, Redox Flow Batteries for Energy Storage: A Technology Review, J. Electrochem. Energy Convers. Storage. 15 (2018) 1–21. https://doi.org/10.1115/1.4037248.

[3] D.K. Kim, **S.J. Yoon**, J. Lee, S. Kim, Parametric study and flow rate optimization of all-vanadium redox flow batteries, Appl. Energy. 228 (2018) 891–901. https://doi.org/10.1016/j.apenergy.2018.06.094.

[4] R. Chen, D. Henkensmeier, S. Kim, **S.J. Yoon**, T. Zinkevich, S. Indris, Improved All-Vanadium Redox Flow Batteries using Catholyte Additive and a Cross-linked Methylated Polybenzimidazole Membrane, ACS Appl. Energy Mater. 1 (2018) 6047–6055. https://doi.org/10.1021/acsaem.8b01116.

[5] **S.J. Yoon**, S. Kim, D.K. Kim, Optimization of local porosity in the electrode as an advanced channel for all-vanadium redox flow battery, Energy. 172 (2019) 26–35. https://doi.org/10.1016/j.energy.2019.01.101.

[6] D.K. Kim, **S.J. Yoon**, S. Kim, Transport phenomena associated with capacity loss of all-vanadium redox flow battery, Int. J. Heat Mass Transf. 148 (2020) 119040. https://doi.org/10.1016/j.ijheatmasstransfer.2019.119040.

[7] **S.J. Yoon**, S. Kim, D.K. Kim, D.M. Yu, S. So, Y.T. Hong, R. Hempelmann, Nitrogen−Doping Through Two−Step Pyrolysis of Polyacrylonitrile on Graphite Felts for Vanadium Redox Flow Batteries, Energy & Fuels. 34 (2020) 5052–5059. https://doi.org/10.1021/acs.energyfuels.0c00689

[8] **S.J. Yoon**, S. Kim, D.K. Kim, S. So, Y.T. Hong, R. Hempelmann, Ionic liquid derived nitrogen doped graphite felt electrodes for vanadium redox flow batteries, Carbon, **accept** (May, 2020).

9.5.2 Posters

[1] **S.J. Yoon**, S. Kim, D.K. Kim, Advanced porous electrodes to improve local electrochemical reactions for vanadium redox flow battery applications, Europe-Korea Conference on Science and Technology (EKC) 2017, Stockholm, Sweden, July 26-29, 2017.

[2] **S.J. Yoon**, D.S. Yang, S. Kim, S. Kim, D.K. Kim, R. Hempelmann, Y.T. Hong, Oleic acid treated graphite felt electrodes for vanadium redox flow batteries, The Korean Society of Industrial and Engineering Chemistry (KSIEC), Daegu, Korea, May 2-4, 2018.

[3] **S.J. Yoon**, Y.T. Hong, S. Kim, R. Hempelmann, Zirconium phosphate composite membrane for vanadium redox flow battery, Bunsentagung 2018, Hannover, Germany, May 10-12, 2018.

[4] **S.J. Yoon**, D.S. Yang, S. Kim, R. Hempelmann, Y.T. Hong, Ionic liquid treated graphite felt electrodes for vanadium redox flow batteries, The Korean Society of Industrial and Engineering Chemistry (KSIEC), Jeju, Korea, November 1-2, 2018.

[5] **S.J. Yoon**, J.H. Han, S. Kim, R. Hempelmann, Y.T. Hong, Polyacrylonitrile (PAN) coated graphite felt electrodes for vanadium redox flow batteries, The Korean Society of Industrial and Engineering Chemistry (KSIEC), Busan, Korea, May 1-3, 2019.